ABSTRACT

STRUCTURAL ARCHITECTURE AND TECTONIC EVOLUTION OF THE ULUKISLA SEDIMENTARY BASIN IN SOUTH-CENTRAL TURKEY

by Can Engin

The E-W-trending Ulukisla basin (UB) in Turkey occurs between the Central Anatolian Crystalline Complex to the north and the Tauride carbonate platform to the south. It contains <5 km-thick, uppermost Cretaceous to Miocene-Pleistocene strata and Eocene magmatic rocks. The Cretaceous–Eocene sedimentary rocks comprise an upward shallowing sequence of clastics. The Eocene sequence includes marine turbidites and is transitional upwards into Oligocene rocks. The upward transition from Lower Oligocene shallow marine, deltaic deposits to Upper Oligocene-Miocene evaporate–terrestrial deposits indicates a record of a successor basin. The Upper Cretaceous–Lower Paleocene rocks and the Middle Eocene–Middle Miocene units are deformed by north- and south-vergent, upright–overturned folds and thrust, strike-slip faults. The E-W normal faults in the Middle Paleocene–Middle Eocene units represent extensional deformation coeval with slab breakoff–induced mafic magmatism. The Ulukisla depocenter initially developed as a successor basin in the latest Mesozoic-early Cenozoic and then evolved into a terrestrial basin in the late Tertiary.

STRUCTURAL ARCHITECTURE AND TECTONIC EVOLUTION OF THE ULUKISLA SEDIMENTARY BASIN IN SOUTH-CENTRAL TURKEY

A Thesis

Submitted to the

Faculty of Miami University

in partial fulfillment of

the requirements for the degree of

Master of Science

Department of Geology & Environmental Earth Science

by

Can Engin

Miami University

Oxford, Ohio

2013

Advisor_____

Dr. Yildirim Dilek

Reader_____

Dr. Brian Currie

Reader_____

Dr. Hailiang Dong

CONTENT

1. INTRODUCTION.....1

2. REGIONAL GEOLOGY.....3

3. STRATIGRAPHY AND SEDIMENTOLOGY OF THE ULUKISLA BASIN.....5

3.1. Ciftehan Formation.....5

3.2. Dedeli Formation.....5

3.3. Aktastepe Formation.....6

3.4. Halkapinar Formation.....6

3.5. Ulukisla Formation.....7

3.6. Hasangazi Formation.....8

3.7. Aktoprak Formation.....9

4. STRUCTURAL GEOLOGY OF THE ULUKISLA BASIN.....10

5. ZIRCON GEOCHRONOLOGY.....13

5.1. Methods.....13

5.2. Detrital Samples.....14

5.3. Magmatic Rock Samples.....16

6. TECTONIC EVOLUTION OF THE ULUKISLA BASIN.....18

7. CONCLUSIONS.....21

8. REFERENCES.....22

9. FIGURE CAPTIONS.....30

LIST OF TABLES

Table 1: Locations, formations and rock types of the collected samples from the Ulukisla Basin and its surroundings **.....85**

Table 2: Strike and dip measurements of bedding planes in different formations in the Ulukisla Basin **.....88**

Table 3: Strike and dip measurements of the faults mapped and observed in the field**.....94**

LIST OF FIGURES

Figure 1: Tectonic map of the eastern Mediterranean region and Anatolia, showing the major plates, plate boundaries and fault systems **.....36**

Figure 2: Geological map of the Central Tauride belt in southern Turkey, showing the major tectonic units, fault zones, ophiolites, and the Ulukisla Basin **.....37**

Figure 3: Total intensity aeromagnetic map of the Central Tauride belt and southern Turkey **...38**

Figure 4: Geological map of the Ulukisla Basin and the Inner–Tauride suture zone in south – central Turkey **.....39**

Figure 5: Stratigraphic columnar section of the Ulukisla Basin and its crystalline basement **.....40**

Figure 6A: Northward overturned basal conglomerate and pelagic limestone of the Ciftehan Formation, resting unconformably over the Cretaceous Alihoca ophiolite **.....41**

Figure 6B: West of the Alihoca Village, the sandstone rocks of the late Maastrichtian – lower Paleocene Aktastepe Formation unconformably resting on the Dedeli Formation and the Alihoca ophiolite **.....41**

Figure 7A: Medium to thin – bedded and laminated sandstone – limestone intercalation in the Kalkankaya Member of the Aktastepe Formation **.....42**

Figure 7B: Fossiliferous neritic limestone (Guneydagi Member) of the Aktastepe Formation **...42**

Figure 8A: Areal view of the Halkapinar Formation, with the younger Hasangazi (Middle – Upper Eocene) and Ulukisla (early – middle Eocene) Formations in the background. **.....43**

Figure 8B: Steeply dipping to southward overturned sandstone and tuffaceous rock intercalations in the Halkapinar Formation west of Gumus Village **.....43**

Figure 9A: Close – up view of the Halkapinar Formation with rounded, undeformed clasts and blocks of Tauride limestone, serpentinite and chert in a muddy – silty matrix **.....44**

Figure 9B: Blocks of blueschist and recrystallized limestone rocks, derived from the Tauride Platform to the south, in a sheared mudstone matrix **.....44**

Figure 10: Photomicrographs of rock blocks within the Halkapinar Formation on the Karagol Road, west of the Alihoca Village **.....45**

Figure 11:.Photomicrographs of sandstone rocks in the Ciftehan Formation **.....46**

Figure 12A: *Nummulites* – bearing calcareous sandstone in the Halkapinar Formation **.....47**

Figure 12B: Coarse – grained sandstone in the Halkapinar Formation with abundant *Nummulites* fossils and quartz grains **.....47**

Figure 13: Photomicrographs of various volcanic rocks intercalated with the sandstone – siltstone and volcanic tuff rocks in the Halkapinar Formation **.....48**

Figure 14: Photomicrographs of the calcareous sandstone – siltstone rocks in the Halkapinar Formation**.....49**

Figure 15: Outcrop photos of the various components of the early – middle Eocene Ulukisla Formation **.....50**

Figure 16: Nearly 200 – m – thick submarine lava flows with mineralized extensional faults within the Ulukisla Basin, exposed at the Caykavak Gap on the Nigde – Ulukisla Road**.....51**

Figure 17: Monzo – syenitic dike – sill intrusions in basalt to basaltic – andesite lava flows near the Gedelli Town in the central part of the Ulukisla Basin **.....52**

Figure 18A: Gently W – SW – dipping lacustrine and fluvial rocks of the Oligo –Miocene Aktoprak Formation unconformably sits on the Kabaktepe evaporites of the underlying Hasangazi Formation **.....52**

Figure 18B: Close-up photo of the stratigraphic contact between the Kabaktepe evaporites and the overlying lacustrine and fluvial rocks of the Aktoprak Formation **.....52**

Figure 19: Sandstone – shale intercalation in the Middle – Upper Eocene Hasangazi Formation, between the Ulukisla and Hasangazi Towns **.....53**

Figure 20: Photomicrographs of lithic sandstones in the Hasangazi Formation **.....54**

Figure 21A: Fluvial (below), lacustrine (above) red-green sandstone and marl-limestone rocks of the Oligo-Miocene Aktoprak Formation in the southwestern part of the Ulukisla Basin **.....55**

Figure 21B: A clayey lacustrine limestone outcrop with a north – vergent thrust fault and a southward overturned parallel backfold**.....55**

Figure 22: Photomicrographs of siltstone – sandstone rocks in the Aktoprak Formation **.....56**

Figure 23: Areal view of the Halkapinar Formation along its southern contact against the Alihoca ophiolite and the Tauride Platform**.....57**

Figure 24: Structural cross – sections through the Ulukisla Basin and the northern edge of the Tauride Platform in the Bolkar Mountains **.....58**

Figure 25: The NE – SW – oriented left – lateral Ecemis Fault Zone truncating the eastern end of the Ulukisla Basin**.....59**

Figure 26: Stereoplots are showing the bedding azimuths and contour diagrams of Ulukisla basin units **.....60**

Figure 27: Stereoplots are showing different fault types in the basin, fault – plane strike and dip azimuth.**.....60**

Figure 28A: Porphyritic Horoz Granite (~ 52 Ma) intruded by a gently – dipping applite – dacite dike near the Horoz Village **.....61**

Figure 28B: A nearly vertical strike – slip fault plane in the Horoz Granite with subhorizontal slickenside lineations **.....61**

Figure 29A: The Uckapili Granite intrusive into the marble, calcschist, and quartz – biotite – muscovite schist rocks of the Nigde metamorphic massif north of the Ulukisla Basin **.....62**

Figure 29B: A granitic dike intrusion in a highly foliated quartz – micaschist rock of the Nigde metamorphic massif **.....62**

Figure 30: Zircon U-Pb geochronology dating of sample 06-ULU-12 **..... 63-65**

Figure 31: Zircon U-Pb geochronology dating of sample 07-ULU-12 **..... 66-67**

Figure 32: Zircon U-Pb geochronology dating of sample 19-ULU-12 **.....68**

Figure 33: Zircon U-Pb geochronology dating of sample 28-ULU-12 **..... 69-70**

Figure 34: Zircon U-Pb geochronology dating of sample 37-ULU-12 **..... 71-72**

Figure 35: Zircon U-Pb geochronology dating of sample 39-ULU-12. **..... 73-74**

Figure 36: Zircon U-Pb geochronology dating of sample 47-ULU-12 **..... 75-77**

Figure 37: Zircon U-Pb geochronology dating of sample 51-ULU-12 **..... 78-80**

Figure 38: Zircon U-Pb geochronology dating of sample 15-ULU-12 **.....81**

Figure 39: Zircon U-Pb geochronology dating of sample 18-ULU-12 **.....82**

Figure 40: Zircon U-Pb geochronology dating of sample 46-ULU-12 **.....83**

Figure 41: Tectonic model of the Ulukisla Basin **.....84**

ACKNOWLEDGEMENTS

My graduate studies at Miami University have been supported by the Turkish Petroleum Corporation (TPC) of Turkey through a fellowship. I am indebted to TPC for providing me with the opportunity to undertake my post-graduate studies in the USA and for the financial support for various components of my thesis research. My research in the Ulukisla Basin (Turkey) was generously supported by a Grants-in-Aid Program grant from the American Association of Petroleum Geologists (AAPG), and I gratefully acknowledge it. Additional financial support for my thesis research was provided by the Distinguished Professor Discretionary Funds of Dr Yildirim Dilek (my thesis advisor), by the Geology Department at Miami University, and by the Graduate School.

The community of the Geology Department at Miami University has given me a sense of belonging and citizenship during my stay, and I have greatly enjoyed the intellectual and social atmosphere here since I joined it in August 2011. I am grateful to Mrs. Cathy Edwards for her help and availability for the needs of the graduate students in the department. The graduate student body in Geology has been great, and I have been very happy to be part of it during the last two years. I would like to extend my special thanks to the fellow Turkish graduate students in the department, Ersin Kaya, Eren Deniz Abus, Sezer Turk, Elif Altikulac, and Furkan Bozukluoglu for their continued support, encouragement and insightful discussions on the geology of Turkey. Special thanks are also due to Dr Zeynep Oner, who provided much help, logistical support and friendship during my first year at Miami University. Dr Burcin Bayram in the Physics Department was always available for engaging discussions and support, and I would like to express my gratitude to her and her family.

My fieldwork in the Ulukisla Basin was made much more enjoyable and productive because of the wonderful hospitality and logistical support of Mrs. Ayse Meral (former Major of Ciftehan) and Mr. Ahmet Meral in the town of Ciftehan. Delicious Turkish meals, evening teas and cherries they shared with us over the course of our stay in the Ulukisla region made my field experience very special, and I would like to extend my warmest thanks and regards to them. Dr. Ender Sarifakioglu at the Mineral Research and Exploration Institute of Turkey (MTA-Ankara) and Mr. Adem Gencer in the Turkish Petroleum Corporation provided geological and

topographic maps of the Central Tauride Mountains in south-central Turkey that were most helpful during my studies. I thank both of these colleagues for their support.

Dr. Andreas Moeller in the Department of Geology at the University of Kansas opened his Geochronology Laboratory to me to undertake the mineral separation and zircon dating work for my samples from the Ulukisla Basin. He and Mr. Josh Feldman gave me plenty training and hand to do the zircon dating in an efficient way, and I would like to express my thanks and gratitude to both of them for educating me for the intricacies of multi-step mineral separation, imaging and zircon dating, and for getting the work done. Mrs. Jolene Neher and Mr. Steve Neher hosted me in their warm and friendly house in Lawrence-Kansas during my multiple stays for the zircon dating work in the University of Kansas. Their friendship and logistical support made my laboratory experience in UK much more efficient and productive, and I greatly appreciated it.

I thank my thesis committee members, Dr. Brian Currie and Dr. Hailiang Dong, for their time, help and support with my research and thesis. I have greatly appreciated my learning experience with them and would like to extend my special thanks to both.

It is really hard to explain how grateful I am to my adviser, Dr. Dilek, for his excellent professional guidance and mentorship during my studies at Miami and throughout the course of my thesis research. I have learned a lot from him. He has taught me how to see the big picture in geology and how to overcome hard problems. His advice, knowledge and sense of humor have greatly helped me throughout my graduate studies. He was not only a great adviser, but also a good friend and even a father figure while I have been far from home. I give my sincere thanks and regards to him.

My wife, Güldane, has always been available for me with her greatest support, encouragement and cheerful attitude throughout my graduate studies at Miami University. It is difficult for me to express my gratitude to her in simple words. She is the most important person in my life. I especially thank her for being part of my life.

Finally, I would like to express my deepest gratitude, thanks and appreciation to my parents. My father and mother have been always there for me at hard times and good times, have supported me through every stage of my educational life, and have provided me with much love, support

and encouragement over the years. Their pride in my accomplishments has been a guiding light in my life.

1. INTRODUCTION

This study is aimed at documenting the internal structure, geochronology and tectonic evolution of a latest Cretaceous – Miocene basin in south-central Turkey that displays a complex history of collision, extension, and strike-slip tectonics superimposed on one of the major Neotethyan suture zones. The Ulukisla Basin occurs north of the Tauride Block and is laterally offset from its northeast counterpart, the Sivas Basin, by the Ecemis Fault Zone (EFZ in Fig. 1). The sedimentary, volcanic and structural record of the Ulukisla Basin provides an excellent opportunity to investigate the mode and nature of regional crustal and mantle processes, following the ophiolite emplacement during the initial stages of the closure of the Inner Tauride Ocean in the late Cretaceous (Dilek et al., 1999). Its evolution from marine conditions of deposition / magmatism to continental fluvial and lacustrine deposition makes the Ulukisla Basin a unique and important successor basin in the region.

The Anatolia plate is situated in a broad convergence zone between Eurasia to the north and Africa and Arabia to the south (Fig. 1). Collision of the Arabia plate to the east since 13 Ma (Dewey et al., 1986) has produced significant shortening across eastern Anatolia, and both the Caucasus and the Zagros. It has also been a major driver for the west-southwestward escape of Anatolia from the Bitlis-Zagros suture zone (Mantovani et al, 2001; Reilinger et al., 2006; Allen et al., 2009). This tectonic escape has been facilitated by the North and East Anatolian transform faults (Fig. 1) and has also caused widespread internal deformation within the Anatolian microplate through mainly strike-slip tectonics (Dhont et al., 2006; Piper et al., 2006; Biryol et al., 2011). The Ulukisla Basin has been affected by this escape-related strike-slip faulting and associated deformation since the late Miocene (Dilek and Whitney, 2000; Sarifakioglu et al., 2013).

The western Anatolian region and the Aegean Sea are currently situated in the upper plate of the Hellenic Subduction (Fig. 1) and are undergoing backarc extension (Jolivet and Brun, 2010). However, the extensional tectonics in this region predates both the initiation of Hellenic subduction and the collision-induced escape tectonics. Extension may have started as early as the middle Eocene, following a continental collision event in the Tethyan system and a subsequent slab breakoff event (Dilek and Sandvol, 2009). This process is also a critical component in the extensional tectonic history of the Ulukisla Basin at about the same time.

This thesis work involved structural field mapping, documentation of bedding and fault orientations systematic collection of rock samples for petrographic and structural analyses, satellite image analyses, and U-Pb zircon dating of both magmatic rocks and basin deposits. In this paper I discuss the stratigraphy and structure of the Ulukisla Basin, document the geometry and nature of different structural elements within the basin strata and analyze the kinematics of deformation associated with different fault systems. I then present the results of our zircon geochronology and discuss their implications for potential sources. The new ages obtained in this study help us better constrain the timing of deposition and magmatism within and around the Ulukisla Basin. In the last part of the paper I introduce a tectonic model for the evolution of the Ulukisla Basin based on the results of this study and the existing literature.

2. REGIONAL GEOLOGY

The Ulukisla Basin is bounded in the south by the Bolkar Mountains, which are part of the Tauride Platform (a continental block) and to the east by the sinistral Ecemis fault zone (Fig. 2). The Nigde metamorphic massif bounds the basin to the north. Ulukisla Basin strata are overlain by the Upper Miocene-Pliocene fluvial rocks and the Quaternary alluvial fan deposits of the Eregli Basin in the west (Fig. 2). The Tauride Platform includes lower Paleozoic to Upper Cretaceous limestone, dolomite, marble, calcschist and metapelitic rocks (Demirtaslı et al., 1984; Alan et al., 2007). These rocks are extensively deformed by folding and faulting, and are intruded by the NE–SW-running Horoz Granite along its northern edge (Fig. 2; Dilek and Whitney 2000; Kadioglu and Dilek, 2010).

Along the southern margin of the Ulukisla Basin, the Alihoca ophiolite rests tectonically above the platform carbonates. In this region, the ophiolite is nearly 2-km-thick and consists of upper mantle harzburgites with minor dunite lenses, ultramafic cumulate rocks, layered to isotropic gabbros, and doleritic dikes (Dilek et al., 1999; Sarifakioglu et al., 2013). Sheeted dikes and volcanic rocks are missing in the Alihoca ophiolite, but blocks of these rocks can be seen in the underlying ophiolitic mélange. Felsic dikes and granitic apophyses also crosscut the gabbros and serpentinized peridotites of the ophiolite.

The Alihoca ophiolite represents a lithospheric fragment of the Inner Tauride Ocean, which has been interpreted to have evolved between the Tauride Platform to the south and the Central Anatolian Crystalline Complex (CACC) to the north. The ophiolite and the Tauride Platform are sharply truncated by the left-lateral Ecemis Fault Zone to the east (Figs. 2 and 3). Although the ophiolitic exposures along the suture zone are covered by the Ulukisla Basin strata, the regional aeromagnetic data indicate the existence of a regionally continuous positive anomaly beneath both the Ulukisla (north) and Eregli (west-northwest) Basins (Fig. 3). (Sarifakioglu et al., 2013). These anomalies are interpreted as indicating the existence of thick slabs of mafic-ultramafic, ophiolitic rocks at depth (Dilek and Whitney, 2000; Sarifakioglu et al., 2013).

To the North of the Ulukisla Basin, the Nigde metamorphic massif to the north (Fig. 2) consists of schists, marble, gneiss, amphibolite and quartzite, and represents a core complex (Whitney and Dilek, 1997; 1998). The protoliths of the Nigde massif were initially deformed and metamorphosed during late Cretaceous-Paleocene contraction (Whitney and Dilek, 2000). Its crustal exhumation path from ~15 to 18 km at depth to about 10 km is recorded by

the high-grade metamorphic rocks in the massif (Whitney and Dilek, 1998). Mylonitic fabrics in these rocks indicate NE-SW-oriented extension that is kinematically consistent with the slip direction along the S-dipping, low-angle detachment fault along its southern edge (Fig. 2; Whitney and Dilek 1998; Dilek and Whitney 2000). The deformed marble, quartzite and minor schist of the Nigde massif in the footwall of this detachment fault are juxtaposed against the undeformed, Middle-Upper Eocene clastic rocks of the Ulukisla Basin in the hanging wall. The calcalkaline Uckapili granite crosscuts all metamorphic and structural fabrics in the Nigde massif (Whitney and Dilek, 1997; 1998).

The NE-SW-trending Ecemis Fault Zone is about 150-km-long and 2- to 8-km-wide (Figs. 2, 4), and is seismically active. It is part of a larger, Tertiary strike-slip fault system crosscutting all geological units and structures in Central Anatolia (Kocyigit and Beyhan, 1998). The Ecemis Fault displaces the Tauride Platform and the Inner Tauride suture zone left-laterally for nearly 80 km, and truncates the metamorphic rocks of the Nigde Massif and the Ulukisla Basin strata in the east (Figs. 2 and 4). Its structural trend and architecture is well defined in the aeromagnetic anomaly map (Fig. 3). The fault system is mostly a transtentional with several major left step-overs and releasing bends that form local pull-apart basins (Kocyigit and Beyhan, 1998; Dilek et al., 1999b). The Ecemis Fault also to played a major role during the unroofing of the Nigde core complex by accommodating top-to-the south shearing and exhumation along the south-dipping Nigde detachment fault (Dilek and Whitney, 2000).

3. STRATIGRAPHY AND SEDIMENTOLOGY OF THE ULUKISLA BASIN

The stratigraphy of the Ulukisla Basin has been well documented in the literature, although the formation names and boundaries vary somewhat depending on the nature of the related studies (Oktay, 1982; Demirtasli et al., 1984; Cevikbas and Oztunali, 1991; Clark and Roberston, 2005). The ages of the stratigraphic units are based entirely on the microfossils recovered from the sedimentary rocks in the basinal strata, and are reported in Demirtasli et al. (1984). There are no radiometric or isotopic age data available from the basinal units, including the volcanic and plutonic rocks. The zircon ages reported in this study represent the first comprehensive dating results from the Ulukisla Basin units and several other intrusive rocks in the region. The doleritic dike intrusions in the Alihoca ophiolite structurally beneath the ophiolite were dated previously at 90 Ma (Dilek et al., 1999a).

In this study I have followed the stratigraphic nomenclature of Demirtasli et al. (1984), and have augmented their formation definitions and descriptions with my own field observations and petrographic data. In the following section all the major formations and stratigraphic units are described briefly, from the oldest to the youngest, providing their areal coverage, lithological makeup, thickness, microfossil contents and known ages. A generalized stratigraphic column for the basin is shown in figure - 5.

3.1. Ciftehan Formation

The Ciftehan Formation is the oldest sedimentary unit in the Ulukisla Basin (Fig. 5). It is best exposed near the town of Ciftehan and Alihoca village in the east and near Maden Village farther west and north of the Bolkar Mountains (Fig. 4). The Ciftehan Formation includes a basal conglomerate containing ophiolitic material, overlain by sandstone and red pelagic limestone (Fig. 6A). Its maximum thickness is ~300 meters. It is laterally transitional into the Dedeli Formation in the west (Demirtasli et al., 1984; this study). Stratigraphically upward and along strike to the west in the basin, the Ciftehan Formation is unconformably overlain by the Aktastepe Formation (Fig. 6B). Based on the occurrence of *Globotruncana* and *Heterohelix* microfossils, Demirtasli et al. (1984) assigned a late Campanian – Maastrichtian age to the Ciftehan Formation.

3.2. Dedeli Formation

Dedeli Formation is coeval with the Ciftehan Formation and is composed of red conglomerate with ophiolitic material at the bottom and gray sandstone and marl at the top. It

is locally transitional into the Kalkankaya Member of the overlying Aktastepe Formation. The uppermost marl rocks have not yielded any fossils, but the limestone-marl units from the middle part of the Dedeli Formation contain *Globotruncana*, *Globigerina* and *Heterohelix* microfossils, indicating its Maastrichtian age (Demirtasli et al., 1984).

3.3. Aktastepe Formation

The type locality of Aktastepe formation is about 5 km west of Alihoca Village. The lower part of the formation contains the Kalkankaya Member, which is composed of a basal conglomerate, and overlying sandstone and limestone (Fig. 5). Sandstone layers are massive / thick-bedded to laminated, and show locally well-developed cross-bedding. Upper limestones contain abundant bivalve shells, rip-up clasts and micrite. The total thickness of this member is about 300 meters. The limestone units in the lower and middle sections of Kalkankaya contain *Orbitoides*, *Loftusia* and *Ompalocyclus* microfossils, indicating a late Maastrichtian age, whereas the limestones from the upper section include *Miscellanea* and Mississippian microfossils characteristic of the lower Paleocene (Demirtasli et al., 1984). Therefore, the Kalkankaya Member has been interpreted as the late Maastrichtian – early Paleocene in age (Fig. 5).

The upper part of the Aktastepe Formation consists of the Guneydagi Member. This unit contains limestone conglomerate, medium- to thick-bedded limestone, and calcarenite (Fig. 7). Near Yassikaya in the southwestern part of the Ulukisla Basin, it is overlain by the Halkapinar Formation (Fig. 4). The uppermost limestone units have yielded *Miscellanean*, *Bolkarina* and *Fabularia* microfossils, that indicate a middle Paleocene age of deposition (Demirtasli et al., 1984).

3.4. Halkapinar Formation

The type locality of the Halkapinar Formation is near Halkapinar Town in the southwestern part of the Ulukisla Basin and near Karagol west of Alihoca Village (Figs. 4 and 8). The formation contains conglomeratic sandstones at the base that are overlain by a sandstone-silstone-shale sequence including blocks of recrystallized limestone, blueschist facies mafic rocks, and quartzites (Figs. 9 and 10). The provenance of these blocks is interpreted to be rocks of the Tauride Plaform to the south (Fig. 4; Dilek and Whitney, 1997).

Halkapinar Formation sandstones are calcarenites (Fig. 11). Graded beds, cross-beds and flute casts are common features in these sandstones. Broken *Nummulites* fossils are locally

abundant in them (Fig. 12). The overlying sandstone-shale sequence of the Halkapinar Formation is interlayered with tuffaceous and volcanogenic sandstones, and basaltic, andesitic and rhyodacitic lava flows in the upper part of the formation (Figs. 8 and 13). The sandstone layers in the upper part of the formation include abundant feldspar, hematite and biotite grains (Figs. 13 and 14).

Vertically upsection, and laterally to the east to the basin, the Halkapinar Formation is gradational with the Ulukisla Formation (Figs. 4 and 5). Where the Ulukisla Formation is absent, the Halkapinar Formation is unconformably overlain by the Hasangazi Formation (Fig. 8A). The total thickness of the Halkapinar Formation is ~1500 meters. Turbiditic sandstones from its middle part of the unit contain the microfossils *Alveolina*, *Nummulites*, *Assilina* and *Discocyclina* which indicates a late Paleocene to middle Eocene ages of deposition.

3.5. Ulukisla Formation

The Ulukisla Formation crops out north of the Halkapinar Formation and is the most extensive unit in the basin (Fig. 4). It overlies the Halkapinar Formation conformably and is overlain by the Hasangazi Formation to the west and the north (Figs. 4 and 5). Near the base of the unit it is composed of a turbiditic sandstone-shale sequence (Fig. 15A) that locally contains blocks and clasts of Upper Cretaceous limestone. This clastic sequence is gradational upward into volcanogenic sandstone, volcanic conglomerate and agglomeratics (Fig. 15B). Red micritic limestone blocks (dm – scale) occur in a volcanic conglomerate in the lower part of the formation (Fig. 15C). Some micritic limestone blocks also include clasts of basaltic lava, indicating that deposition of this limestone was synchronous with basaltic volcanism in the depocenter.

Volcanic rocks in the middle part of the formation are made largely of pillow lavas (Fig. 15D) with basaltic and trachybasaltic compositions (Sarifakioglu et al., 2013). Locally, the pillow lava unit is up to 200-m-thick (i.e. Caykavak Gap, Nigde-Ulukisla Road), with numerous mineralized, high- to low-angle normal faults (Fig. 16). Pillow lava, pillow breccia and hyaloclastites are intercalated, and alternate with massive lava flows. Farther north in the Ulukisla Formation andesitic to dacitic lavas, local dacitic dome structures and agglomerates become more widespread. The massive lava flows in the central part of the formation are intruded by extensive networks of red-colored monzo-syenitic dikes and sills, and small

stocks (Fig. 17). Two NE-SW-oriented and sheared monzo-syenitic plutons occur near the town of Gedelli in the south-central part of the formation (Fig. 4).

The total thickness of the Ulukisla Formation is estimated to be between 1500 and 2000 meters (Oktay, 1982; Cevikbas and Oztunali, 1991; Clark and Robertson, 2005). Microfossils of *Nummulites*, *Vernevillina*, *Assilina*, and *Operculina* recovered from the sandstone and limestone units indicate a Lutetian (early-middle Eocene) age of the Ulukisla Formation (Demirtasli et al., 1984).

3.6. Hasangazi Formation

The Hasangazi Formation crops out mainly in the western part of the basin, and unconformably covers the Ulukisla and Halkapinar Formations (Figs. 4 and 18). It is also unconformably overlain by the Oligo-Miocene Aktoprak Formation in the south and late-Neogene aged fluvial-lacustrine deposits adjacent to the Eregli Basin in the west.

The oldest unit in the Hasangazi Formation is a basal conglomerate with abundant volcanic clasts in a carbonaceous matrix that is overlain by coarse-grained limestone (calcarenite) with coral and algal fragments and abundant fossil remainings. Demirtasli et al. (1984) and Clark and Robertson (2005) interpreted this limestone unit as a coral build-up accumulated above a volcanic high in the basin. The microfossils recovered from these limestone rocks include *Nummulites*, *Gypsina* and *Discocycline* representing a late Lutetian age (Demirtasli et al., 1984).

Stratigraphically upward in the formation, sandstone–shale intercalations (Boztepe Member of Demirtasli et al., 1984) become prominent (Fig. 19). Sandstone layers are commonly massive and thickly bedded, and show graded-bedding, cross-lamination, and flute-casts. Volcanic material (i.e. feldspar-plagioclase, hornblende and hematite grains) are common in the sandstone layers (Fig. 20). Shale layers include abundant volcanic mud. The total thickness of this sequence is estimated to be around 300-400 meters. Demirtasli et al. (1984) reported *Globorotalia*, *Gypsina* and *Discocyclina* microfossils from the sandstone units in this formation, indicating a late Lutetian age of deposition.

In the southwestern part of the basin, the sandstone / shale sequence is transitional upward into ~200 m of thinly bedded siltstone, mudstone and selenitic gypsum (Fig. 18). This gypsum-clastic unit is known as the Kabaktepe Evaporites (Demirtasli et al., 1984). The

upper gypsum layers are unconformably overlain by fluvial and lacustrine rocks of the Aktoprak Formation (Figs. 4 and 18).

The estimated total thickness of the Hasangazi Formation is less than 600 meters. The microfossils obtained from its various members constrain its depositional age as the late Lutetian (~42-40 Ma).

3.7. Aktoprak Formation

The non-marine Aktoprak Formation is composed of fluvial and lacustrine rocks, that outcrop in a broad syncline in the western end of the Ulukisla Basin. The unit is unconformably overlain by the Miocene–Pliocene rocks to the north and the Quaternary alluvial fan deposits of the Eregli Basin to the west (Fig. 4). Its type locality is near Aktoprak (Kilan) Village, about 12 km to the S–SW of Ulukisla Town.

The base of the Aktoprak Formation consists of red-green, conglomerate and coarse-grained sandstone with siltstone intercalations. Sandstone locally shows well-developed graded-bedding and cross-bedding (Fig. 21A). Clasts in the conglomerate and sandstone are well rounded and mostly made of recrystallized limestone (derived from the Tauride Platform), micritic limestone, basaltic and andesitic volcanic rocks, and quartz. Stratigraphically upward, the conglomerate–sandstone unit becomes rich in a carbonaceous matrix and is overlain by blue-gray marl and limestone (Fig. 21B) that contains abundant gastropod fossils. Gypsum and biotite grains are common in this marl – limestone unit (Fig. 22). Blumenthal (1956) estimated the age of these gastropods and hence the age of the lacustrine marl-limestone unit as Chattian–Aquitanian (latest Oligocene–Lower Miocene). The total thickness of the Aktoprak Formation is about 1000 meters.

4. STRUCTURAL GEOLOGY OF THE ULUKISLA BASIN

In this section, the internal structure of the Ulukisla Basin and the spatial and temporal relationships of a different fault systems that affected the basinal strata are discussed. Sedimentary and magmatic rocks of the basin were deformed by contractional, extensional and strike – slip tectonics during its evolution. Macroscopic and mesoscopic structures associated with these deformational events are documented with field photos, and their attitudes have been measured systematically in the field. The azimuths of bedding planes in different formations and the various fault planes observed and recorded in the field are plotted in stereonet projections (Figs. 26 and 27) and are given in table – 2 and 3.

Ulukisla Basin is a NE-SW-oriented depocenter with a rhombic geometry (Fig. 2), and it is bounded on its three sides by major fault systems. To the south, it is juxtaposed against the Paleozoic- Mesozoic recrystallized carbonate rocks of the Tauride Platform along an ENE-trending left-lateral oblique-slip fault system (Bolkar Frontal Fault) with a significant down-to-the north normal component (Figs. 4 and 23). This Bolkar Frontal Fault system has multiple splays within the northern edge of the Tauride Platform, affecting its rocks, as well as the Alihoca ophiolite underlying the basinal strata (Fig. 24).

To the north, the Ulukisla Basin strata rest tectonically on the metamorphic rocks of the Nigde Massif along an E-W-striking, S-dipping detachment fault (Nigde Detachment of Whitney and Dilek, 1997). Clastic and volcanic rocks of the Ulukisla and Hasangazi Formations are situated in the hanging wall of the Nigde detachment fault, which is bounded on the east by the NE-trending Ecemis Fault Zone (Figs. 2 and 25). The tectonic exhumation of the Nigde core complex and the formation of the Ulukisla Basin might have been thus partly coeval (Dilek and Whitney, 2000; Gautier et al., 2002).

To the east, the Ulukisla Basin strata are abruptly truncated by the left-lateral Ecemis Fault Zone and its strands (Figs. 2 and 4). Along this segment bordering the Ulukisla Basin the Ecemis Fault system is mainly transtensional in character with its left-stepover physiographic features, and locally includes pull-apart depocenters filled with Oligo-Miocene sedimentary and volcanic rocks (Fig. 25).

To the west, the Ulukisla Basin strata are unconformably overlain by the Upper Miocene-Pliocene fluvial and alluvial fan deposits, which may have formed as part of the initial Eregli Basin (Fig. 2).

Internally the Ulukisla Basin strata have been deformed by a series of ENE-WSW-trending broad folds that display both north-and-south vergence (Fig. 24). The rock units in the older Ciftehan and Aktastepe Formations are generally dipping to the NE at moderate to steep angles (55^{o}-75^{o}), whereas those in the Halkapinar Formation have a prodominatly E-W strike with gentle to steep dip angles both to north and south (Fig. 26). Turbitiditic rocks in the Middle to Upper Eocene Hasangazi Formation exhibit two well-defined maxima in Figure 26, defining steeply to moderately NW- and SE-dipping layers. The terrestrial rocks of the Oligo-Miocene Aktoprak Formation nearly mimic the same pattern as with the Hasangazi units, indicating that these two formations were affected by the same deformational event in a similar fashion. The more northwesternly orientation of the layers in the older Ciftehan (U. Cretaceous), Aktastepe (Lower Paleocene) and Halkapinar (Middle Paleocene-Middle Eocene) Formations are distinctly different from the northeasterly orientation of the layers in younger formations.

The rock units in the Ulukisla Formation and the underlying ophiolitic basement (Alihoca ophiolite) are deformed extensively by different fault systems (Fig. 24). The Ciftehan and Aktastepe Formations in the southern part of the Ulukisla Basin display two sets of fault systems with distinctly different orientations. One set of faults, represented by reverse and left-lateral strike-slip faults, run generally WNW-ESE and dip steeply to the south (Fig. 27). A second set of reverse, thrust and oblique-slip faults run NNW-SSE with steep to moderate dips both to the east and the west. No crosscutting relationships of these two fault systems were observed in the field. Therefore, it is not possible to constrain their relative timing of formation. However, these two fault sets were clearly a result of contractional deformation with a strong oblique-slip component and might have formed synchronously.

The Halkapinar (Middle Paleocene-Middle Eocene) and Ulukisla (Lower-Middle Eocene) Formations are strongly affected by pure extensional normal faults and transtensional fault systems (Fig. 27). The NW-SE-trending normal faults have low-to-high angle dips to the NE or SW, and generally occur in the submarine volcanic units of these two formations. The faults display hydrothermal mineralization effects (Fig. 16) as evidenced by widespread epidote+chlorite+quartz+hematite and calcite precipitation (greenschist facies metamorphic minerals), indicating the possibility of a syn-magmatic origin. Turbiditic rocks intercalated with the submarine pillow and massive lava flows and volcaniclastic rocks are also deformed by these NW-SE-oriented extensional normal faults.

The transtensional normal faults in the Halkapinar and Ulukisla Formations generally have a NE-SW general orientation with steep to moderate dips both to the E and the W (Fig. 27). They are, therefore, nearly perpendicular to the general strike of the NW-SE extensional normal faults. Displacement direction, slip sense, slickenside lineations, and other kinematic indicators along these faults indicate their oblique-slip nature with a strong extensional component. The relative timing of the development of these NE-SW transtensional faults with respect to the formation of the NW-SE normal fault systems is not constrained because of the lack of the clear crosscutting relationships in the field. However, they appear to be kinematically compatible in accommodating NE-SW-oriented extensional deformation during synchronous deposition and volcanism in the Ulukisla Basin throughout the Middle Paleocene and Middle Eocene.

Both the Halkapinar and Ulukisla Formations are also affected by contractional reverse and thrust faults (Fig. 15C), although not as extensively as by the normal faults. Since mainly N-vergent thrust and reverse faults crosscut the extensional normal faults, they are interpreted as post-extensional and late Eocene or younger in age.

The Middle Eocene and younger Hasangazi and Aktoprak Formations mainly display WNW-ESE- and ENE-WSW-running and vertically to steeply S-dipping reverse faults with major strike-slip components (Fig. 24). These N-vergent faults are commonly associated with tight, N-vergent folds and locally with southward-overturned backfolds (Fig. 21). The existence of subhorizontal to gently plunging slickenside lineations on some of the fault planes (Fig. 28) and the spatially associated contractional structures, such as folds and parasitic folds with moderately to vertically plunging fold axes, suggest that these oblique-slip faults are transpressional faults that developed in the Oligo-Miocene and later. The WNW-ESE-oriented oblique-slip faults in the older Ciftehan and Aktastepe Formations are geometrically and kinematically compatible with the transpressional faults observed in the younger formations. Thus, it is inferred that all these faults may have formed as a result of a transpressional stress regime during the Oligo-Miocene or later.

5. ZIRCON GEOCHRONOLOGY

5.1. Methods

Eleven (11) rock samples were collected from different locations in the Ulukisla basin to carry out zircon U-Pb geochronology. Three samples were picked from possible source rocks in the region, including the Horoz Granite and felsic intrusions within the Tauride Block to the south (Fig. 28A), and the Uckapili Granite in the Nigde metamorphic massif to the north (Fig. 29). In addition, eight sandstone samples from different formations in the Ulukisla basin were collected for detrital zircon analysis. During the sampling in the field, we tried to pick the rock samples with the most characteristic features of the stratigraphic formation they represent, relatively unaltered and fresh, and away from major faults and shear zones. The purpose of this geochronological work is to constrain the potential provenance of the basin deposits and determine the maximum deposition ages of basin formations. The overall goal of this component of the study was to better understand the tectonically controlled palaeo-topography and the tectonic evolution of the region from the late Cretaceous through the Miocene. Sand-size clastic rocks constitute the best material for zircon analysis, and the felsic igneous rocks provided abundant zircon grains. The amount of rock sampled from each site was 3 to ~5 kg.

Zircon separation and analyses were done in the Geochronology Laboratory at the University of Kansas. Zircon crystals were separated by standard separation techniques, including crushing, grinding, water tabling, sieving, heavy liquids, magnetic separation and handpicking as a last step. Magmatic zircon grains were handpicked and mounted on double-sided tape. Three magmatic samples were analyzed without polishing and SEM imaging. Even though one of them gave clear and accurate results, two of them gave unclear results. Subsequently, these magmatic zircons were polished and imaged by using the Scattering Electron Microscope. Unbroken and euhedral grains were picked for magmatic samples because their cores and rims need to be well imaged in order to decide a domain for laser ablation.Zircons from eight detrital samples, all with different shapes and colors, were picked, polished, and imaged before analyzing.

For magmatic samples, approximately 50-60 zircon grains for each sample are considered sufficient (Fu et al., 2009). Conversely, 120-150 zircon grains for each detrital sample are required to document potentially different age populations, the sample might contain. LEO 1550 field emission scanning electron microscope with CL (cathodoluminescence) imaging

to document the texture and internal structure of the zircon grains. Zircon grains were set in epoxy then grinded and polished to approximately half their original thickness for the LA-ICP-MS analysis.

LA-ICP-MS Uranium-Lead zircon measurements were analyzed on a The Element2 high resolution magnetic sector field ICP-MS coupled with a 193 nm UV laser ablation system with a 30 nm laser-spot diameter. The ablated material is transferred into the spectrometer by argon carrier gas (for solution) or an Ar/He mixture for laser ablation. The GJ1 zircon was used as a major reference standard (e.g., Jackson et al. 2004) to avoid instrumental mass-bias. Plesovice zircon standards (Slama et al. 2008) were used as a secondary standard within each analytical session at the KU LA-ICP-MS laboratory as a quality control target.

5.2. Detrital Samples

06-ULU-12 (Darbogazi Town Entrance - N37^{o}28'.995"/E034^{o}34'.185"): Fig. 30

This sandstone sample was collected near the entrance of Darbogaz Town in the southwestern part of the Ulukisla Basin. I picked 120 zircon grains for this sample. One zircon grain gave a discordant age of ca. 900 Ma. Another grain yielded an age of ca. 60 Ma, and the rest 118 grain analyses gave a concordant $^{206}Pb/^{238}U$ age of ca. 50 Ma.

07-ULU-12 (After exiting Darbogazi – N37^{o}28'.382"/E034^{o}34'.227"): Fig. 31

This sample was taken from the south-central part of the basin. I analyzed 130 grains; 114 of those are less than 10% discordant. The youngest grain gave a $^{206}Pb/^{238}U$ age of 53.4±2.4 Ma. The probability density diagram indicates major age groups at ca. 90-100 Ma, 190-220 Ma, 245 Ma, a very major and broad group at 280-360 Ma, one grain at 380 Ma, small groups at 430-450 Ma, 470-490 Ma, then another broad group between 520-730 Ma with a maximum at 600 Ma, another group 790 Ma and a broader group at 860-1000 Ma. We prefer 7/6 Pb age for the groups, which are bigger than 1 Ga. There are groups at ca. 1030 Ma with a maximum at 1000 Ma, a few grains at ca. 1100 Ma and ca. 1220, 1600 and 1900 Ma. There are eight grains older than 2 Ga which are at 2.0, 2.1, 2.2, 2.4 (n=2), 2.6 and 2.85 Ga. The oldest grain has a concordant $^{207}Pb/^{206}Pb$ age of 3140 Ga.

19-ULU-12 (Ciftehan-Pozanti Road - N37^{o}30'.402"/E034^{o}47'.158"): Fig. 32

The sample was collected between the Towns of Ciftehan and Pozanti on Highway E-5. This location corresponds to the southern edge of the Ulukisla Basin. I selected 123 zircon grains

for this sample, and 112 of them were less than 10%discordant. The youngest grain gave a $^{206}Pb/^{238}U$ age of 48.5±2.4 Ma. There is a small group of ca. 55-60 Ma spots, one at 72 Ma, one at 80 Ma, and all other grains are older than 200 Ma. In the probability density plot, there are further distinct modes at ca. 300 Ma, 400 Ma, a broad peak at ca. 550-750 Ma, another group at 900-1100 Ma and then a few older grains. There are only 11 grains older than 1.1, 1.6, 1.7, 1.95 (n=2), 2.0 (n=2), 2.1, 2.4 and 2.9 (n=2) Ga.

28-ULU-12 (Elmali Road - N37°32'.689"/E034°46'.323"): Fig. 33

This sample is collected from the eastern part of the basin, located within the left-lateral Ecemis Fault Zone. Totally 106 grains were analyzed. The zircons from this sample did not yield any older zircons than ca. 58 Ma. The youngest analysis gave a $^{206}Pb/^{238}U$ age of 52.7±1.6 Ma. This marks the maximum age of deposition. The robust median for the weighted average $^{206}Pb/^{238}U$ age of 100 spots that are less than 10%discordant is 55.9 Ma+0.3-02 Ma.

37-ULU-12 (Elmali Road - N37°35'.636"/E034°44'.557"): Fig. 34

This sample was taken on the Elmali Road located in the eastern part of the basin. I expected to get different age populations from this sample, but 99% of the results show the identical age group that is 53.9±0.18 Ma. Eighty-eight zircon grains provided this identical age with $^{206}Pb/^{238}U$. The interpretation of this result may be that: (1) there was a very local, single magmatic source for the provenance; (2) This sample can be a volcanosedimentary rock with direct volcanic input.

39-ULU-12 (Between Hasangazi and Ciftehan - N37°31'.576"/E034°42'.382"): Fig. 35

This was taken on Highway E-5 between the Towns of Hasangazi and Ciftehan. The results look similar to the results from Sample 37-UlU-12. Almost 95% of the zircons, which is 109 grains, provided identical age group of 49.75±0.14 with $^{206}Pb/^{238}U$. As with Sample 37-ULU-12, this sample may also have a very local single magmatic source, or it can be a volcanosedimentary unit with direct volcanic input.

47-ULU-12 (Nigde-Ulukisla Road - N37°42'.646"/E034°33'.291"): Fig. 36

The location of this sample is in the northeastern part of the basin. I analyzed 90 grains, and 83 of the analyses were near concordant (discordance<10%). Seventy-four zircon grains have $^{206}Pb/^{238}U$ ages between ca. 48 and 58 Ma. The youngest concordant population has a

weighted average $^{206}Pb/^{238}U$ age of 48.3±0.3 Ma, and this result reflects the maximum age of deposition. There are nine zircons older than 60 Ma. A group of three analyses gave a Concordia age of 74.0±0.9 Ma. All older zircons do not form groups, but different ages are represented by a single grain at $^{206}Pb/^{238}U$ dates of ca. 91 Ma, 280 Ma, 280 Ma, 310 Ma, 450 Ma and 680 Ma. There is one zircon, which provided an age older than 1 Ga, with a $^{207}Pb/^{206}Pb$ age of 1040 Ma.

51-ULU-12 (Aktoprak Village - N37°28'.843"/E034°27'.190"): Fig. 37

This sample was collected in Aktoprak (Kilan) Village in the center of the Ulukisla Basin. A large amount of zircons (104 grains) gave the average age of 51±0.7/0.6; another zircon group (12 grains) with $^{206}Pb/^{238}U$ gave an age of 72.1+3.5/-2.1. In the probability density, there are different ages at 93.8, 103.9, 132.3, 249.5, 282, 342, 384, 576, 590 and the oldest one 928 Ma.

5.3. Magmatic Rock Samples

15-ULU-12 (Horoz Village – Horoz Granite - N37°29'.191"/E034°48'.474"): Fig. 38

Horoz granite occurs along the southern border of the basin, and is one of the potential source rocks for basin sediments. We collected a sample from this granite on the Horoz Village road. The Horoz granite crosscuts the Permian to Cretaceous rocks of the Tauride Platform and the tectonically overlying Alihoca ophiolite. The youngest population age weighted with $^{206}Pb/^{238}U$ is of 52±0.5 (95% conf.).

18-ULU-12 (Horoz Village Road – Felsic dike - N37°28'.639"/E034°47'.184"): Fig. 39

This sample was taken from a dike intrusion in the Horoz granite near the southern margin of the basin. There are networks of felsic (aplitic to rhyolitic) dike intrusions within the Horoz granite, and they are compositionally and geochemically similar to the granitic host rock (Kadioglu and Dilek, 2009). I calculated a lower intercept age of 48.5±0.9 Ma with an MSWD=2.6. There are a lot of data which is highly discordant to an upper intercept with the isotopic composition of common Pb. This is caused by the numerous inclusions of relatively unradiogenic but Pb-rich apatite in the analyzed zircons that could not be avoided during laser ablation. The lower intercept of this Discordia between the youngest zircon and the common Pb component appears to give the most reliable date.

46-ULU-12 (Nigde Massif – Uckapili Granite - N37°54'.412"/E034°54'.391"): Fig. 40

The Nigde metamorphic massif is located to the north of the Ulukisla Basin, and is part of the Central Anatolian Crystalline Complex (Whitney and Dilek, 1998). It consists of metapelites, amphibolites and migmatites, intruded by granitic dikes and plutons. The Nigde massif is hence a potential source rock for the basin depositions. I calculated a Concordia age of 72.5±1.1 Ma (95% confidence), with an MSDW (concordance and equivalence) = 2.1. This is the youngest near concordant population, so it can be interpreted as the age of magmatic crystallization for this sample. There is another concordant population at 79±1.0, Ma which may be part of the earlier magmatic history.

6. TECTONIC EVOLUTION OF THE ULUKISLA BASIN

The stratigraphy and sedimentology of the Ulukisla Basin show an upward shallowing sequence of Upper Cretaceous through Lower Eocene clastic units. Extensive submarine magmatism that produced mostly alkaline, high-K volcanic and intrusive rocks intercalated with turbiditic sandstones mark the early to middle Eocene history of the basin. This was a spatially and temporally focused magmatic activity, which is also part of the tectonic evolution of the coeval Sivas Basin to the northeast in central Turkey (Fig. 1). The Middle to Upper Eocene record of the Ulukisla Basin is represented by marine turbidites, which are transitional upwards into mudstone-gypsum intercalations and nearly 200-m-thick selenitic gypsum deposits. These evaporites characterize hypersaline depositional conditions and indicate basin shallowing by the late Eocene. The Oligo-Miocene fluvial and lacustrine rocks unconformably overlying the evaporate deposits indicate the onset and operation of terrestrial depositional processes in the latest stage of the Ulukisla Basin evolution. The ophiolitic basement of the basinal strata and the occurrence of widespread ophiolitic material in the Upper Cretaceous-Paleocene sedimentary units in the lowest stratigraphic levels suggest that Ulukisla Basin evolved as the Inner Tauride Ocean was closing, following the emplacement of its oceanic lithosphere southward onto northern continental margin of the Tauride Block. This evolutionary history indicates a complete stratigraphic and tectonic record of a successor basin.

Based on the stratigraphic and structural record of the basinal strata as documented in this study and in previous work by other researchers, and on the regional geological constraints, a tectonic model is developed to explain the evolution of the Ulukisla Basin (Fig. 41). The 92 Ma Alihoca Ophiolite was emplaced onto the Tauride margin by the Campanian, marking the Inner Tauride suture zone in southern Turkey (Dilek at al., 1999; Sarifakioglu et al., 2013). The metamorphic sole of the Kiziltepe ophiolite in the Bolkar Mountains (Tauride Block) and the Tauride Carbonates display the textural and mineralogical evidence of a blueschist facies metamorphic overprint (Dilek and Whitney, 1997), indicating that the partially subducted continental margin beneath the ophiolitic slab underwent high-P metamorphism (Fig. 41). Clastic to pelagic sediments of the Ciftehan and Dedeli Formations were deposited in the remnant Inner Tauride basin, with abundant ophiolitic material shed off to the depocenter.

The widespread occurrence of blocks and clasts of blueschist rocks and recrystallized limestones of the Tauride Block in the Middle Paleocene–Lower Eocene Halkapinar

Formation indicates that the partially subducted continental margin and the high-P metamorphosed sole of the Kiziltepe ophiolite were exposed at the surface, providing detritus to the basin in the north. This requires the exhumation and uplift of the Tauride Block in the lower plate that coincided with the onset of mafic volcanism in the Ulukisla Basin (Fig. 41). Kadioglu and Dilek (2009) and Sarifakioglu et al. (2013) suggested that this volcanism with high-K, alkaline to shoshonitic products was a result of a slab breakoff event, following the ophiolite emplacement and the partial subduction of the Tauride continental margin. The asthenospheric window created by this inferred slab breakoff provided the necessary heat and the melt flux to cause partial melting of the subduction-metasomatized mantle beneath the basin, producing the alkaline volcanic and plutonic rocks during the late Paleocene through Middle Eocene (Fig. 41). The similar and coeval volcanic and plutonic products within the adjacent Sivas Basin to the northeast (Dirik et al., 1999) indicate that slab breakoff and subsequent magmatism were regional in scale within the Neothyan realm (Altunkaynak and Dilek, 2013).

It is well documented in the literature that slab breakoff-induced magmatism is associated with tectonic extension and sedimentary basin formation along and across suture zones (Davies and von Blackenburg, 1995; Atherton and Ghani, 2002; Koprubasi and Aldanmaz, 2004; Haschke et al., 2002; Maheoa et al., 2002; Chun et al., 2005; Dilek and Altunkaynak, 2007; Keskin et al., 2008; Xu et al., 2008). The NW-SE-striking, numerous normal faults both in the turbiditic rock sequences and the submarine lava flows in the Ulukisla Basin are consistent with this tectonic model and indicate a NE-SW-oriented extensional stress regime within the basin during the Middle Paleocene-Middle Eocene (Fig. 26). This inferred extension direction is parallel to the general trend of the left-lateral Ecemis Fault Zone to the east of the Ulukisla Basin and is also compatible with the kinematics of extension along the Nigde detachment and within the Nigde core complex to the north (Fig. 2) (Whitney and Dilek, 1997; 1998; Faya et al., 2001).

Detrital zircons obtained from the Halkapinar, Ulukisla, and Hasangazi Formations have revealed U-Pb isotopic ages of the early- Middle Eocene (54-48 Ma), the Mississippian (349-341 Ma), the Proterozoic (~ 600 Ma, ~ 900 Ma) and the Archean (~ 2000 Ma). The Oligo-Miocene Aktoprak Formation has yielded detrital zircons with U-Pb ages of 73 Ma. This last detrital zircon age (Campanian) is the same as the magmatic zircon age I have obtained from the Uckapili granite in the Nigde massif to the north. Therefore, it is inferred that the exhumed Nigde core complex was providing detrital material to the Ulukisla Basin during the

Oligo- Miocene. The Eocene detrital zircon ages are coeval with the magmatic zircon ages of the Horoz granite and the felsic dike intrusions in it. It is hence possible that the Horoz granite may have been exposed by the middle-late Eocene as a provenance for the early Eocene detrital zircons in the basin. The most likely source of the Mississippian and Precambrian detrital zircons is the Pontide belt in northern Turkey and in the Caucasus in the Republic of Georgia where the remnants of a Paleozoic Hercynian orogenic belt and Precambrian terranes are exposed (Zakariadze et al., 2007). Major S-SW running river systems draining the Caucasus and Eastern Pontide Mountains may have carried the Paleozoic and Precambrian zircons through the Sivas Basin in the east and then to the Ulukisla Basin in the southwest during the late Cenozoic. Further detrital zircon analyses on the Ulukisla and Sivas Basin strata will help us better constrain this hypothesis.

The middle-late Eocene history of the Ulukisla Basin involved strike-slip faulting with mostly transpressional deformation (Fig. 41). This tectonic regime caused contraction, shortening, uplift and emergence of the basinal units, and played a major role in ending the marine conditions. Basin shoaling produced local lagoons and ponds, in which evaporite deposition took place in the latest Eocene. The Ulukisla Basin became a terrestrial depocenter by the early Oligocene, with extensive fluvial and lacustrine deposition throughout the Oligo-Miocene (Fig. 41). With the onset of the North Anatolian transform faulting and the Arabia collision-driven escape tectonics, central Anatolia started to experience widespread strike-slip deformation in the late Miocene (~7 Ma) and onwards. Most of the left-lateral strike-slip faults in the Miocene and younger rocks in the Ulukisla Basin and its vicinity are the results of this tectonic escape regime, including the seismically active NE-SW-striking Ecemis Fault Zone.

7. CONCLUSIONS

The late Cretaceous-Miocene Ulukisla Basin in south-central Turkey represents a successor basin developed along a major Neotethyan suture zone. Its tectonic evolution encompasses early marine and late terrestrial conditions of deposition. Its stratigraphic record shows that the Tauride continental block and the late Cretaceous Alihoca ophiolite were the major source of clastic material for its depocenter throughout the latest Cretaceous and early Eocene. Slab breakoff-induced magmatism and extension controlled its evolution during the early to middle Eocene. The extensional tectonics and thermal subsidence may have produced the deep marine conditions of sedimentation, coeval with submarine volcanism at this time. Transpressional strike-slip faulting, as a manifestation of an oblique collision of the Tauride Block with the Central Anatolian Crystalline Complex in the middle Eocene, caused widespread contractional deformation across the basin and terminated its marine nature by the early Oligocene. The Oligo-Miocene terrestrial rocks of the Ulukisla Basin were deformed by left-lateral strike-slip faults, which were developed as part of the Anatolian escape tectonics the late Miocene and onwards.

8. REFERENCES

Akay, E., and Uysal, S., 1988, Post – Eocene tectonics of the central Taurus Mountains: Mineral and Research Exploration Bulletin, v. 108, p. 23-34.

Alan, I., ¸ Sahin, ¸ S., Keskin, H., Altun, I., Bakırhan, B., Balcı, V., Böke, N., Saçlı, L., Pehlivan, ¸ S., Kop, A., Haniçili, N., and Çelik, Ö.F., 2007, The geodynamic evolution of the intermediate Taurus Zone: Eregli (Konya)-Ulukı¸sla (Nigde)-Karsantı (Adana)-Namrun (Içel) surroundings: MTA Raport Number 11006 (in Turkish).

Allen, M., J. Jackson, and R. Walker (2004), Late Cenozoic reorganization of the Arabia-Eurasia collision and the comparison of short-term and long-term deformation rates, Tectonics, 23, TC2008, doi:10.1029/ 2003TC001530.

Allen, P.A., Allen, J.R., 1990, Basin Analysis – Principles and Applications: Blackwell Scientific Publications, Oxford.

Altunkaynak, S. and Dilek, Y., 2013, Eocene mafic volcanism in northern Anatolia: Its causes and mantle sources in the absence of active subduction: International Geology Review, v.55(13), p.1641-1659.

Atabey, E., Goncuoglu, M.C., Turhan, N., 1990, Turkish geological map series: No. 33, section J19, Maden Tetkik ve Arama Genel Mudurlugu (General Directorate of Mineral Research and Exploration), Ankara.

Atherton, M.P. and Ghani, A.A., 2002, Slab breakoff: a model for Caledonian, Late Granite syn-collisional magmatism in the orthotectonic (metamorphic) zone of Scotland and Donegal, Ireland: Lithos, v. 62, p. 65-85.

Biryol, C.B., Beck, S.L., Zandt, G., and Ozacar, A.A., 2011, Segmented African lithosphere beneath the Anatolian region inferred from teleseismic P-wave tomography. Geophysycal Journal International, v. 184, p. 1037–1057.

Blumental, M., 1956, Yuksek Bolkardaginin Kuzey Kenari Bolgelerinin ve Bati Uzantilarinin Jeolojisi: Mineral Research and Exploration Institute of Turkey (MTA) Publication, v. D, Special Publication Series No. 7, p. 1-153.

Boztug, D., Cevikbas, A., Demirkol, C., Oztunali, O., 2001, The coexistence of the crustal thickening and thinning related plutons in the Middle Taurus Mountains, Turkey:

Abstract of the Fourth International Turkish Geological Symposium, 24 – 28 September, 2001, Cukurova University, Adana, Turkey.

Celik, O.F., and Chiaradia, M., 2008, Geochemical and petrological aspects of dike intrusions in the Lycian ophiolites (SW Turkey): A case study for the dike emplacement along the Tauride Belt Ophiolites: International Journal of Earth Sciences, v. 97, p. 1151 – 1164, doi: 10.1007/s00531-007-0204-0.

Cemen, I., Goncuoglu, M.C., Dirik, K., 1999, Structural evolution of the Tuzgolu Basin in Central Anatolia, Turkey: Geol. V. 107, p. 693 – 706.

Cevikbas, A., Oztunali, O., 1991, Ulukisla – Camardi (Nigde) havzasinin maden yataklari:jeoloji Muhendisligi, v. 39, p. 22 – 40.

Chun, S.L., Chu, M.-F., Zhang, Y., Xie, Y., Lo., Y.-H., Lee, T.Y., Lan, C.Y., Li, X., Zhang, Q., and Wang, Y., 2005, Tibetan tectonic evolution inferred from spatial and temporal variations in post-collisional magmatism: Earth-Science Reviews, v. 68, p. 173–196.

Clark, M., and Robertson, A.H.F., 2002, The role of the Early Tertiary Ulukisla Basin, southern Turkey, in suturing of the Mesozoic Tethys ocean: Journal of the Geological Society, London, v. 159, p. 673-690.

Clark, M., and Robertson, A.H.F., 2005, Uppermost Cretaceous – Lower Tertiary Ulukisla Basin, south – central Turkey: Sedimentary evolution of part of a unified basin complex within an evolving Neotethyan suture zone: Sedimentary Geology, v. 173, no. 1-4, p. 15-51, doi: 10.1016/j.sedgeo.2003.12.010.

Davies, J.H., and von Blanckenburg, F., 1995, Slab breakoff: A model of lithosphere detachment and its test in the magmatism and deformation of collisional orogens: Earth and Planetary Science Letters, v. 129, no. 1–4, p. 85–102.

DeCelles, P.G., and Giles, K.A., 1996, Foreland Basin Systems: Basin Research,v. 8, p. 105-123.

Dhont, D., Chorowicz, J., and Luxey, P., 2006, Anatolian escape tectonics driven by Eocene crustal thickening and Neogene–Quaternary extensional collapse in the eastern Mediterranean region. In, Dilek, Y. and Pavlides, S. (Editors), Geological Society of America Special Paper 409, p. 441-462. doi: 10.1130/2006.2409(21).

Dellaloglu, A.A., and Aksu, R., 1986, Eregli (Kona)-Ulukisla-Ciftehan-Camardi (Nigde) Dolayinin Jeolojisi ve Petrol Olanaklari: TPAO Rapor, Ankara, 2205, 11-15.

Demirtasli, E., Bilgin, A.Z., Erenler, W., Isiklar, S., Sanli, D.Y., Selim, M., Turhan, N., 1975, Geology of the Bolkar Mountains: in: Alpan, S. (Ed), Congress of Earth Sciences 50th Year of the Republic, Mineral Research Institute of Turkey (MTA), Special Publication, Ankara, p. 42 – 57.

Demirtasli, E., Turhan, N., Bilgin, A.Z., and Selim, M., 1984, Geology of the Bolkar Mountains, in Tekeli, O., and Goncuoglu, M.C., eds., Geolgy of Taurus Belt: Proceedings of the International Symposium, Mineral Research and Expolaration Instutute of Turkey (MTA), Ankara, Turkey, p. 125-141.

Dilek, Y., and Moores, E.M, 1990, Regional Tectonics of the Eastern Mediterranean ophiolites, in Malpas, J., Moores, E.M., Panayiotou, A., and Xenophontos, C., eds., Ophiolites, oceanic crustal analogues, proceedings of the symposium "Troodos 1987": Niscosia, Cyprus: The Geological Survey Department, p. 295-309.

Dilek, Y., and Whitney, D.L. , 1997, Counterclockwise *P-T-t* trajectory from the metamorphic sole of a Neo-Tethyan ophiolite (Turkey): Tectonophysics, v.280 (3-4), p.295-310.

Dilek, Y., Garver, J.I., and Whitney, D.L., 1997, Extensional exhumation, uplift, and crustal cooling in a collision orogen and the geomorphic response, Central Anatolia – Turkey: GSA Abstract with Programs, v. 29, p. A474.

Dilek, Y., and Whitney, D.L., 1998, Syn-metamorphic to neotectonic evolution of the Ecemis strike-slip fault zone (Turkey): EOS Transactions: American Geophysical Union, v. 80, p. F915.

Dilek,Y., Thy, P., Hacker, B., and Grundvic, S., 1999a, Structure and petrology of Tauride ophiolites and mafic dike intrusions (Turkey): Implications for the Neo-Tethyan ocean: Geological Society of America Bulletin, v. 111, no. 8, p. 1192-1216, doi: 10.1130/0016-7606(1999)111<1192:SAPOTO>2.3.CO;2.

Dilek, Y., Whitney, D.L., and Tekeli, O., 1999b, Links between tectonic processes and landscape morphology in an alpine collision zone, south – central Turkey: Annals of Geomorphology (Z. Geomorph. N.F.) v. 118, p. 147 – 164.

Dilek, Y., 2006, Collision tectonics of the Eastern Mediteranean region: Causes and consequences, in Dilek, Y., and Pavlides, S, eds., Postcollisional Tectonics and Magmatism in the Mediterranean Region and Asia: Geological Society of America Special Paper 409, p. 1 – 13, doi: 10.1130/2006.2409(1).

Dilek, Y. and Altunkaynak, S., 2007, Cenozoic crustal evolution and mantle dynamics of post-collisional magmatism in western Anatolia: International Geology Review, v. 49, p. 431-453.

Dilek, Y., and Altunkaynak, S., 2009, Cenozoic crustal evolution and mantle dynamics of post-collisional magmatism in western Anatolia: International Geology Review, v. 49, p. 431-453, DOI: 10.2747/0020-6814.49.5.431.

Dilek, Y., and Altunkaynak, S., 2009, Geochemical and temporal evolution of Cenozoic magmatism in western Turkey: Mantle response to collision, slab breakoff, and litospheric tearing in an orogenic belt, in van Hinsbergen , D.J.J., Edwards, M.A., and Govers, R., eds., Collison and Collapse at the Africa-Arabia-Eurosia subduction Zone: Geological Society of London Special Publications, v. 311, p. 213-233, DOI: 10.1144/SP311.8.

Dilek, Y., and Sandyol, E., 2009, Seismic structure, crustal architecture and tectonic evolution of the Anatolian – African plate boundary and the Cenozoic orogenic belts in the Eastern Mediterranean region, in Murphy, J.B., Kappie, J.D., and Hynes, A.J., eds., Ancient Orogens and Modern Analogues: Geological Society of London Special Publication 327, p. 127 – 160.

Dirik et al., 1999, Stratigraphy and pre-Miocene tectonic evolution of the southwestern part of the Sivas Basin, Central Anatolia, Turkey: Geological Journal, v.34: p.303-319.

Dixon, J.E., and Robertson, A.H.F., eds., 1984, The Geological Evolution of the Eastern Mediterranean: Geological Society of London Special Publication 17, 824 p.

Fayon, A.K., Whitney, D.L., Teyssier, C., Garver, J.I., and Dilek, Y., 2001, Effects of plate convergence obliquity on timing and mechanisms of exhumation of a mid-crustal terrain, the Central Anatolian Crystalline Complex: Earth and Planetary Science Letters, v. 192, p. 191-205.

Fedo, C.H., Sircombe, K.M., Rainbird, R.H., 2003, Detrital zircon analysis of the sedimentary record: In: Hanchar, J., Hoskin, P., (Ed): Zircon. Reviews in mineralogy and Geochemistry, v. 53, p. 277-303.

Fu, B., Mernagh, T.P., Kita, N.T., Kemp, A.I.S., Valley, J.W., 2009, Distinguishing magmatic zircon from hydrothermal zircon: A case study from the Gidginbung high-sulphidation Au–Ag–(Cu) deposit, SE Australia. Chemical Geology, v. 259, p. 131–142.

Gautier, P., Bozkurt, E., Hallot, E., and Dirik, K., 2002, Dating the exhumation of a metamorphic dome: Geological evidence for pre-Eocene unroofing of the Nigde massif (Central Anatolia, Turkey): Geological Magazine, v. 139, p. 559-576.

Gehrel, G.E., 2000, Introduction to detrital zircon studies of Paleozoic and Triasic strata in western Nevada and northern California: Geol. Society of America Special Papers, v.347, p. 1 – 17.

Gehrel, G.E., Dickinson, W.R., 1995, Detrital zircon provenance of Cambrian to Triassic miogeoclinal and eugeoclinal strata in Nevada: American Journal of Science, v. 295, p. 18-48.

Goncuoglu, M.C., 1986, Geochronologic data from the southern part (Nigde area) of the Central Anatolian Massif: Maden Tetkik ve Arama Dergisi, v. 105/106, p. 83 – 96.

Goncuoglu, M.C., Teker, I.O., Cemen, I., 2000, Exhumation of the Nigde Massif, southern central crystalline complex, Turkey: International Earth Science Colloq. Agean Region, Dokuz Eylul University, Izmir, p. 141.

Gorur, N., Oktay, F.Y., Seymen, I., and Sengor, A.M.C., 1984, Paleotectonic evolution of the Tuzgolu Basin Complex, Central Turkey: Sedimentary Record of a Neo-Tethyan Closure, in Dixon, J.E., and Robertson, A.H.F., eds., Geological evolution of the Eastern Mediterranean: Geological Society of London Special Publications, v. 17, p. 467-482.

Gorur, N., Tuysuz, O., and Sengor, A.M.C., 1998, Tectonic evolution of the central Anatolian basins: International Geology Review, v. 40, p. 831-850.

Haschke, M.R., Scheuber, E., Günther, A., and Reutter, K.-J., 2002, Evolutionary cycles during the Andean orogeny: repeated slab breakoff and flat subduction?: Terra Nova, v. 14, p. 49–55.

Jolivet, L., Brun, J.P., 2010,Cenozoic geodynamic evolution of the Aegean: Int J Earth Sci (Geol Rundsch), v. 99, p.109–138.

Kadioglu, Y.K., Dilek, Y., Gulec, N., and Forland, K.A., 2003, Tectonomagmatic evolution of bimodal plutons in the Central Anatolian Crystalline Complex, Turkey: Journal of Geology, v. 111, p. 671-690.

Kadioglu, Y.K., Dilek, Y., and Forland, K.A, 2006, Slab breakoff and syncollisional origin of the Late Cretaceous magmatism in the Central Anatolian Crystalline Complex, Turkey, in Dilek Y., and Pavlides, S., eds., Postcollisional tectonics and magmatism in the Mediterranean Region and Asia: Geological Society of America Special paper, v. 409, p. 381-415, doi: 10.1130/2006/2409(19).

Kadioglu, Y.K., and Dilek, Y., 2009,Structure and geochemistry of the adakitic Horoz granitoid, Bolkar Mountains, south-central Turkey, and its tectonomagmatic evolution: International Geology Review, v. 52, No. 2-3, p.

Kadioglu, Y.K., and Dilek, Y., 2010, Structure and geochemistry of the adakitic Horoz granitoid, Bolkar Mountains, south-central Turkey, and its tectonomagmatic evolution: International Geology Review, v. 52, p. 505-535.

Keskin,M., Genç, S.C., and Tuysuz, O., 2008, Petrology and geochemistry of post-collisional Middle Eocene volcanic units in north-central Turkey: Evidence for magma generation by slab breakoff following the closure of the Northern Neotethys Ocean: Lithos, v. 104, p. 267–305.

Kocyigit, A., and Beyhan, A., 1998, A new intracontinental transcurrent structure: the Central Anatolian Fault Zone, Turkey:Tectonophysics, v. 284, p. 317-336.

Koprubasi N., and Aldanmaz, E., 2004, Geochemical constraints on the petrogenesis of Cenozoic I-type granitoids in Northwest Anatolia, Turkey: Evidence for magma generation by lithospheric delamination in a post-collisional setting: International Geology Review, v. 46, p. 705–729.

Maheoa, G., Guillota, S., Blichert-Tofta, J., Rollandb, Y., and Pecherb, A., 2002, A slab breakoff model for the Neogene thermal evolution of South Karakorum and South Tibet: Earth and Planetary Science Letters, v. 195, p. 45-58.

Mantovani, E., M. Viti, N. Cenni, and D. Babbucci (2001), Short and long term deformation patterns in the Aegean-Anatolian system: Insights from space-geodetic data (GPS), Geophys. Res. Lett., 28, 2325–2328.

Okay, A.I., Tansel, I., Tuysuz, O., 2001, Obduction subduction and collision as reflected in the Upper Cretaceous – Lower Tertiary sedimentary record of western Turkey: Geological Magazine, v. 138, p. 117 – 142.

Oktay, F.Y., 1982, Ulukisla ve cevresinin stratigrafisi ve jeolojik evrimi: Bulletin of the Geoogical Society of Turkey (in Turkish, v. 25, p. 1-23.

Piper, J.D.A., Tatar, Gursoy, H., Koçbulut, F., and Mesci, B.L., 2006, Paleomagnetic analysis of neotectonic deformation in the Anatolian accretionary collage, Turkey. In, Dilek, Y. and Pavlides, S. (Editors), Geological Society of America Special Paper 409, p. 417-439. DOI: 10.1130/2006.2409(20).

Reilinger, R. McClusky, S., Vernant, P., Lawrence, S., Ergintav, S., Cakmak, R., Ozener, H., Kadirov, F., Guliev, I., Stepanyan, R., Nadariya, M., Hahubia, G., Mahmoud, S., Sakr, K., ArRajehi, A., Paradissis, D., Al-Aydrus, A., Prilepin, M., Guseva, T., Evren, E., Dmitrotsa, A.,Filikov, S.V., Gomez, F., Al-Ghazzi, R., and Karam, G., 2006, GPS constraints on continental deformation in the Africa-Arabia- Eurasia continental collision zone and implications for the dynamics of plate interactions. Journal of Geophysical Research, v. 111, B05411, doi:10.1029/2005JB004051.

Robertson, A.H.F., and Dixon, J.E., 1984, introduction: Aspects of the geological evolution of the eastern Mediterranean, in Dixon, J.E., and Robertson, A.H.F., eds., The geological evolution of the eastern Mediterranean: Geological Society of London Special Publication, v. 17, p. 1-74.

Robertson, A.H.F., and Grasso, M., 1995, Overview of the Late Tertiary – Recent tectonic and paleoenvironmental development of the Mediterranean region: Terra Nova, v. 7, p. 114 – 127, doi:10.1111/j.1365 – 3121.1995.tb00680.x.

Sarifakioglu et al., 2013, Interactive comment on "Jurassic–Paleogene intra-oceanic magmatic evolution of the Ankara Mélange, North-Central Anatolia, Turkey": Solid Earth Discuss., 5, C758–C762.

Sengor, A.M.C., and Yilmaz, Y., 1981, Tethyan evolution of Turkey: A plate tectonic approach: Tectonophysics, v. 75, p. 181 – 241, doi:10.1016/0040 – 1951(81)90275 – 4.

Sengor, A.M.C., Yilmaz, Y., and Sungurlu, O., 1984, Tectonics of the Mediterranean Cimmerides: Nature and evolution of the western termination of Paleo-Tethys, in Dixon, J.E., and Robertson, A.H.F., eds., The geological evolution of the Eastern Mediterranean: Geological Society of London Special Publication, v. 17, p. 447-471.

Whitney, D.L., and Dilek, Y., 1997, Core complex development in Central Anatolia, Turkey: Geology, v. 25, p. 1023 – 1026, doi: 10.1130/0091 – 7613 (1997)025<1023: CCDICA>2.3.CO;2.

Whitney, D.L., and Dilek, Y., 1998, Metamorphism during crustal thickening and extension in central Anatolia: The Nigde metamorphic core complex: Journal of Petrology, v. 39, P. 1-466.

Whitney, D.L. and Dilek, Y., Synkinematic andalusite-sillimanite-quartz veins as indicators of P-T-t conditions during late-stage unroofing of a metamorphic core complex, Turkey: Journal of Metamorphic Geology, vol. 18, No. 1, p. 59-66.

Xu, Y.-G., Lan, J.-B., Yang, Q.-J., Huang, X.-L., and Qiu, H.-N., 2008, Eocene break-off of the Neo-Tethyan slab as inferred from intraplate-type mafic dykes in the Gaoligong orogenic belt, eastern Tibet: Chemical Geology, v. 255, p. 439–453.

Yetis, C., 1984, Geology of the Camardi (Nigde) region and characteristics of the Ecemis Fault Zone between Maden Bogazi and Kamisli: Istanbul Uni. Fen Fak. Mem. Seri B 43, p. 41 – 61.

Yilmaz, Y., Tuysuz, O., Yigitbas, E., Genc, S.C., Sengor, A.M.C., 1997, Geology and tectonic evolution of the Pontides: In: Robinson, A.G., (Ed.), Regional and petroleum geology of the Black Sea and surrounding region, American Association Petroleum Geol. Mem., v. 68, p. 183 – 226.

Zakariadze, G.S., Dilek, Y., Adamia, Sh. A., Oberhaensli, R.E., Karpenko, S.F., Bazylev, B.A., and Solov'eva, N., 2007, Geochemistry and geochronology of the Neoproterozoic Pan-African basement of the Transcaucasian Massif (Republic of Georgia) and implications for island arc evolution in the Late Precambrian Arabian-Nubian Shield: Gondwana Research, v. 11, p. 92-108.

9. FIGURE CAPTIONS

Figure 1: Tectonic map of the eastern Mediterranean region and Anatolia, showing the major plates, plate boundaries and fault systems. The Ulukisla and the coeval Sivas sedimentary basins are marked. Modified from Barrier et al. (2001). Key to lettering: DSF – Dead Sea Fault, BFZ – Burdur fault zone, NAFZ – North Anatolian Fault zone, NEAFZ – Northeast Anatolian Fault zone, KOTJ – Karliova triple junction, TF – Tabriz Fault, MTJ – Maras triple junction, EFZ – Ecemis fault zone, TGF – Tuzgolu Fault, KF – Kefali Fault.

Figure 2: Geological map of the Central Tauride belt in southern Turkey, showing the major tectonic units, fault zones, ophiolites, and the Ulukisla Basin.

Figure 3: Total intensity aeromagnetic map of the Central Tauride belt and southern Turkey (from MTA, 20 ?). High positive anomalies represent the mafic – ultramafic rocks of the Inner Tauride Ocean remnants (i.e. Alihoca, Aladag, Mersin ophiolites).

Figure 4: Geologic map of the Ulukisla Basin and the Inner – Tauride suture zone in south – central Turkey. Data are from: Demirtasli et al., 1984; Cevikbas, 1991; MTA Paftasi (1/100.000); and this study.

Figure 5: Stratigraphic columnar section of the Ulukisla Basin and its crystalline basement. Depositional environments of different stratigraphic units and various deformational events that affected these units are also shown. Data are from: Demirtasli et al. , 1984; Sarifakioglu et al., 2013; Dilek et al., 1999; Clark and Robertson, 2002; Cevikbas, 1991, Oktay, 1982.

Figure 6A: Northward overturned basal conglomerate and pelagic limestone of the Ciftehan Formation, resting unconformably over the Cretaceous Alihoca ophiolite. The Tauride Platform is juxtaposed agains the Alihoca ophiolite along the Bolkar Frontal Fault System.

Figure 6B: West of the Alihoca Village, the sandstone rocks of the late Maastrichtian – lower Paleocene Aktastepe Formation unconformably resting on the Dedeli Formation and the Alihoca ophiolite.

Figure 7A: Medium to thin – bedded and laminated sandstone – limestone intercalation in the Kalkankaya Member of the Aktastepe Formation. A parasitic S – shape fold and a mini fault are also seen in this outcrop.

Figure 7B: Fossiliferous neritic limestone (Guneydagi Member) of the Aktastepe Formation.

Figure 8A: Areal view of the Halkapinar Formation, with the younger Hasangazi (Middle – Upper Eocene) and Ulukisla (early – middle Eocene) Formations in the background. The Hasangazi Formation sits in a westward plunging syncline on top of the Ulukisla and Halkapinar Formations.

Figure 8B: Steeply dipping to southward overturned sandstone and tuffaceous rock intercalations in the Halkapinar Formation west of Gumus Village. Sandstone layers make "razor – back ridges" in a softer mudstone country rock in the field.

Figure 9A: Close – up view of the Halkapinar Formation with rounded, undeformed clasts and blocks of Tauride limestone, serpentinite and chert in a muddy – silty matrix.

Figure 9B: Blocks of blueschist and recrystallized limestone rocks, derived from the Tauride Platform to the south, in a sheared mudstone matrix.

Figure 10: Photomicrographs of rock blocks within the Halkapinar Formation on the Karagol Road, west of the Alihoca Village.

A: Meta – dolerite with a blueschist facies overprint. *Glocophane*, quartz and hornblende make up the rock. The provenance of this block in the Halkapinar Formation is the Kiziltepe ophiolite, resting tectonically on the Tauride platform carbonates. Polarized light. Sample location: N 37^{o}.25'.637", E034^{o}.34'.487", 2318 meters.

B: Quartzite rock with recrystallized, strain – free large quartz grains with triple junctions and fine – grained quartz that underwent grain – size reduction during deformation. The provenance of this block is Triassic or older meta – politic rocks in the Tauride Platform to the south. Polarized light.

Figure 11: Photomicrographs of sandstone rocks in the Ciftehan Formation.

A: *Globotruncana* and *Globigerina* – bearing, fine – grained sandstone – siltstone with a mudstone matrix. Polarized light.

B: Hematite, K – feldspar, quartz and chlorite clasts in a carbonaceous matrix. Normal light.

Figure 12A: *Nummulites* – bearing calcareous sandstone in the Halkapinar Formation.

Figure 12B: Coarse – grained sandstone in the Halkapinar Formation with abundant *Nummulites* fossils and quartz grains.

Figure 13: Photomicrographs of various volcanic rocks intercalated with the sandstone – siltstone and volcanic tuff rocks in the Halkapinar Formation.

A: Basaltic lava flow capped by a chert layer; the volcanic rocks is highly fractured and brecciated in the outcrop. Plagioclase and Clinopyroxene (cpx) are still recognizable. Polarized light.

B: Rhyodacite lava with zoned plagioclase and biotite. Polarized light.

C: Rhyolite lava with plagioclase phenocrysts and aligned plagioclase microlites. Polarized light.

D: Fine – grained rhyodacite lava with K – feldspar and biotite grains. Polarized light.

Figure 14: Photomicrographs of the calcareous sandstone – siltstone rocks in the Halkapinar Formation.

A: Carbonate and clay matrix with clasts of feldspar and broken *Nummulites*. This sample was taken immediately below the Kabaktepe evaporites in the uppermost part of the Halkapinar Formation. Polarized light.

B: Carbonate matrix with clasts of altered albite, quartz and broken *Nummulites* fossils. Normal light.

Figure 15: Outcrop photos of the various components of the early – middle Eocene Ulukisla Formation.

A: Turbiditic sandstone layers in a sandstone – shale sequence along the Ciftehan – Pozanti Road in the southernmost part of the Ulukisla Formation.

B: Siltstone –mudstone, sandstone, volcanic conglomerate and tuffaceous rock intercalations with steeply N – dipping layers north of the Gedelli Town in the central part of the Ulukisla Formation.

C: Volcanic sandstone and agglomerate outcrop with micritic limestone clasts and blocks in the south – central part of the Ulukisla Formation. Limestone block and the matrix are deformed by a low – angle, N – vergent thrust fault.

D: Nearly 15 – 20 m – thick pillow – lava sequence resting conformably on the volcanic tuff + siltstone –mudstone units shown in B. Pillow lavas top to the North with steeply inclined inter pillow lava surfaces.

Figure 16: Nearly 200 – m – thick submarine lava flows with mineralized extensional faults within the Ulukisla Basin, exposed at the Caykavak Gap on the Nigde – Ulukisla Road.

A: Pillow breccias with W – NW – dipping bedding surfaces and S – and N – dipping faults with chlorite + epidote + hematite + calcite mineralization.

B: Trachybasalt, trachyandesite and alkaline basalt pillow lavas separated from hyaloclastite and pillow breccia rocks by S – dipping extensional normal faults.

Figure 17: Monzo – syenitic dike – sill intrusions in basalt to basaltic – andesite lava flows near the Gedelli Town in the central part of the Ulukisla Basin.

Figure 18A: Gently W – SW – dipping lacustrine and fluvial rocks of the Oligo –Miocene Aktoprak Formation unconformably sits on the Kabaktepe evaporites of the underlying Hasangazi Formation. The older Ulukisla Formation is seen in the background, in the southern limb of a broad E – W – oriented anticline.

Figure 18B: Close – up photo of the stratigraphic contact between the Kabaktepe evaporites (Hasangazi Formation) and the overlying lacustrine and fluvial rocks of the Aktoprak Formation.

Figure 19: Sandstone – shale intercalation in the Middle – Upper Eocene Hasangazi Formation, between the Ulukisla and Hasangazi Towns.

A: Steeply – dipping to vertical, left – lateral strike – slip fault with a normal component.

B: A NNW – SSE oriented, left –lateral transtensional fault system in the same sandstone – shale sequence in the Hasangazi Formation. Sandstone layers are dipping steeply to the north.

Figure 20: Photomicrographs of lithic sandstones in the Hasangazi Formation.

A: Fine – grained carbonaceous sandstone with clasts of hematite and plagioclase. Polarized light.

B: Graywacke – volcanic ash with highly altered plagioclase, hornblende, hematite and quartz grains. Very fine – grained rock. Polarized light.

Figure 21A: Fluvial (below) and lacustrine (above) red – green sandstone and marl – limestone rocks of the Oligo – Miocene Aktoprak Formation in the southwestern part of the Ulukisla Basin.

Figure 21B: A clayey lacustrine limestone outcrop with a north – vergent thrust fault and a southward overturned parallel backfold.

Figure 22: Photomicrographs of siltstone – sandstone rocks in the Aktoprak formation.

A: Clasts of gypsum – anhydrite and calcite in a mudstone matrix. Polarized light.

B: Clasts of gypsum – anhydrite, calcite and biotite in a mudstone – marl matrix. Polarized light.

Figure 23: Areal view of the Halkapinar Formation along its southern contact against the Alihoca ophiolite and the Tauride Platform. The Bolkar Frontal Fault System is a network of steeply N – dipping en – echelon faults along which the platform carbonates have been uplifted. The blueschist – bearing Kiziltepe ophiolite resting tectonically on the Tauride Platform Carbonates is also shown.

Figure 24: Structural cross – sections through the Ulukisla Basin and the northern edge of the Tauride Platform in the Bolkar Mountains.

Figure 25: The NE – SW – oriented left – lateral Ecemis Fault Zone truncating the eastern end of the Ulukisla Basin. The photo in A is taken just north of the on in B. The Tauride Platform carbonates are uplifted along the transtensional Ecemis Fault Zone. The most recently active fault strand follows the current river channel in the west – central part of the fault zone.

Figure 26: Stereoplots showing the bedding azimuths and contour diagrams of the Ulukisla Basin sedimentary units.

Figure 27: Stereoplots are showing different fault types in the basin, fault – plane strike and dip azimuth.

Figure 28A: Porphyritic Horoz Granite (~ 52 Ma) intruded by a gently – dipping applite – dacite dike near the Horoz Village.

Figure 28B: A nearly vertical strike – slip fault plane in the Horoz Granite with subhorizontal slickenside lineations.

Figure 29A: The Uckapili Granite intrusive into the marble, calcschist, and quartz – biotite – muscovite schist rocks of the Nigde metamorphic massif north of the Ulukisla Basin.

Figure 29B: A granitic dike intrusion in a highly foliated quartz – micaschist rock of the Nigde metamorphic massif.

Figure 30A-B-C: Zircon U-Pb geochronology dating of sample 06-ULU-12.

Figure 31A-B: Zircon U-Pb geochronology dating of sample 07-ULU-12.

Figure 32: Zircon U-Pb geochronology dating of sample 19-ULU-12.

Figure 33A-B: Zircon U-Pb geochronology dating of sample 28-ULU-12.

Figure 34A-B: Zircon U-Pb geochronology dating of sample 37-ULU-12.

Figure 35A-B: Zircon U-Pb geochronology dating of sample 39-ULU-12.

Figure 36A-B-C: Zircon U-Pb geochronology dating of sample 47-ULU-12.

Figure 37A-B-C: Zircon U-Pb geochronology dating of sample 51-ULU-12.

Figure 38: Zircon U-Pb geochronology dating of sample 15-ULU-12.

Figure 39: Zircon U-Pb geochronology dating of sample 18-ULU-12.

Figure 40: Zircon U-Pb geochronology dating of sample 46-ULU-12.

Figure 41: Tectonic model of the Ulukisla Basin. It shows the evolution of the Ulukisla basin from Maastrichtian to Oligo-Miocene.

Figure 1

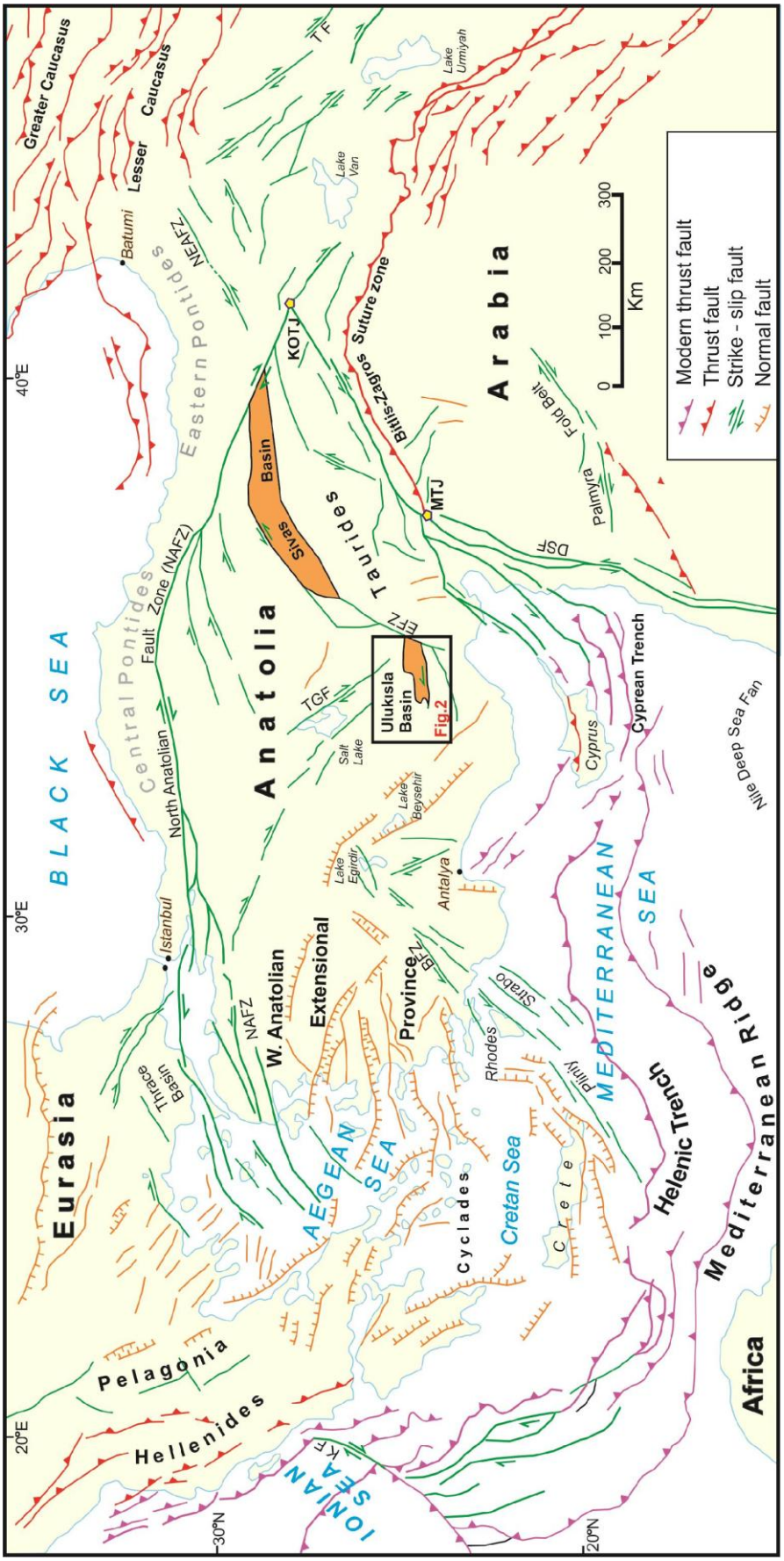
Greater Caucasus
Lesser Caucasus
Batumi
Eastern Pontides
NEAFZ
TF
Lake Urmiyah
Lake Van
KOT.J
Bitlis-Zagros Suture zone
Arabia
Fold Belt
Palmyra
MTJ
DSF
EFZ
Sivas Basin
Central Pontides
Fault Zone (NAFZ)
North Anatolian
Anatolia
Taurides
TGF
Salt Lake
Ulukisla Basin
Fig.2
Lake Beysehir
Lake Egirdir
Antalya
Cyprus
Cyprean Trench
Nile Deep Sea Fan
BLACK SEA
Istanbul
W. Anatolian Extensional Province
NAFZ
Thrace Basin
EGF
Rhodes
Strabo
Pliny
MEDITERRANEAN SEA
AEGEAN SEA
Cyclades
Cretan Sea
Crete
Helenic Trench
Mediterranean Ridge
Eurasia
Pelagonia
Hellenides
KTF
IONIAN SEA
Africa
20°E
30°E
40°E
30°N
20°N
0 100 200 300 Km
Modern thrust fault
Thrust fault
Strike - slip fault
Normal fault

Figure 2

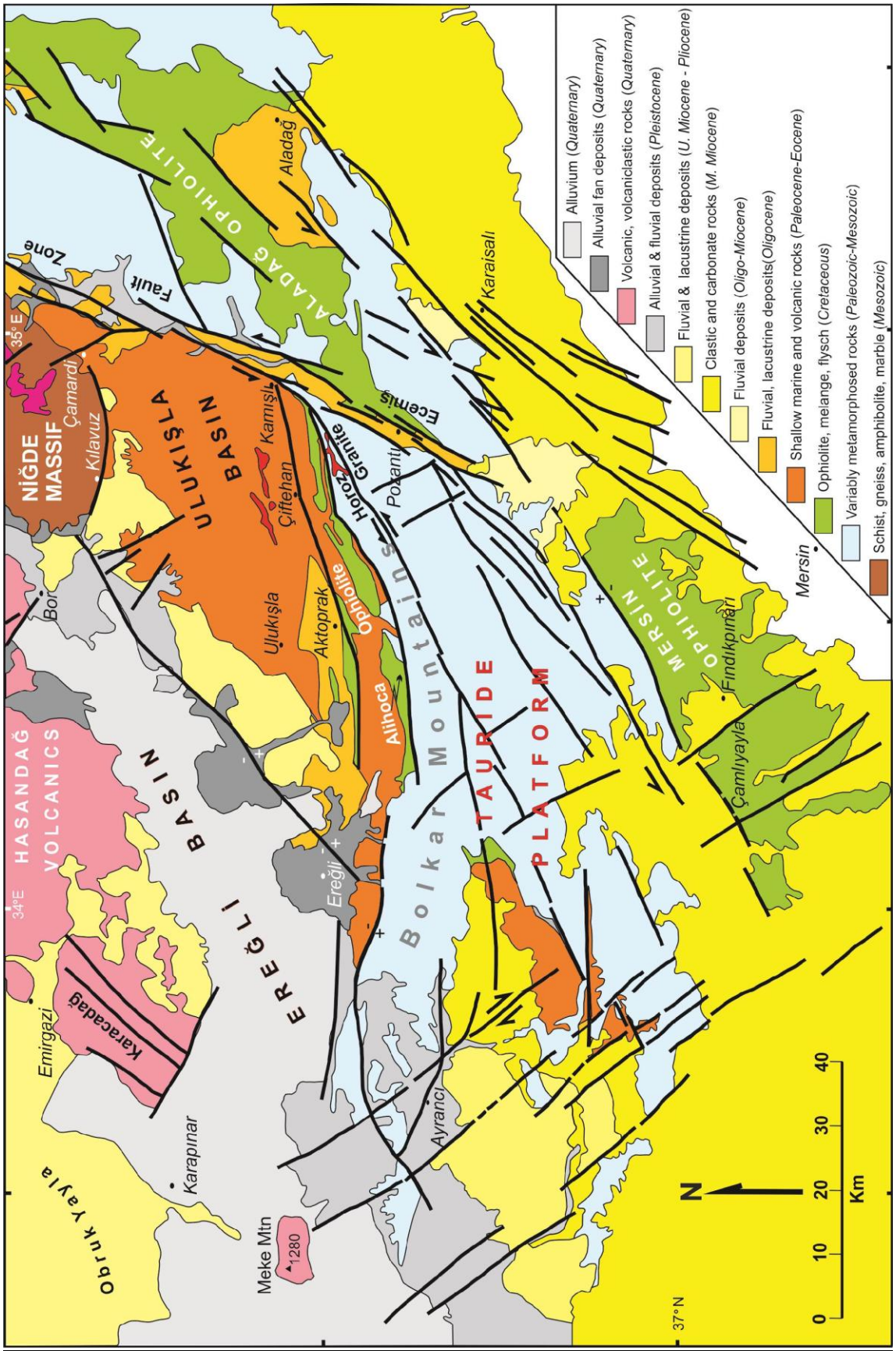
Alluvium (Quaternary)
Alluvial fan deposits (Quaternary)
Volcanic, volcaniclastic rocks (Quaternary)
Alluvial & fluvial deposits (Pleistocene)
Fluvial & lacustrine deposits (U. Miocene - Pliocene)
Clastic and carbonate rocks (M. Miocene)
Fluvial deposits (Oligo-Miocene)
Fluvial, lacustrine deposits(Oligocene)
Shallow marine and volcanic rocks (Paleocene-Eocene)
Ophiolite, melange, flysch (Cretaceous)
Variably metamorphosed rocks (Paleozoic-Mesozoic)
Schist, gneiss, amphibolite, marble (Mesozoic)
ALADAĞ OPHIOLITE
Aladağ
Karaisalı
Ecemiş Fault Zone
NİĞDE MASSIF
Çamardı
Kılavuz
ULUKIŞLA BASIN
Kamışlı
Çiftehan
Horoz Granite
Pozantı
Ulukışla
Aktoprak
Ophiolite
Alihoca
Bolkar Mountains
TAURIDE PLATFORM
MERSİN OPHIOLITE
Mersin
Findıkpınarı
Çamlıyayla
HASANDAĞ VOLCANICS
EREĞLİ BASIN
Karacadağ
Emirgazi
Karapınar
Ereğli
Ayrancı
Meke Mtn
1280
Obruk Yayla
34°E
35° E
37° N
N
0
10
20
30
40
Km

Figure 3

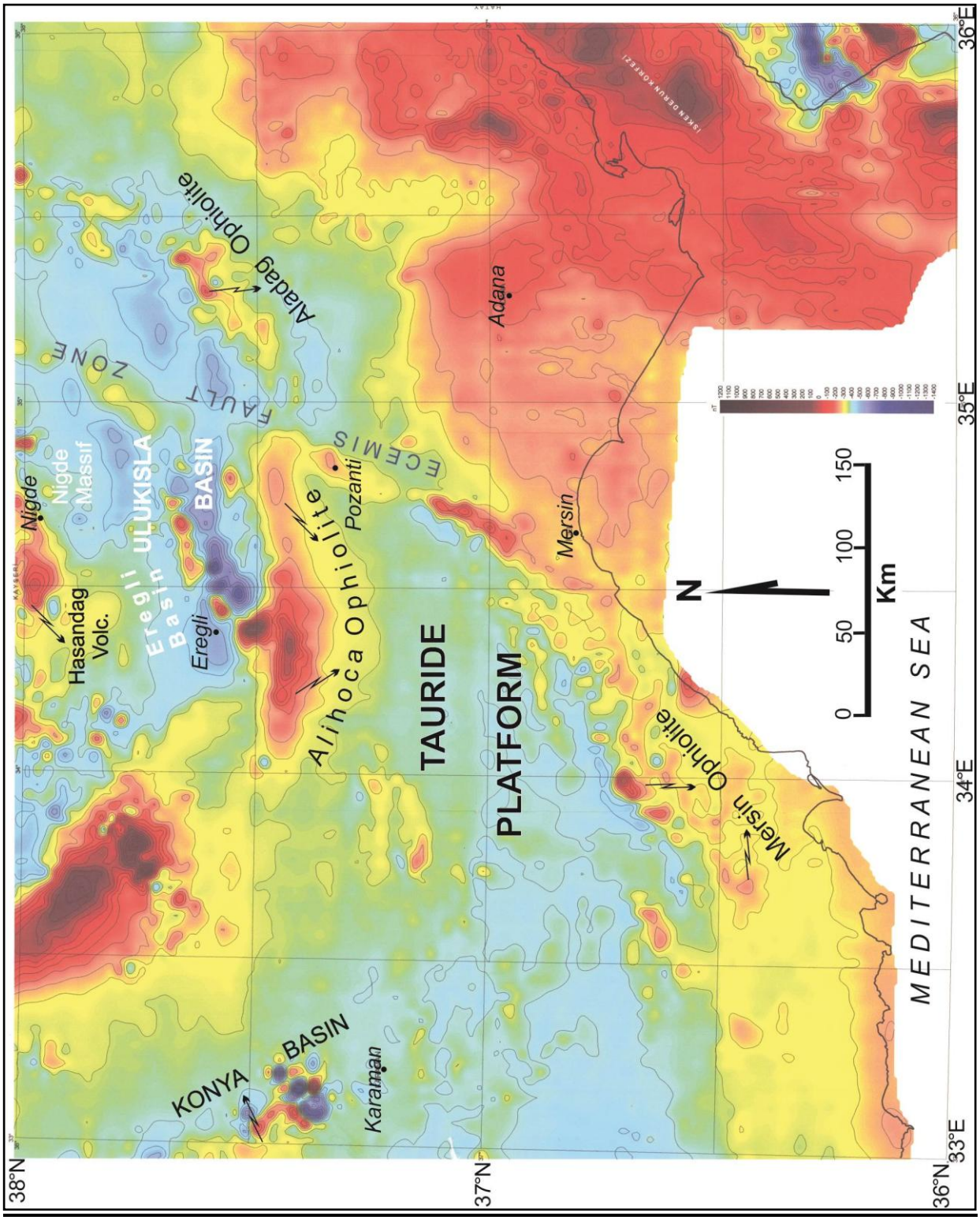
Nigde
Nigde Massif
Hasandag Volc.
Eregli ULUKISLA Basin
BASIN
Eregli
FAULT ZONE
Aladag Ophiolite
ECEMIS
Pozanti
Alihoca Ophiolite
TAURIDE
PLATFORM
Adana
Mersin
Mersin Ophiolite
KONYA BASIN
Karaman
MEDITERRANEAN SEA
N
0
50
100
150
Km
38°N
37°N
36°N
33°E
34°E
35°E
36°E

Figure 4

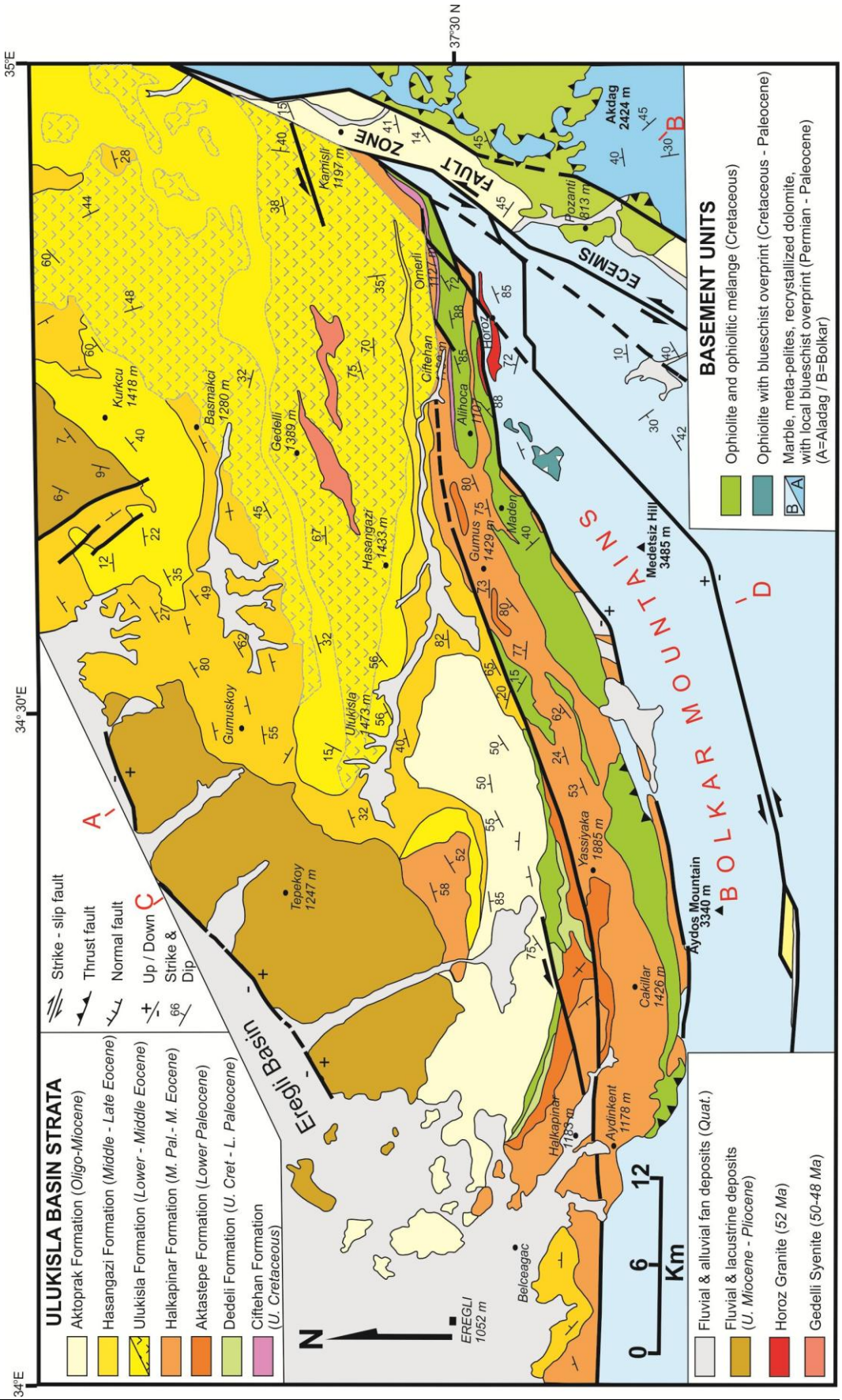
ULUKISLA BASIN STRATA
Aktoprak Formation (Oligo-Miocene)
Hasangazi Formation (Middle - Late Eocene)
Ulukisla Formation (Lower - Middle Eocene)
Halkapinar Formation (M. Pal.- M. Eocene)
Aktastepe Formation (Lower Paleocene)
Dedeli Formation (U. Cret - L. Paleocene)
Ciftehan Formation (U. Cretaceous)
Strike - slip fault
Thrust fault
Normal fault
Up / Down
Strike & Dip
Eregli Basin
BOLKAR MOUNTAINS
ECEMIS FAULT ZONE
BASEMENT UNITS
Ophiolite and ophiolitic mélange (Cretaceous)
Ophiolite with blueschist overprint (Cretaceous - Paleocene)
Marble, meta-pelites, recrystallized dolomite, with local blueschist overprint (Permian - Paleocene)
(A=Aladag / B=Bolkar)
Fluvial & alluvial fan deposits (Quat.)
Fluvial & lacustrine deposits (U. Miocene - Pliocene)
Horoz Granite (52 Ma)
Gedelli Syenite (50-48 Ma)
Km
0
6
12
N
EREGLI 1052 m
Belceagac
Halkapinar 1185 m
Aydinkent 1178 m
Cakillar 1426 m
Aydos Mountain 3340 m
Yassiyaka 1885 m
Tepekoy 1247 m
Gumuskoy
Ulukisla 1473 m
Hasangazi 1433 m
Gedelli 1389 m
Basmakci 1280 m
Kurkcu 1418 m
Kamisli 1197 m
Ciftehan
Omerli
Horoz
Alihoca
Gumus 1429 m
Maden
Medetsiz Hill 3485 m
Pozanti 813 m
Akdag 2424 m
34°E
34°30'E
35°E
37°30 N
A
B
C
D

Figure 5

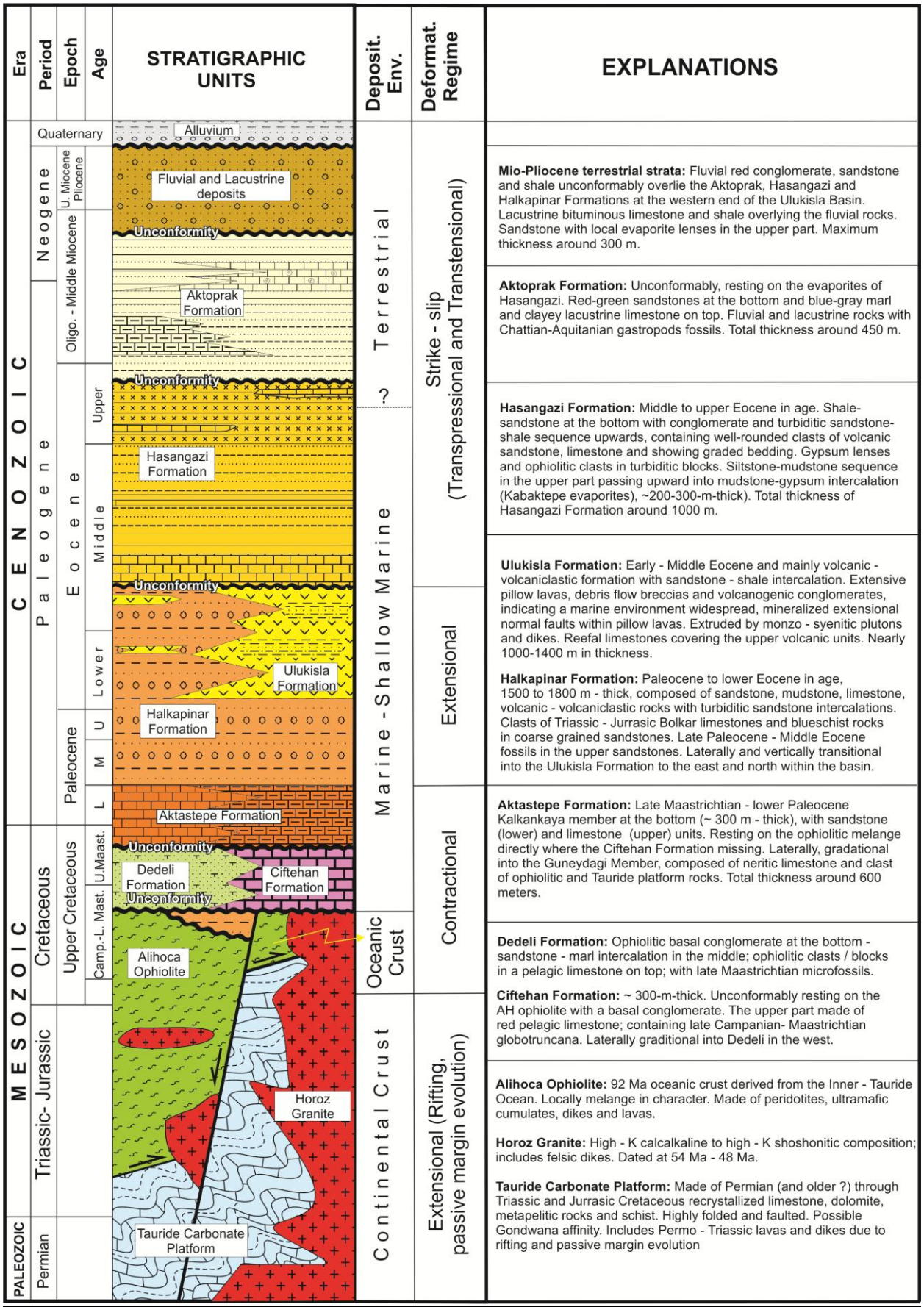
Era
Period
Epoch
Age
STRATIGRAPHIC UNITS
Deposit. Env.
Deformat. Regime
EXPLANATIONS
CENOZOIC
MESOZOIC
PALEOZOIC
Paleogene
Neogene
Quaternary
Cretaceous
Triassic- Jurassic
Permian
Eocene
Paleocene
Upper Cretaceous
U. Miocene Pliocene
Oligo. - Middle Miocene
Upper
Middle
Lower
U
M
L
U.Maast.
Camp.-L. Mast.
Alluvium
Fluvial and Lacustrine deposits
Unconformity
Aktoprak Formation
Unconformity
Hasangazi Formation
Unconformity
Ulukisla Formation
Halkapinar Formation
Aktastepe Formation
Unconformity
Dedeli Formation
Ciftehan Formation
Unconformity
Alihoca Ophiolite
Horoz Granite
Tauride Carbonate Platform
Terrestrial
?
Marine - Shallow Marine
Oceanic Crust
Continental Crust
Strike - slip (Transpressional and Transtensional)
Extensional
Contractional
Extensional (Rifting, passive margin evolution)
Mio-Pliocene terrestrial strata: Fluvial red conglomerate, sandstone and shale unconformably overlie the Aktoprak, Hasangazi and Halkapinar Formations at the western end of the Ulukisla Basin. Lacustrine bituminous limestone and shale overlying the fluvial rocks. Sandstone with local evaporite lenses in the upper part. Maximum thickness around 300 m.
Aktoprak Formation: Unconformably, resting on the evaporites of Hasangazi. Red-green sandstones at the bottom and blue-gray marl and clayey lacustrine limestone on top. Fluvial and lacustrine rocks with Chattian-Aquitanian gastropods fossils. Total thickness around 450 m.
Hasangazi Formation: Middle to upper Eocene in age. Shale-sandstone at the bottom with conglomerate and turbiditic sandstone-shale sequence upwards, containing well-rounded clasts of volcanic sandstone, limestone and showing graded bedding. Gypsum lenses and ophiolitic clasts in turbiditic blocks. Siltstone-mudstone sequence in the upper part passing upward into mudstone-gypsum intercalation (Kabaktepe evaporites), ~200-300-m-thick). Total thickness of Hasangazi Formation around 1000 m.
Ulukisla Formation: Early - Middle Eocene and mainly volcanic - volcaniclastic formation with sandstone - shale intercalation. Extensive pillow lavas, debris flow breccias and volcanogenic conglomerates, indicating a marine environment widespread, mineralized extensional normal faults within pillow lavas. Extruded by monzo - syenitic plutons and dikes. Reefal limestones covering the upper volcanic units. Nearly 1000-1400 m in thickness.
Halkapinar Formation: Paleocene to lower Eocene in age, 1500 to 1800 m - thick, composed of sandstone, mudstone, limestone, volcanic - volcaniclastic rocks with turbiditic sandstone intercalations. Clasts of Triassic - Jurrasic Bolkar limestones and blueschist rocks in coarse grained sandstones. Late Paleocene - Middle Eocene fossils in the upper sandstones. Laterally and vertically transitional into the Ulukisla Formation to the east and north within the basin.
Aktastepe Formation: Late Maastrichtian - lower Paleocene Kalkankaya member at the bottom (~ 300 m - thick), with sandstone (lower) and limestone (upper) units. Resting on the ophiolitic melange directly where the Ciftehan Formation missing. Laterally, gradational into the Guneydagi Member, composed of neritic limestone and clast of ophiolitic and Tauride platform rocks. Total thickness around 600 meters.
Dedeli Formation: Ophiolitic basal conglomerate at the bottom - sandstone - marl intercalation in the middle; ophiolitic clasts / blocks in a pelagic limestone on top; with late Maastrichtian microfossils.
Ciftehan Formation: ~ 300-m-thick. Unconformably resting on the AH ophiolite with a basal conglomerate. The upper part made of red pelagic limestone; containing late Campanian- Maastrichtian globotruncana. Laterally graditional into Dedeli in the west.
Alihoca Ophiolite: 92 Ma oceanic crust derived from the Inner - Tauride Ocean. Locally melange in character. Made of peridotites, ultramafic cumulates, dikes and lavas.
Horoz Granite: High - K calcalkaline to high - K shoshonitic composition; includes felsic dikes. Dated at 54 Ma - 48 Ma.
Tauride Carbonate Platform: Made of Permian (and older ?) through Triassic and Jurrasic Cretaceous recrystallized limestone, dolomite, metapelitic rocks and schist. Highly folded and faulted. Possible Gondwana affinity. Includes Permo - Triassic lavas and dikes due to rifting and passive margin evolution

Figure 6A-B

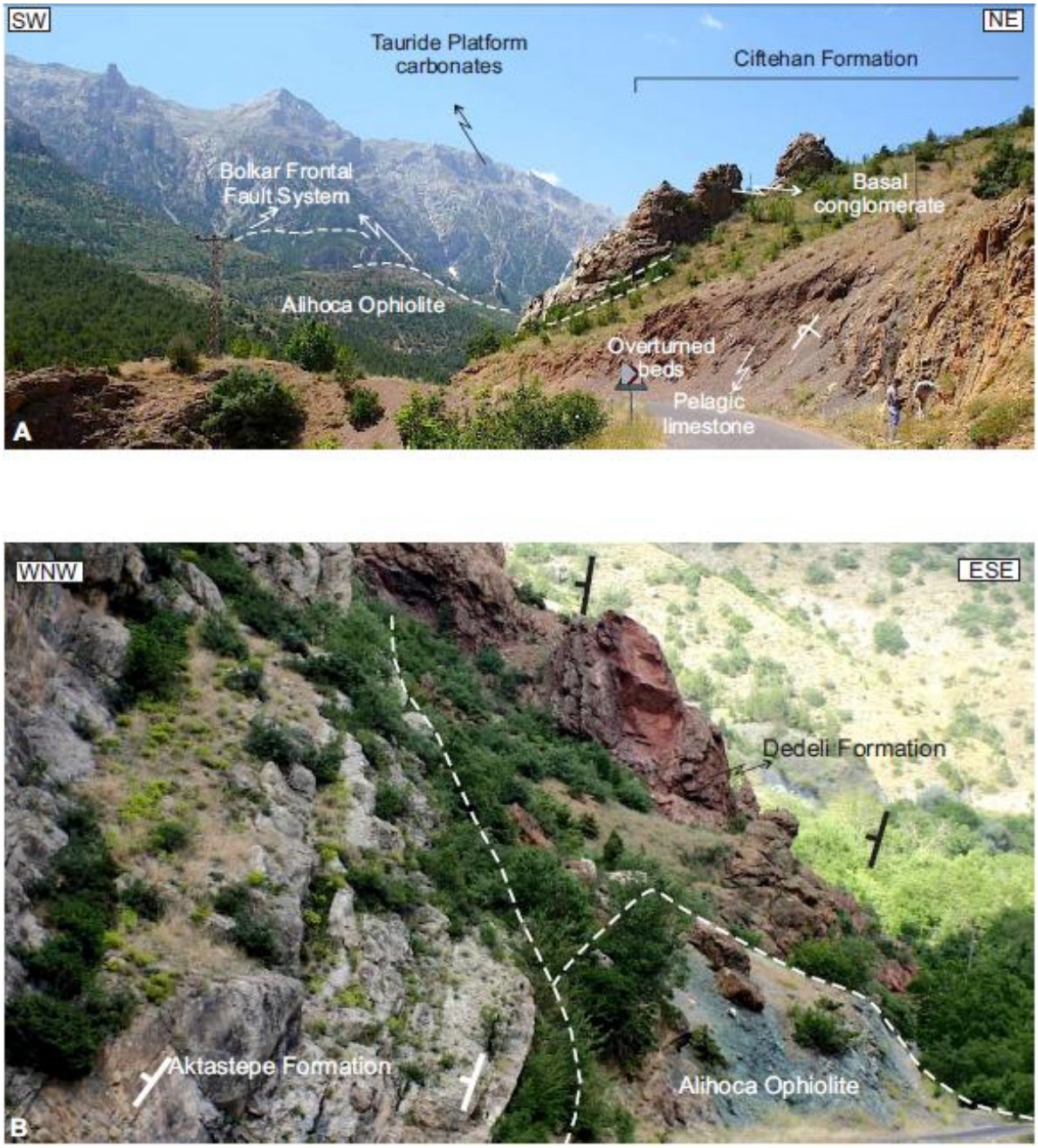
SW
NE
Tauride Platform carbonates
Ciftehan Formation
Bolkar Frontal Fault System
Basal conglomerate
Alihoca Ophiolite
Overturned beds
Pelagic limestone
A
WNW
ESE
Dedeli Formation
Aktastepe Formation
Alihoca Ophiolite
B

Figure 7A-B

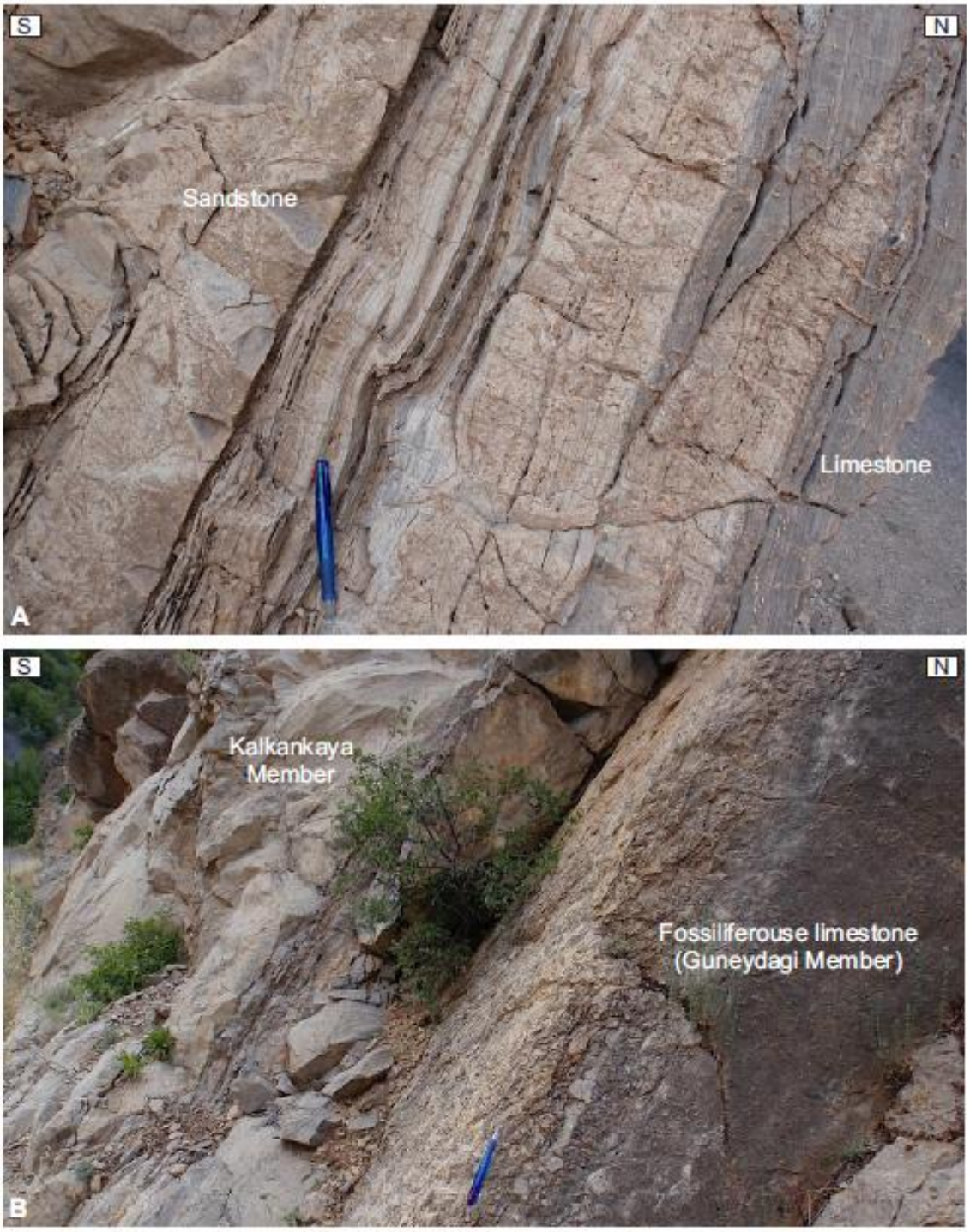
S
N
Sandstone
Limestone
A
S
N
Kalkankaya
Member
Fossiliferouse limestone
(Guneydagi Member)
B

Figure 8A-B


W
E
Ulukisla Formation
(volcanic rocks)
Hasangazi Formation
Sandstone - mudstone
intercalation
Halkapinar Formation
A
N
S
Tuffaceous rocks
Sandstone
Halkapinar Formation
B

Figure 9A-B


Serpentinite
Limestone
Chert
A
Recrystallized limestone
(Tauride)
Blueschist rocks
B

Figure 10

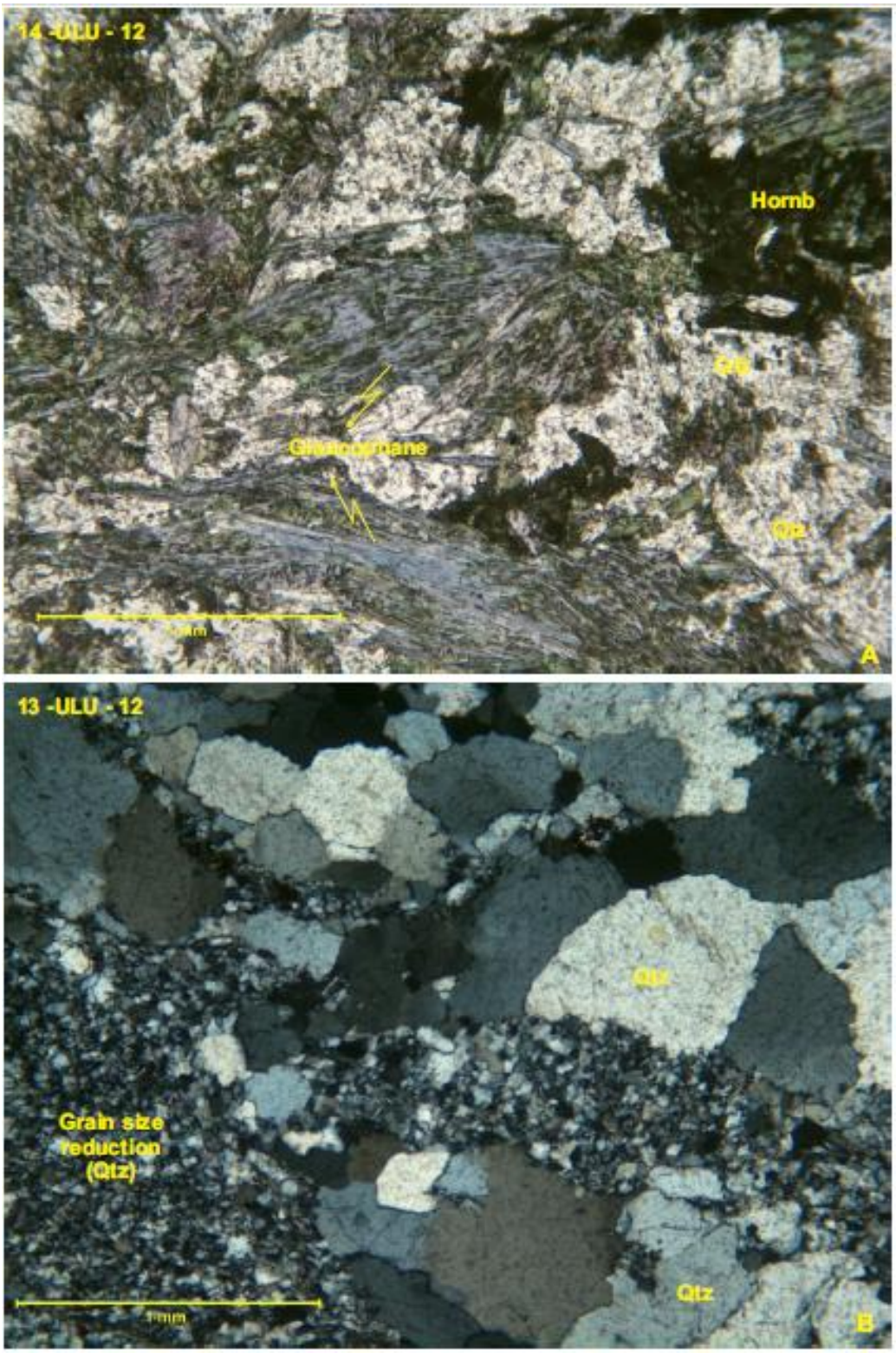
14 -ULU - 12
Hornb
Qtz
Glaucophane
Qtz
1mm
A
13 -ULU - 12
Qtz
Grain size
reduction
(Qtz)
Qtz
1mm
B

Figure 11

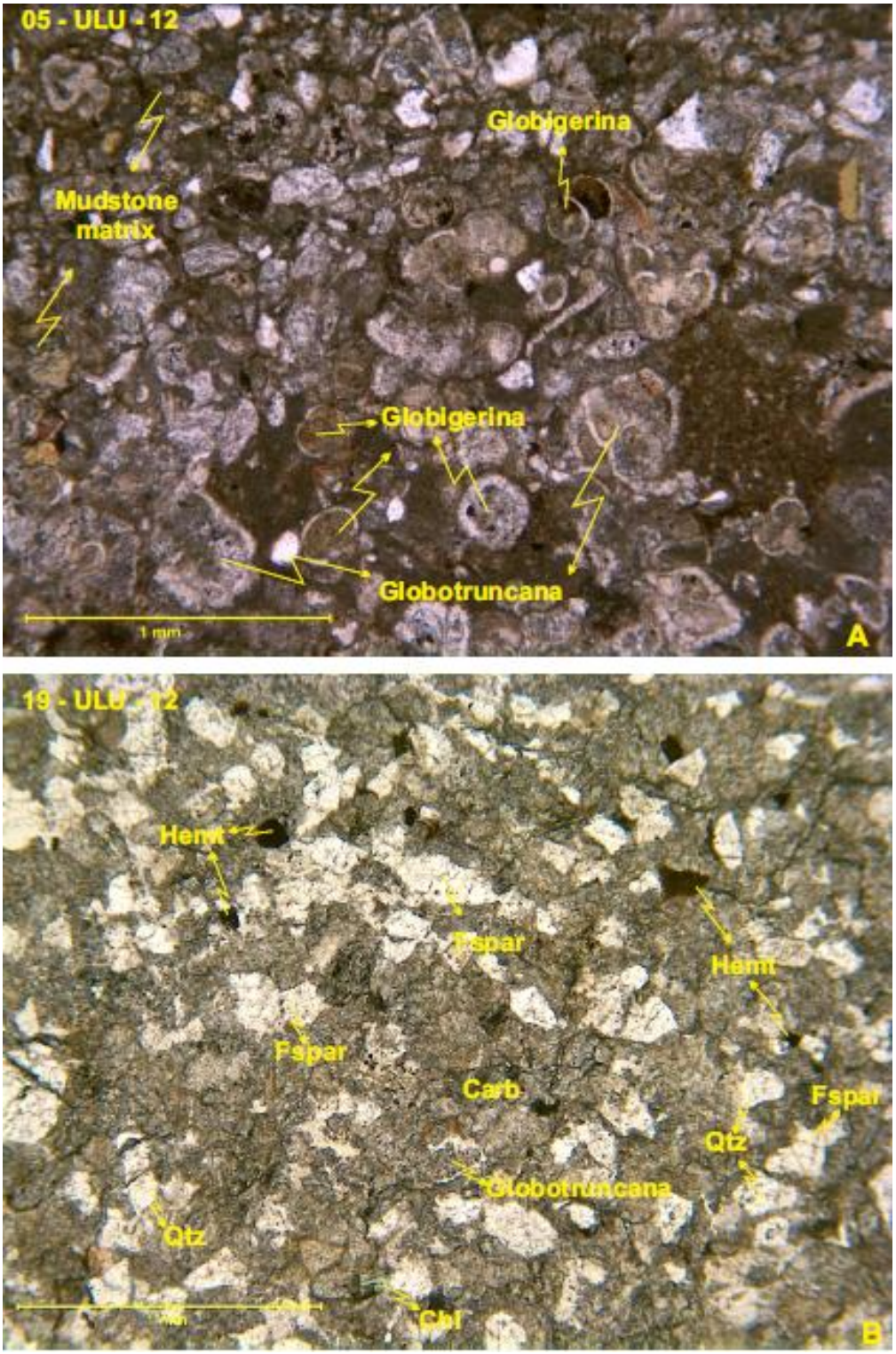
05 - ULU - 12
Globigerina
Mudstone matrix
Globigerina
Globotruncana
1 mm
A
19 - ULU - 12
Hemt
Fspar
Hemt
Fspar
Carb
Fspar
Qtz
Globotruncana
Qtz
Chl
B

Figure 12A-B

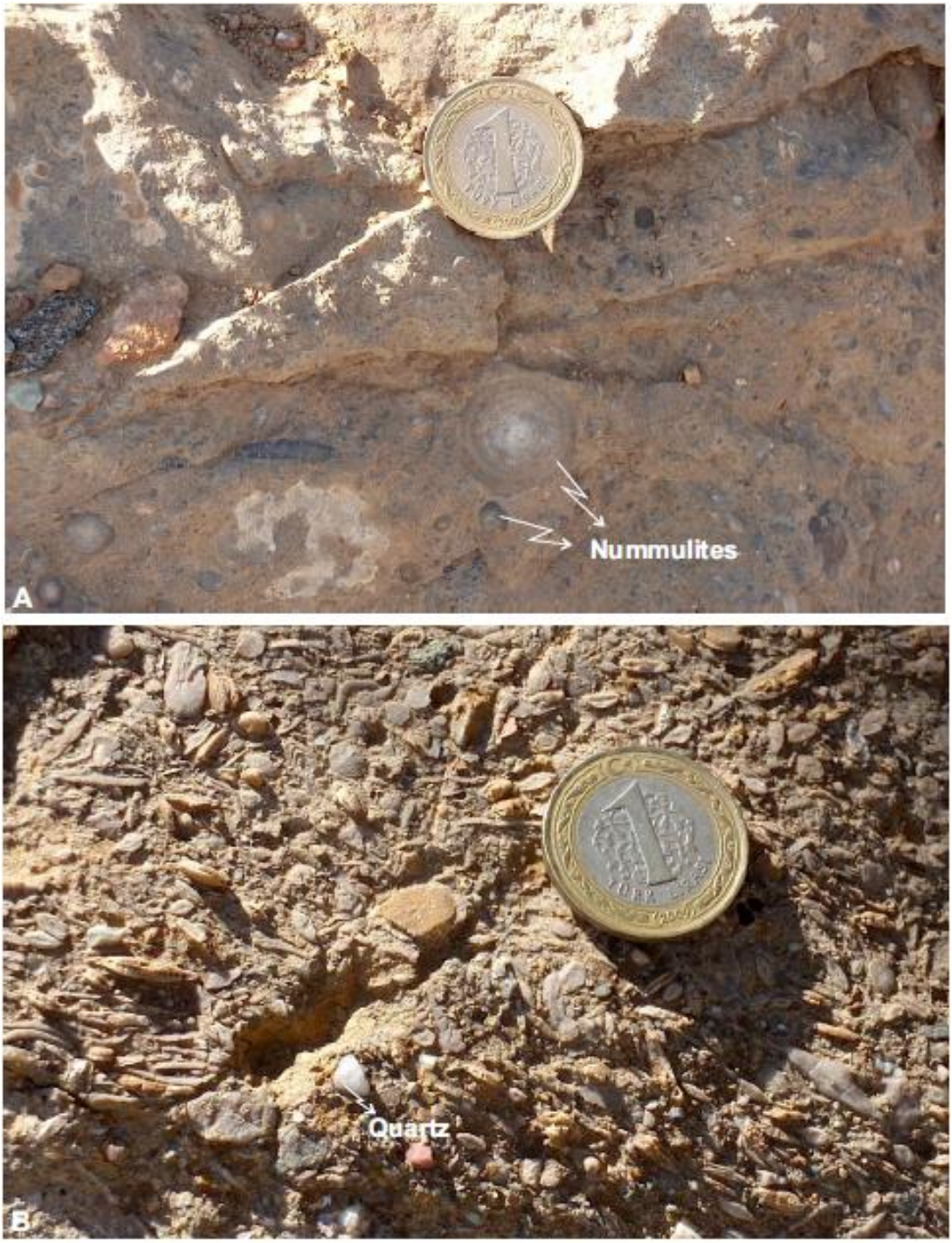

Figure 13

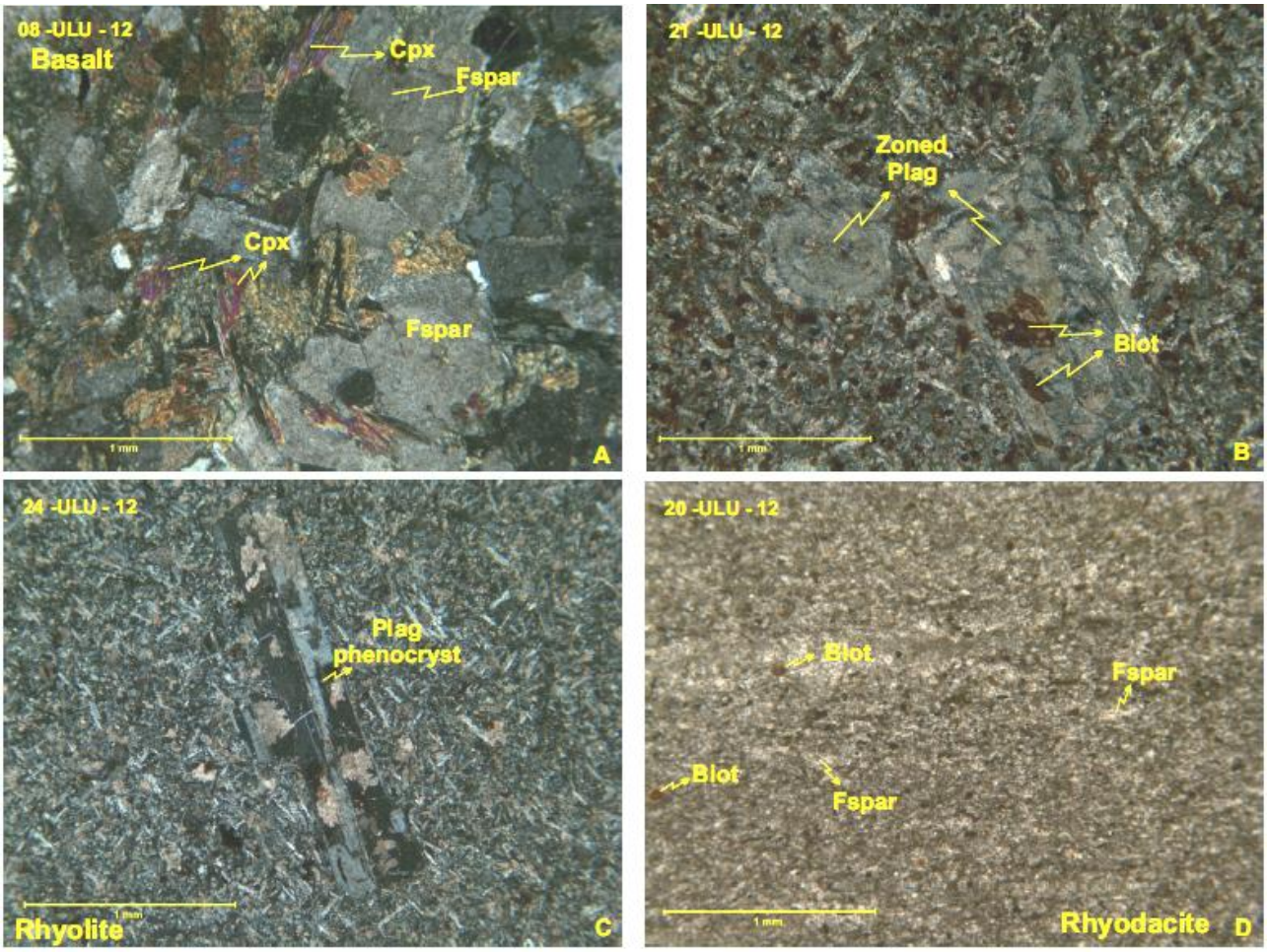
08 -ULU - 12
Basalt
Cpx
Fspar
Cpx
Fspar
1 mm
A
21 -ULU - 12
Zoned
Plag
Biot
1 mm
B
24 -ULU - 12
Plag
phenocryst
1 mm
Rhyolite
C
20 -ULU - 12
Biot
Fspar
Biot
Fspar
1 mm
Rhyodacite
D

Figure 14

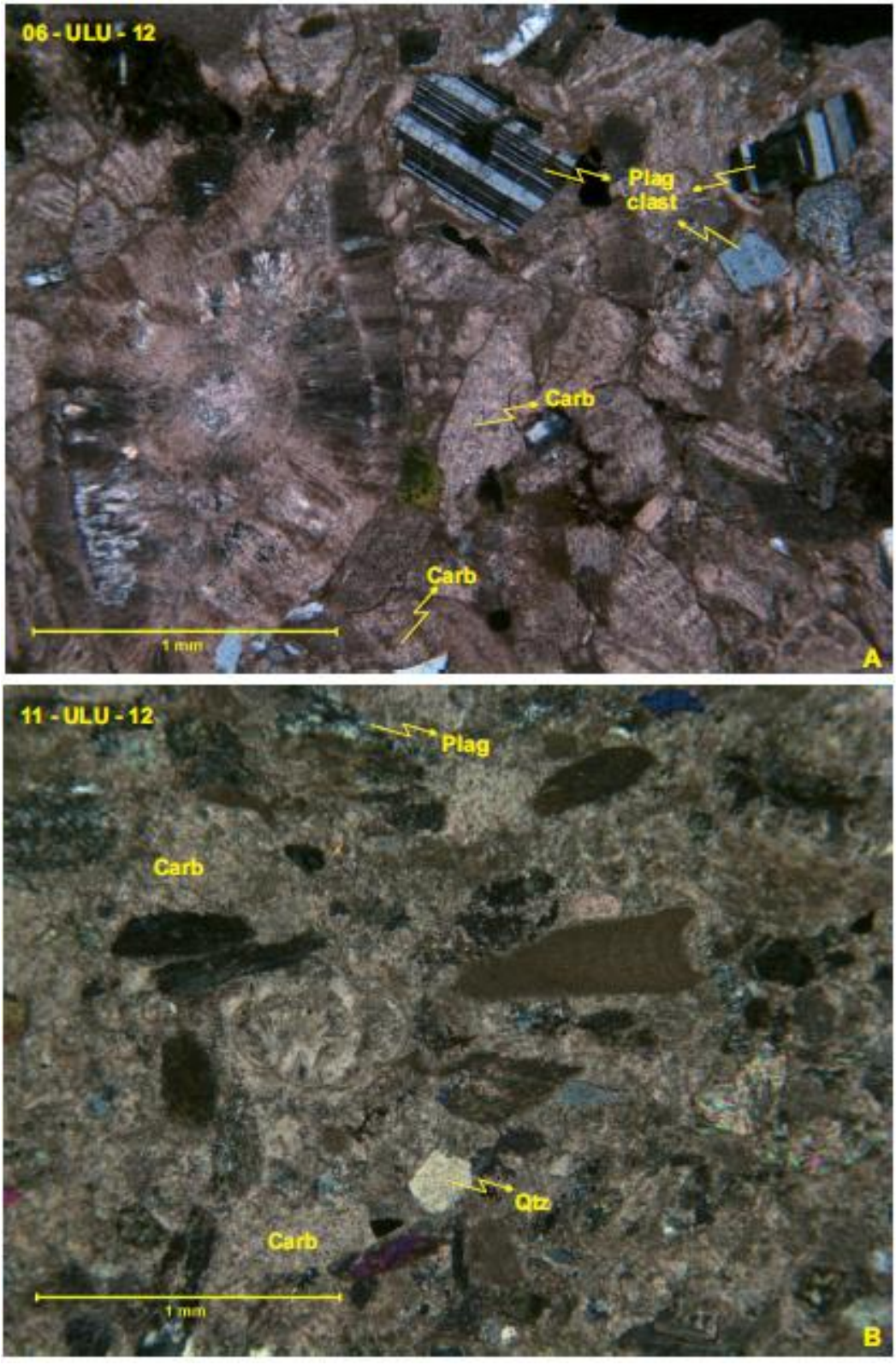
06 - ULU - 12
Plag clast
Carb
Carb
1 mm
A
11 - ULU - 12
Plag
Carb
Qtz
Carb
1 mm
B

Figure 15

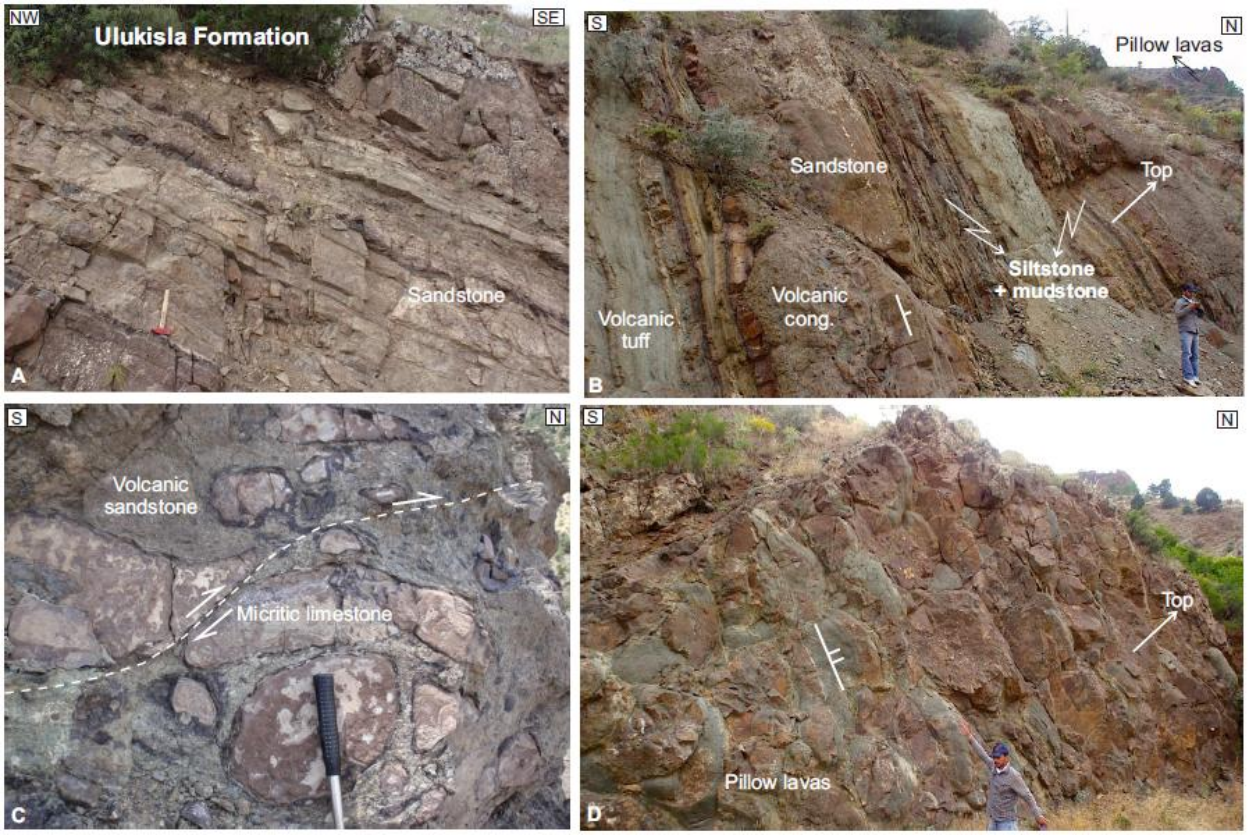
NW
Ulukisla Formation
SE
Sandstone
A
S
N
Pillow lavas
Sandstone
Top
Siltstone
+ mudstone
Volcanic
tuff
Volcanic
cong.
B
S
N
Volcanic
sandstone
Micritic limestone
C
S
N
Top
Pillow lavas
D

Figure 16

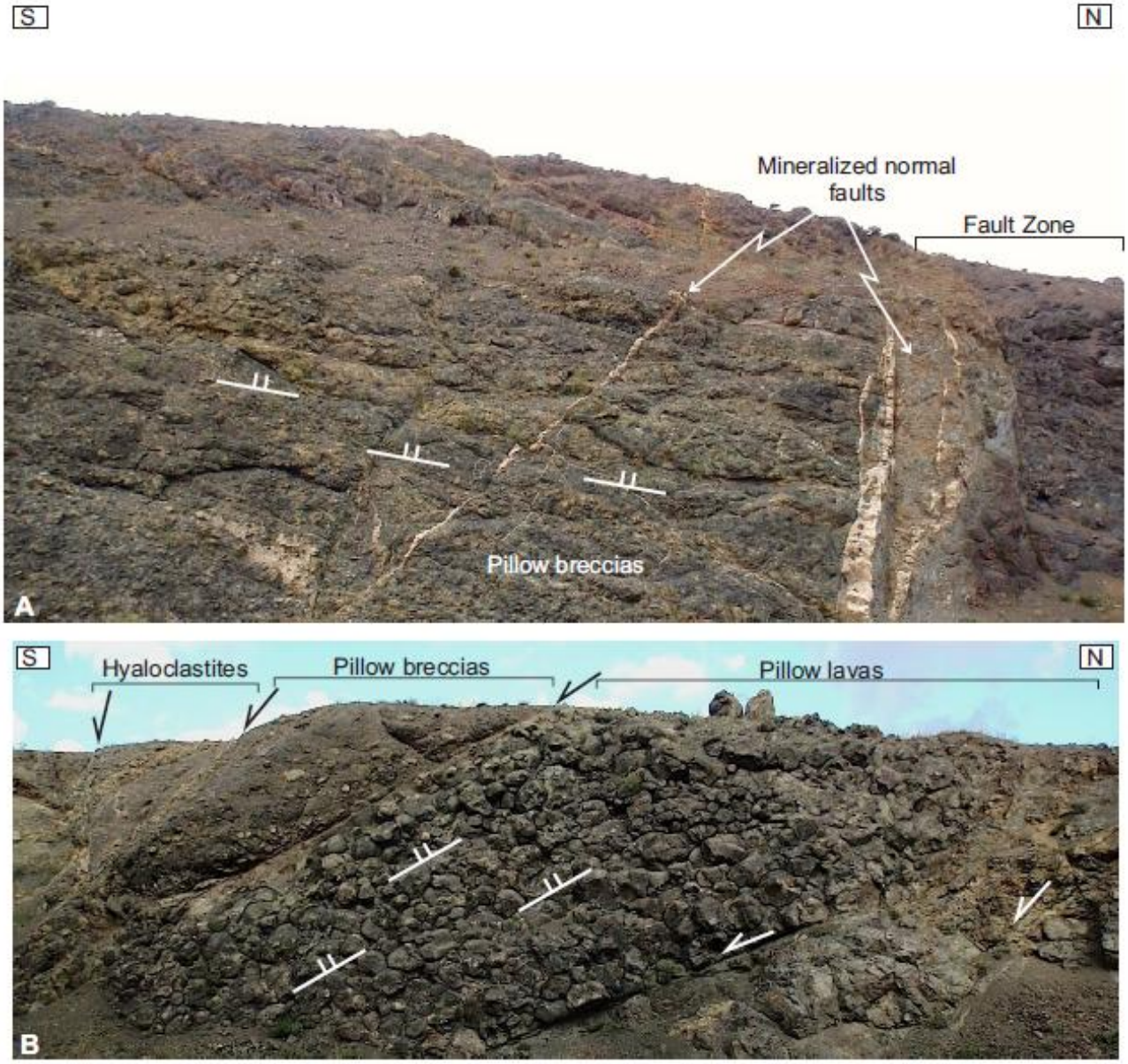
S
N
Mineralized normal faults
Fault Zone
Pillow breccias
A
S
Hyaloclastites
Pillow breccias
Pillow lavas
N
B

Figure 17

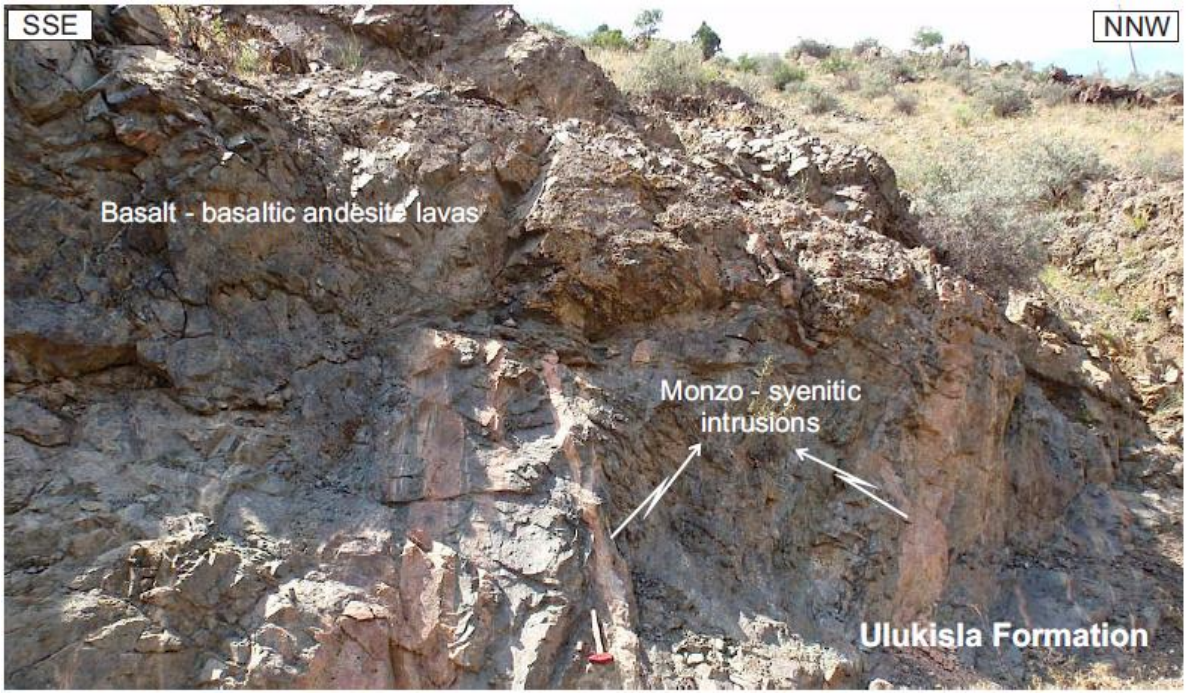

Figure 18A-B

Figure 19


NNW
SSE
Sandstone
Sandstone
Shale
Shale
Hasangazi Formation
A
NNW
SSE
Transtension Zone
Sandstone
Shale
Hasangazi Formation
B

Figure 20

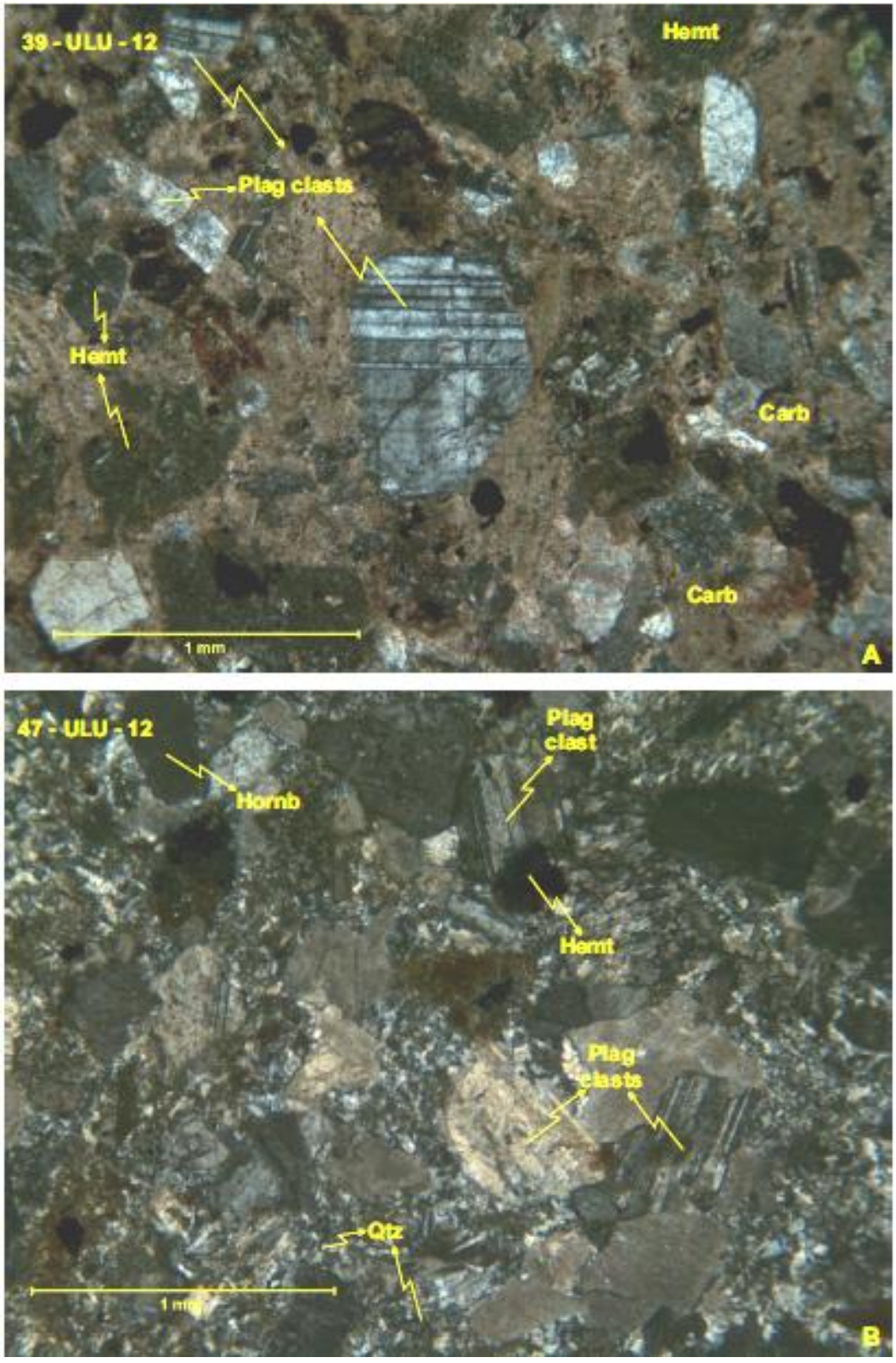
39 - ULU - 12
Hemt
Plag clasts
Hemt
Carb
Carb
1 mm
A
47 - ULU - 12
Plag clast
Hornb
Hemt
Plag clasts
Qtz
1 mm
B

Figure 21A-B

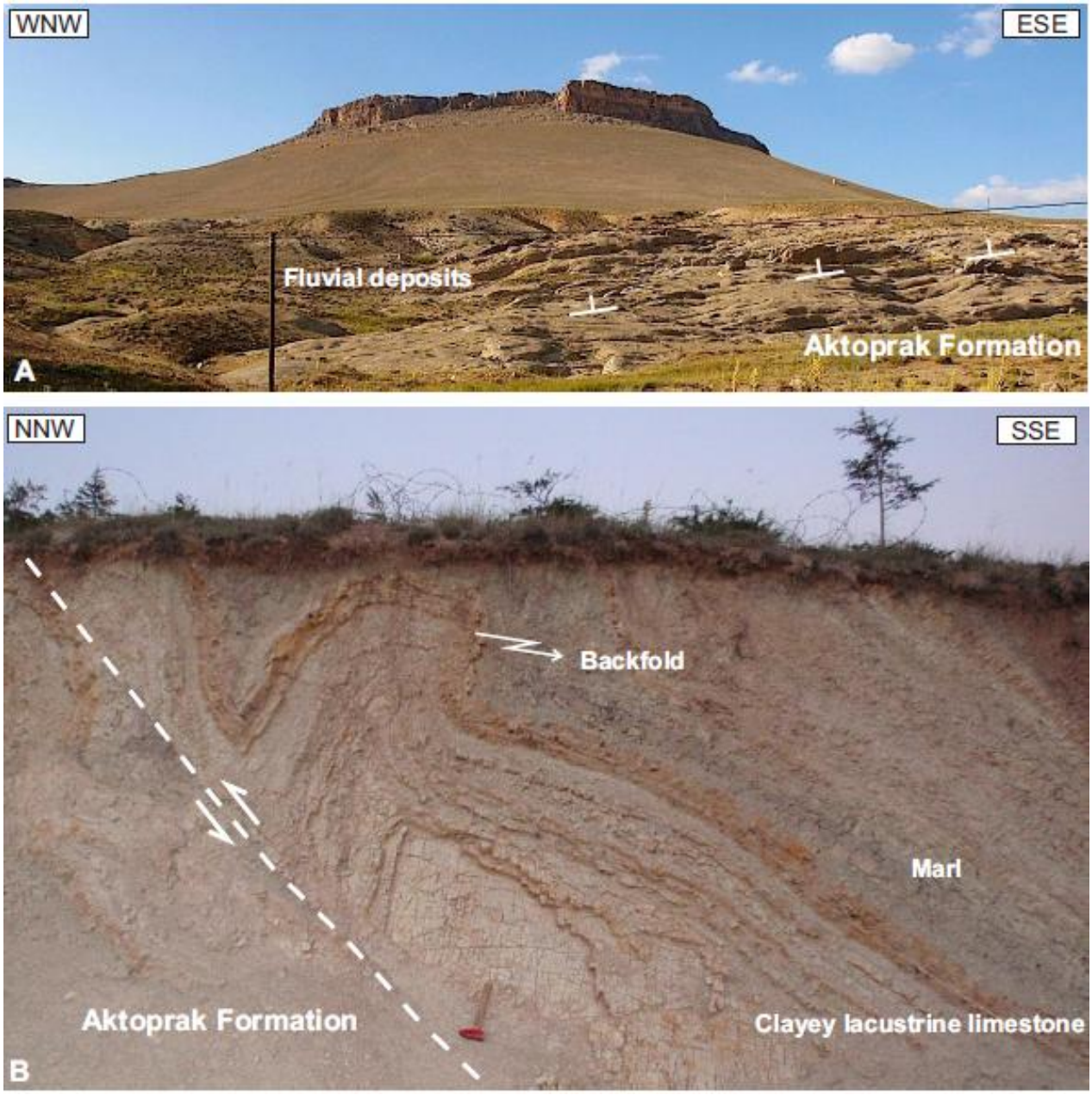
WNW
ESE
Fluvial deposits
Aktoprak Formation
A
NNW
SSE
Backfold
Marl
Aktoprak Formation
Clayey lacustrine limestone
B

Figure 22

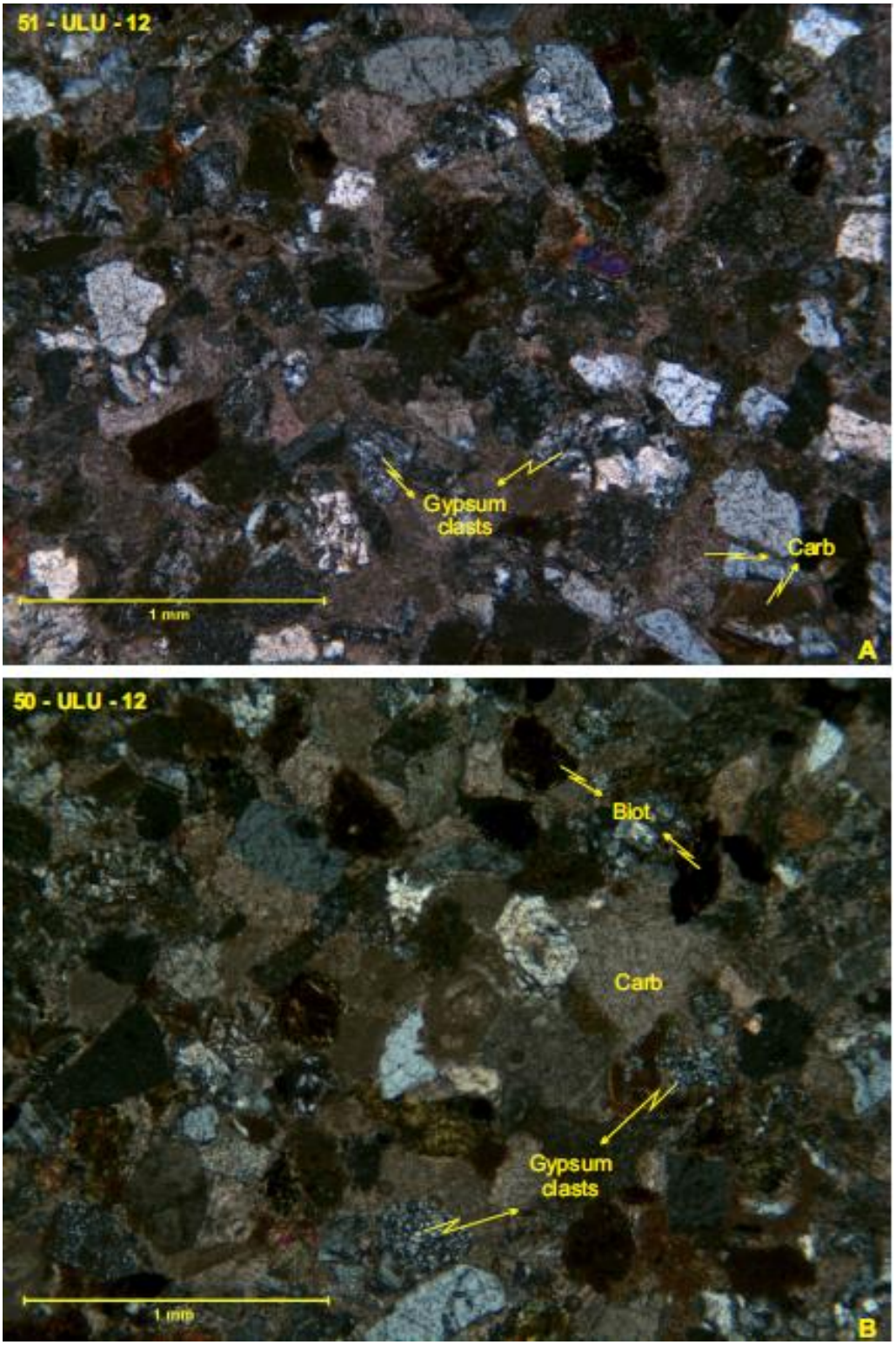
51 - ULU - 12
Gypsum clasts
Carb
1 mm
A
50 - ULU - 12
Biot
Carb
Gypsum clasts
1 mm
B

Figure 23

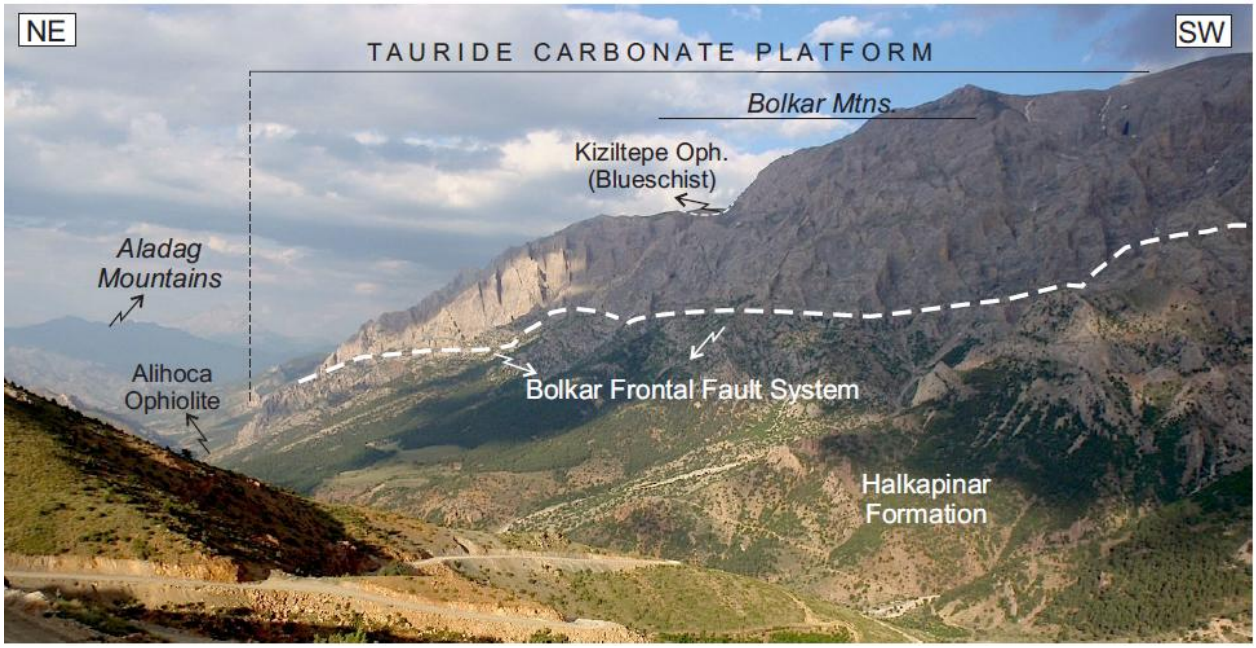
NE
SW
TAURIDE CARBONATE PLATFORM
Bolkar Mtns.
Kiziltepe Oph.
(Blueschist)
Aladag
Mountains
Alihoca
Ophiolite
Bolkar Frontal Fault System
Halkapinar
Formation

Figure 24

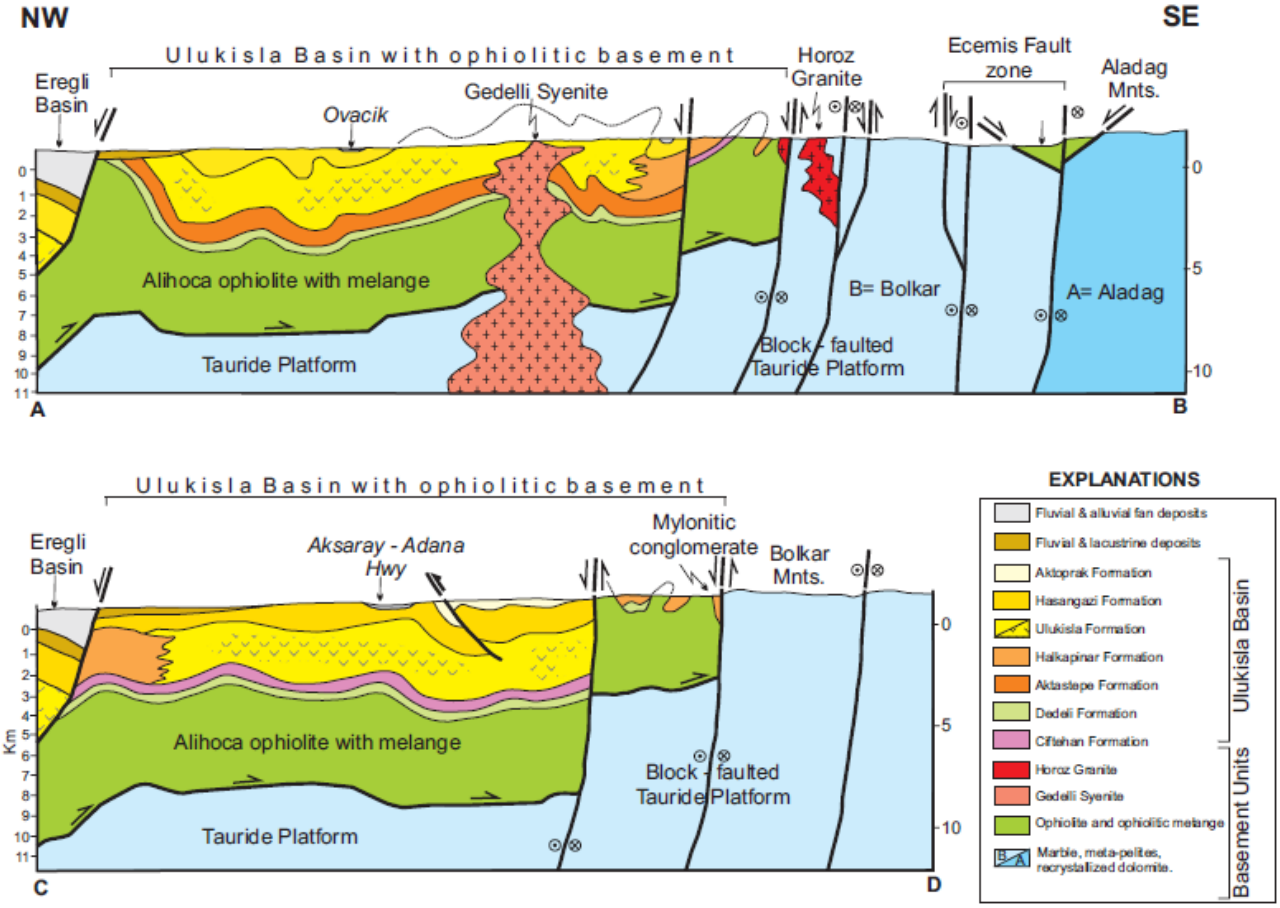
NW
SE
Ulukisla Basin with ophiolitic basement
Eregli Basin
Ovacik
Gedelli Syenite
Horoz Granite
Ecemis Fault zone
Aladag Mnts.
Alihoca ophiolite with melange
Tauride Platform
B= Bolkar
A= Aladag
Block - faulted Tauride Platform
A
B
Ulukisla Basin with ophiolitic basement
Eregli Basin
Aksaray - Adana Hwy
Mylonitic conglomerate
Bolkar Mnts.
Km
Alihoca ophiolite with melange
Tauride Platform
Block - faulted Tauride Platform
C
D
EXPLANATIONS
Fluvial & alluvial fan deposits
Fluvial & lacustrine deposits
Aktoprak Formation
Hasangazi Formation
Ulukisla Formation
Halkapinar Formation
Aktastepe Formation
Dedeli Formation
Ciftehan Formation
Horoz Granite
Gedelli Syenite
Ophiolite and ophiolitic melange
Marble, meta-pelites, recrystallized dolomite.
Ulukisla Basin
Basement Units

Figure 25

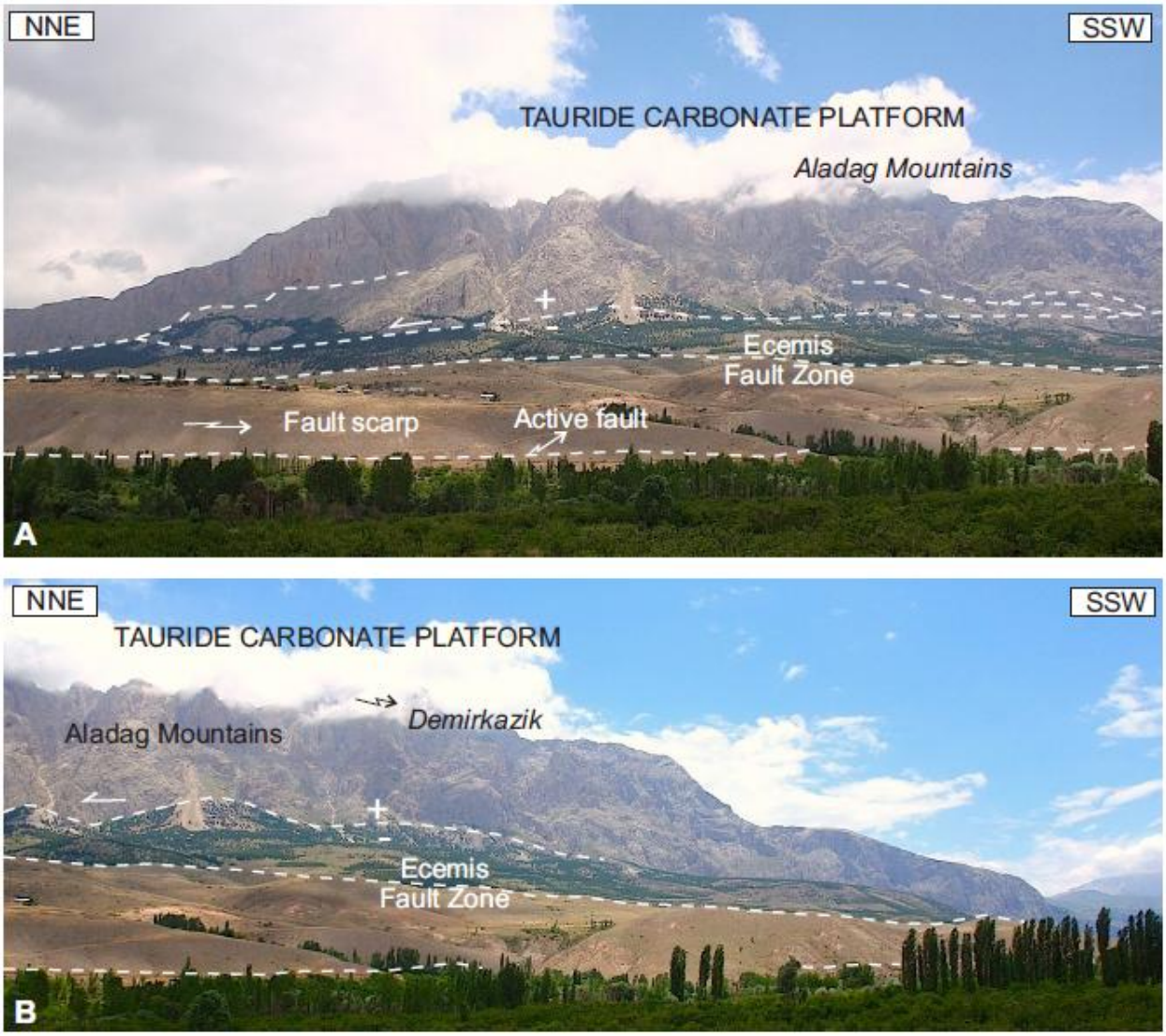
NNE
SSW
TAURIDE CARBONATE PLATFORM
Aladag Mountains
Ecemis
Fault Zone
Fault scarp
Active fault
A
NNE
SSW
TAURIDE CARBONATE PLATFORM
Aladag Mountains
Demirkazik
Ecemis
Fault Zone
B

Figure 26

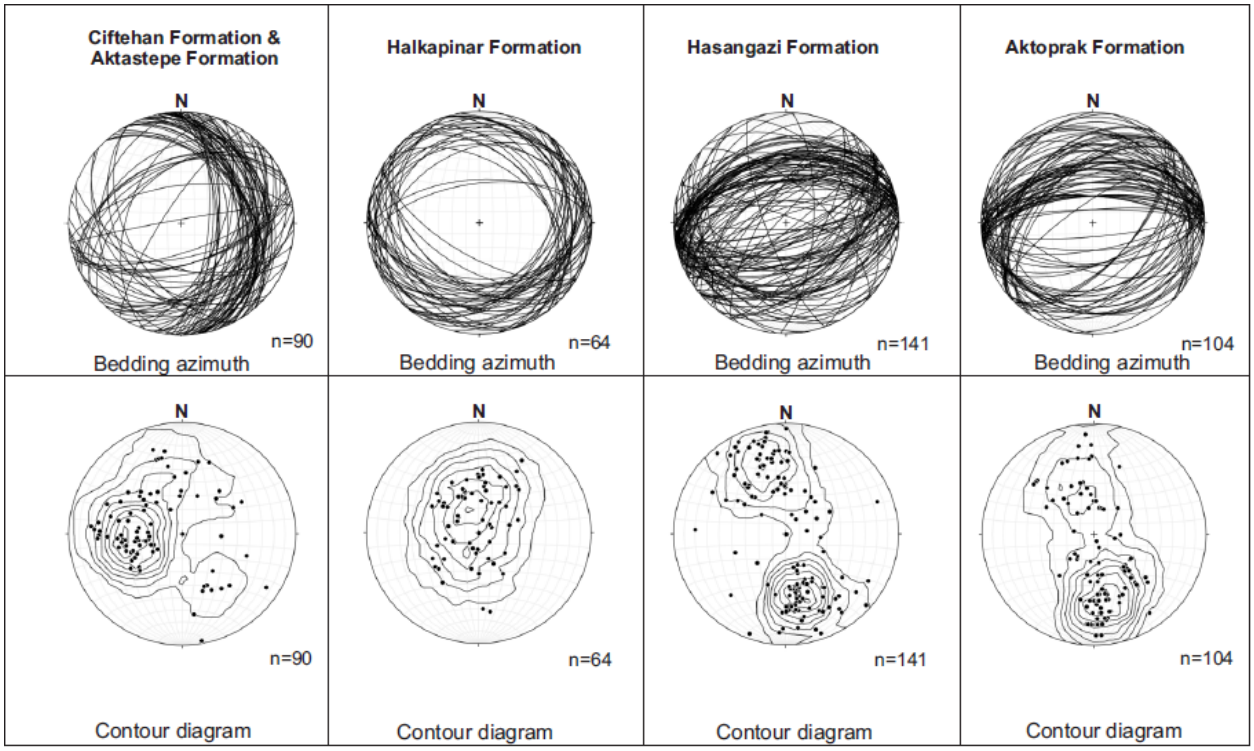

Figure 27

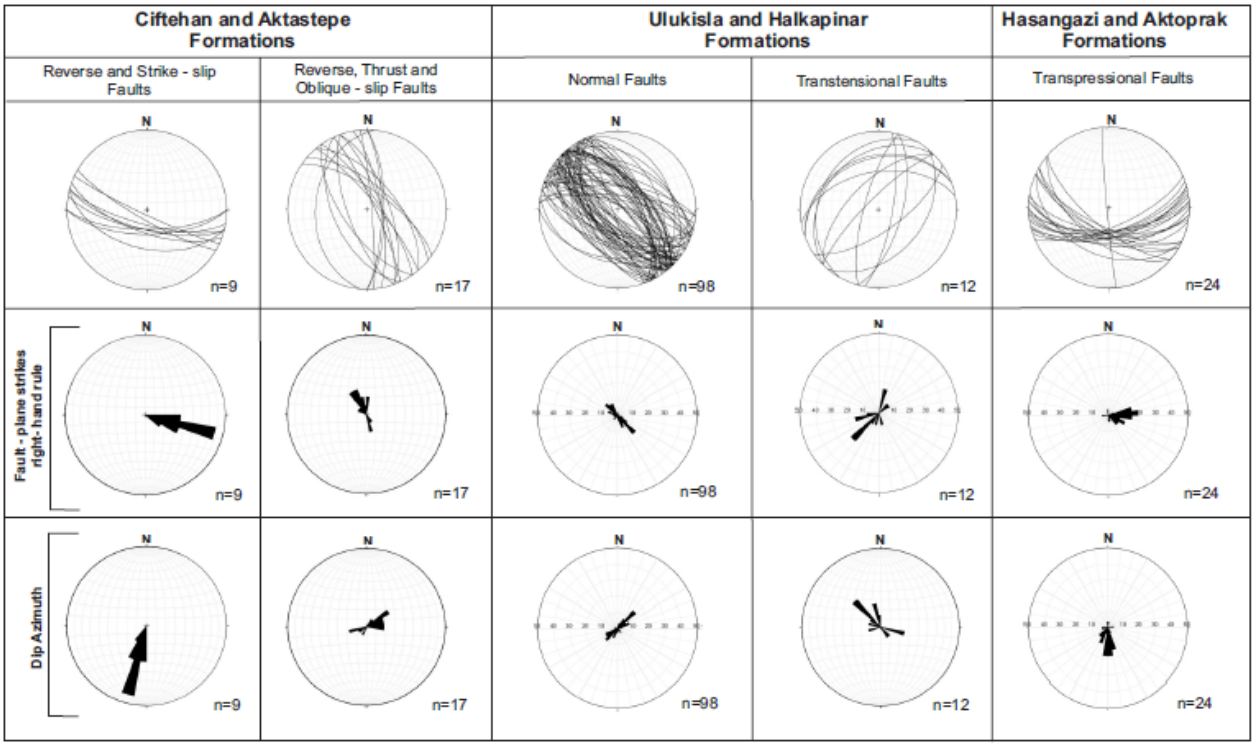

Figure 28A-B

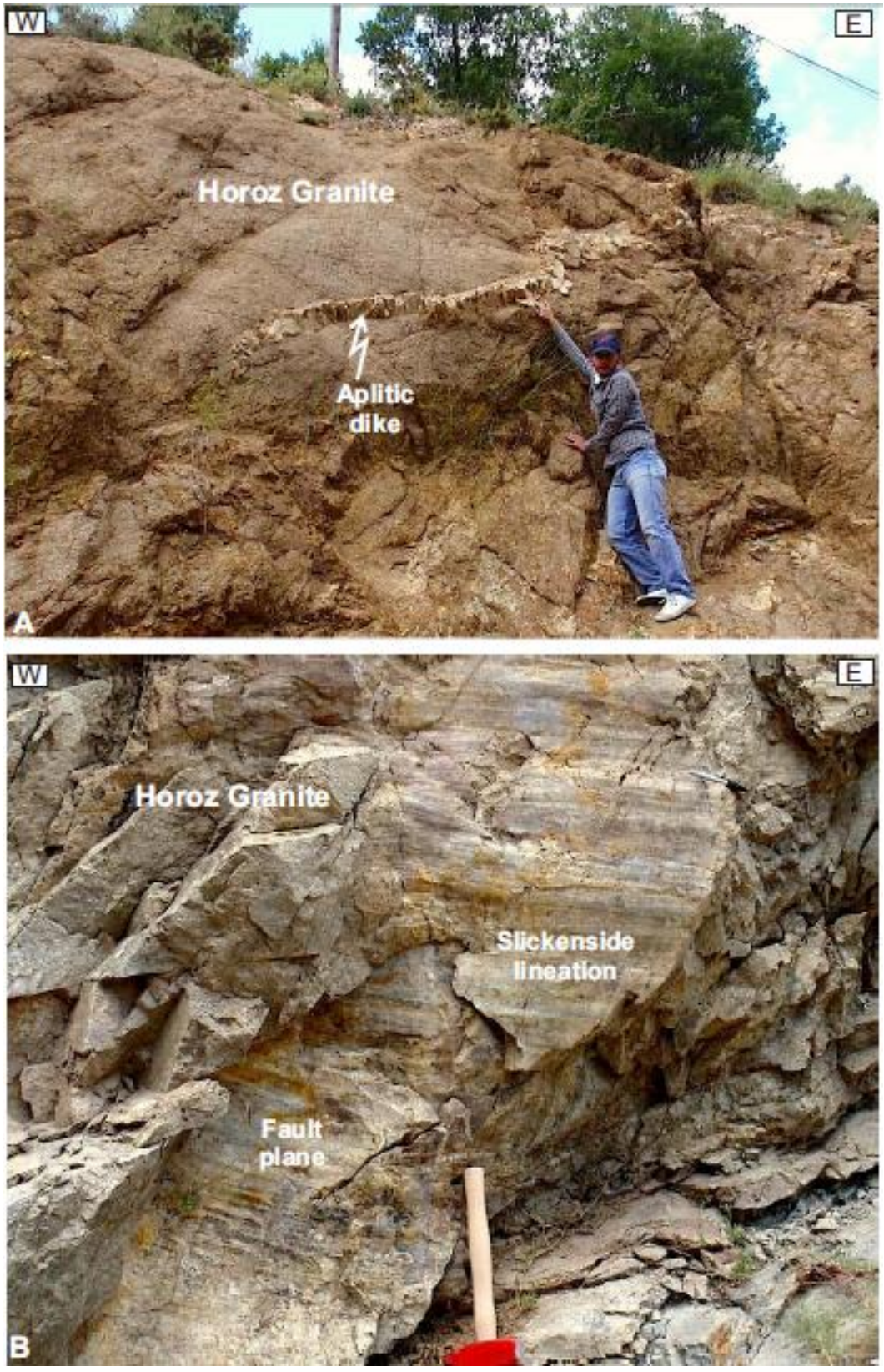
W
E
Horoz Granite
Aplitic dike
A
W
E
Horoz Granite
Slickenside lineation
Fault plane
B

Figure 29A-B


SW
Nigde Massif
metamorphic rocks
Uckapili
Village
NE
Uckapili Granite
A
SW
NE
Granitic
dike
Nigde Massif
metamorphic rocks
B

Figure 30A

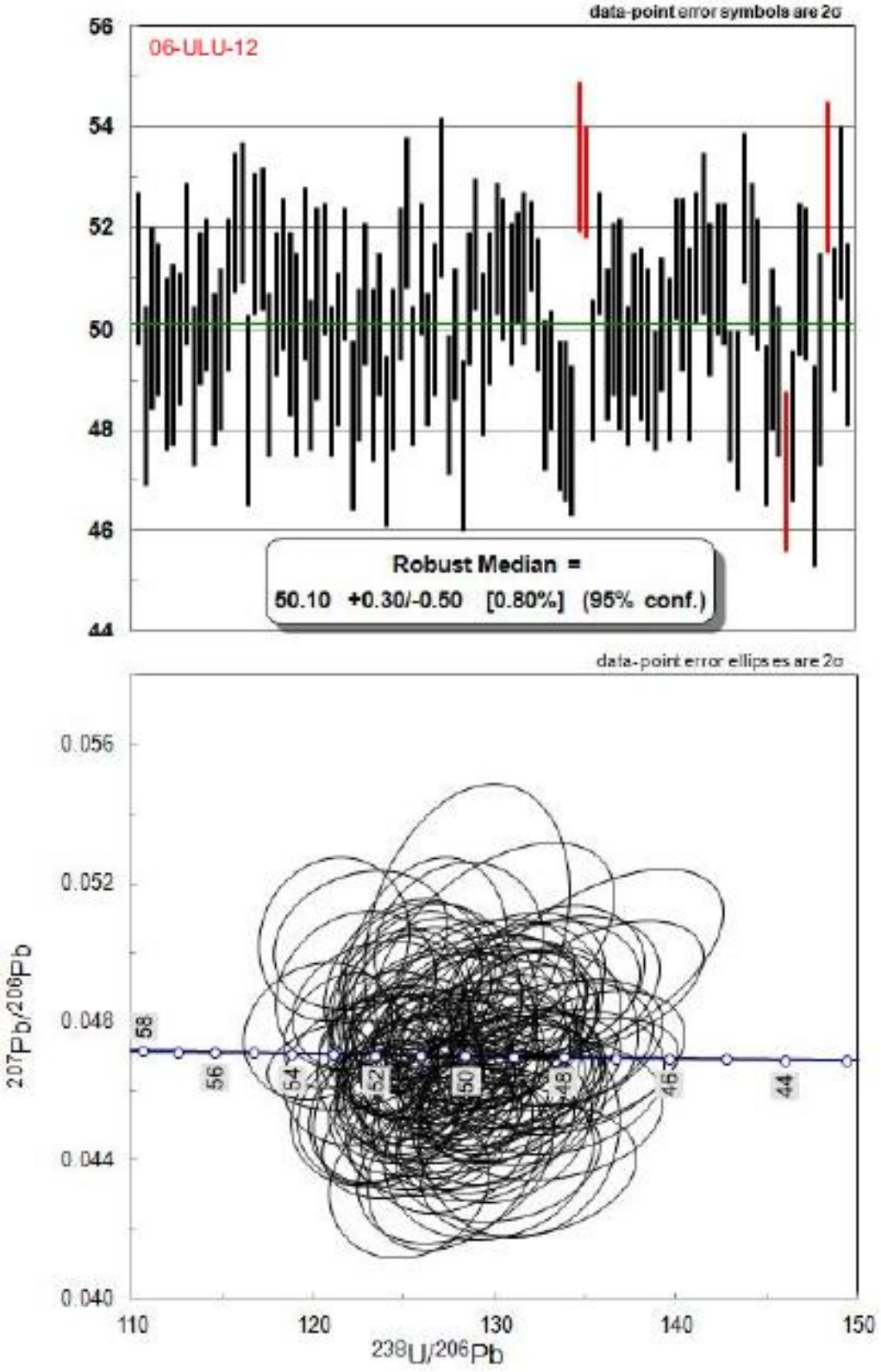
data-point error symbols are 2σ
06-ULU-12
56
54
52
50
48
46
44
Robust Median =
50.10 +0.30/-0.50 [0.80%] (95% conf.)
data-point error ellipses are 2σ
0.056
0.052
0.048
0.044
0.040
207Pb/206Pb
58
56
54
52
50
48
46
44
110
120
130
140
150
238U/206Pb

Figure 30B

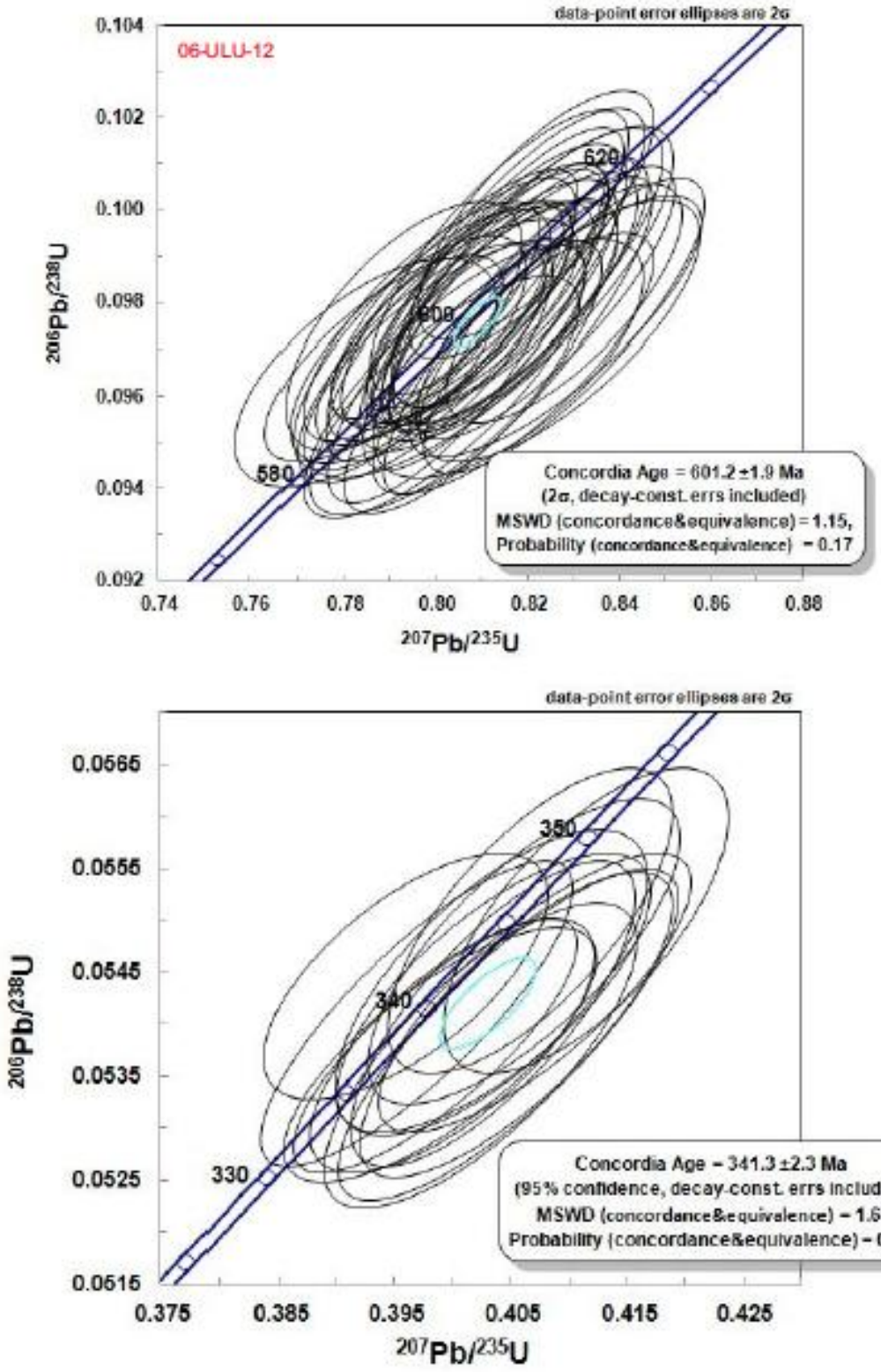
data-point error ellipses are 2σ
06-ULU-12
620
600
580
Concordia Age = 601.2 ±1.9 Ma
(2σ, decay-const. errs included)
MSWD (concordance&equivalence) = 1.15,
Probability (concordance&equivalence) = 0.17
$^{206}Pb/^{238}U$
$^{207}Pb/^{235}U$
data-point error ellipses are 2σ
350
340
330
Concordia Age = 341.3 ±2.3 Ma
(95% confidence, decay-const. errs included)
MSWD (concordance&equivalence) = 1.6,
Probability (concordance&equivalence) = 0.02
$^{206}Pb/^{238}U$
$^{207}Pb/^{235}U$

Figure 30C

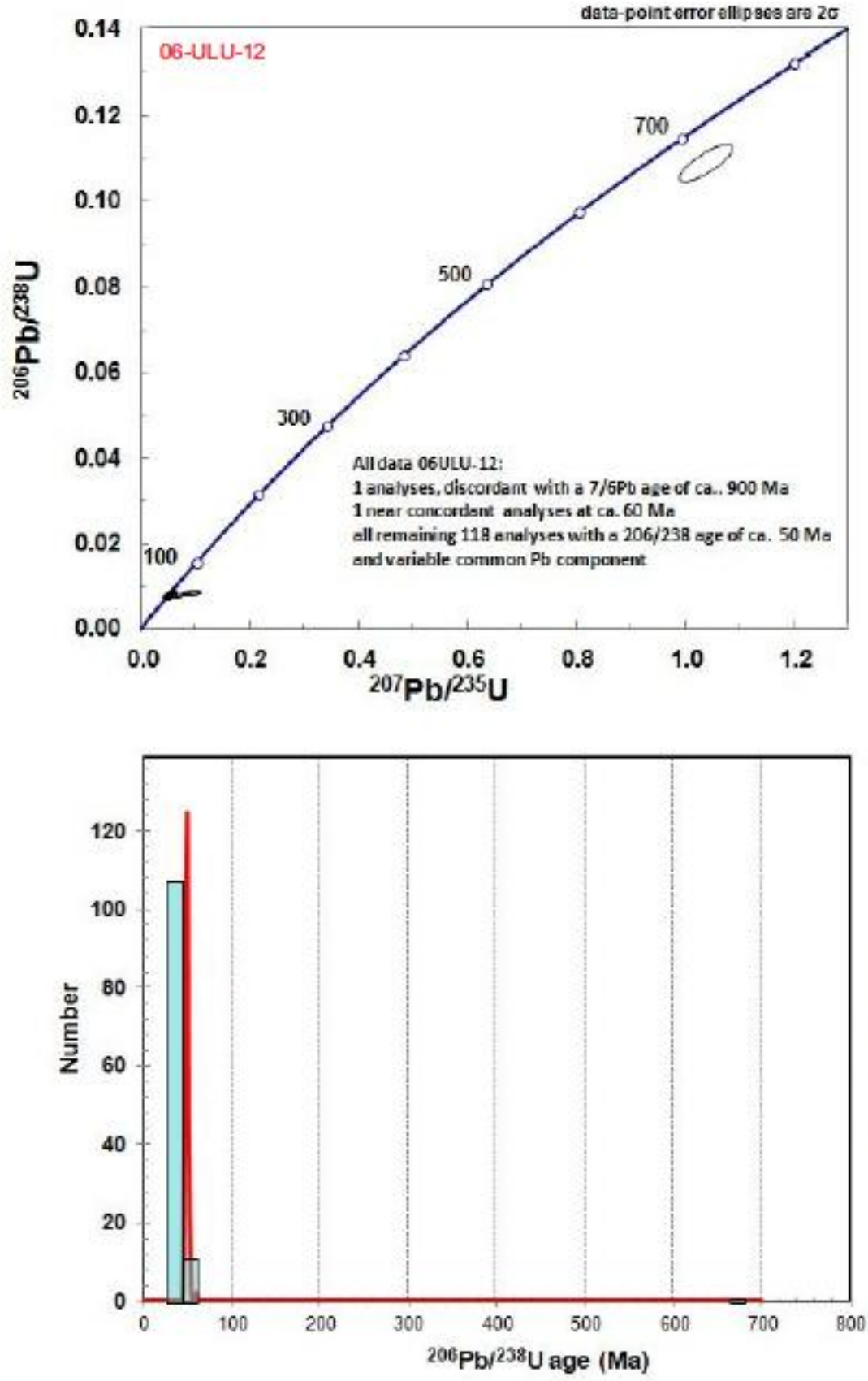
data-point error ellipses are 2σ
06-ULU-12
700
500
300
100
All data 06ULU-12:
1 analyses, discordant with a 7/6Pb age of ca.. 900 Ma
1 near concordant analyses at ca. 60 Ma
all remaining 118 analyses with a 206/238 age of ca. 50 Ma
and variable common Pb component
$^{206}Pb/^{238}U$
$^{207}Pb/^{235}U$
0.00
0.02
0.04
0.06
0.08
0.10
0.12
0.14
0.0
0.2
0.4
0.6
0.8
1.0
1.2
Number
Relative probability
$^{206}Pb/^{238}U$ age (Ma)
0
20
40
60
80
100
120
0
100
200
300
400
500
600
700
800

Figure 31A

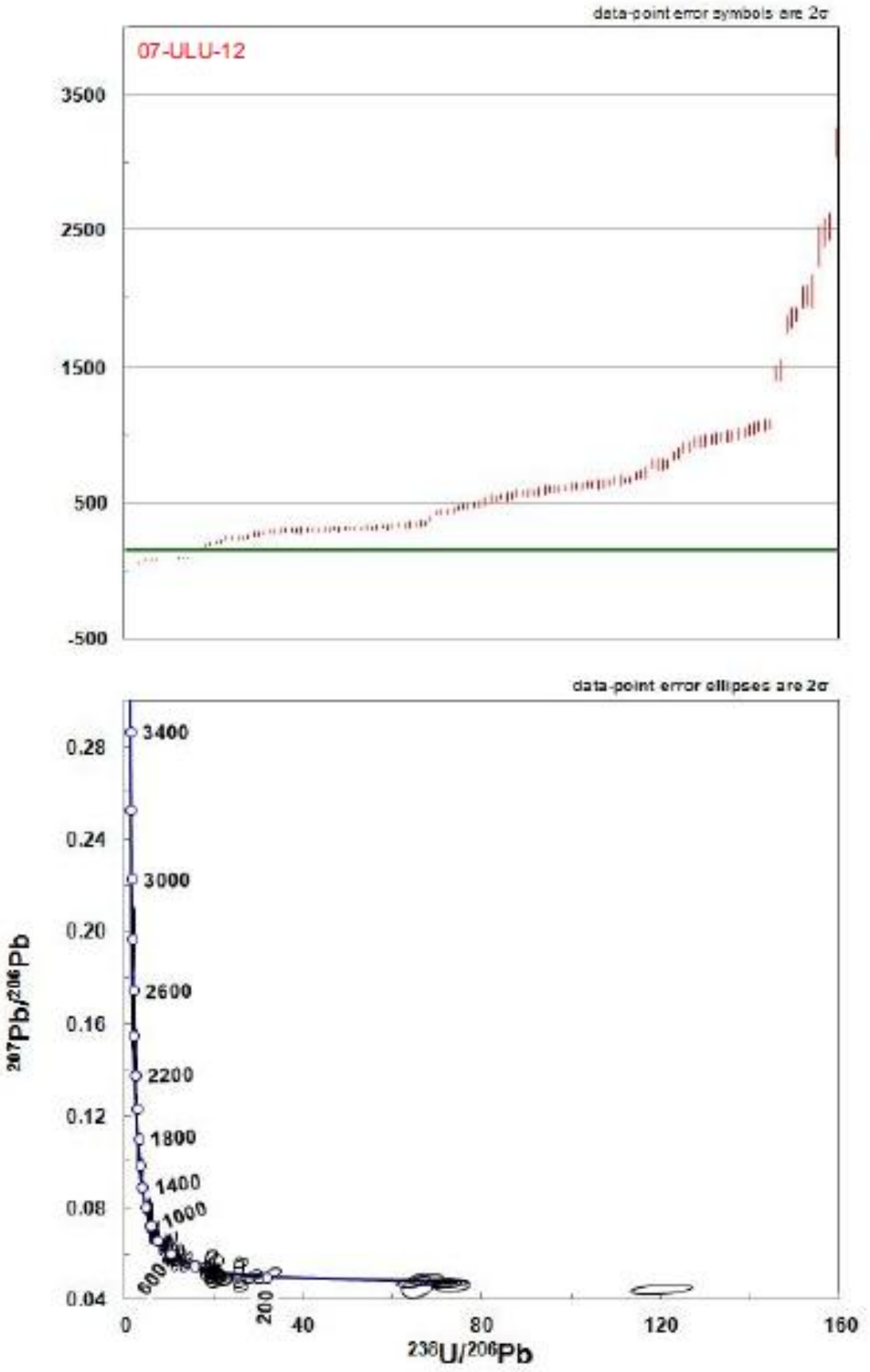
data-point error symbols are 2σ
07-ULU-12
3500
2500
1500
500
-500
data-point error ellipses are 2σ
0.28
0.24
0.20
0.16
0.12
0.08
0.04
$^{207}Pb/^{206}Pb$
3400
3000
2600
2200
1800
1400
1000
600
200
0
40
80
120
160
$^{238}U/^{206}Pb$

Figure 31B

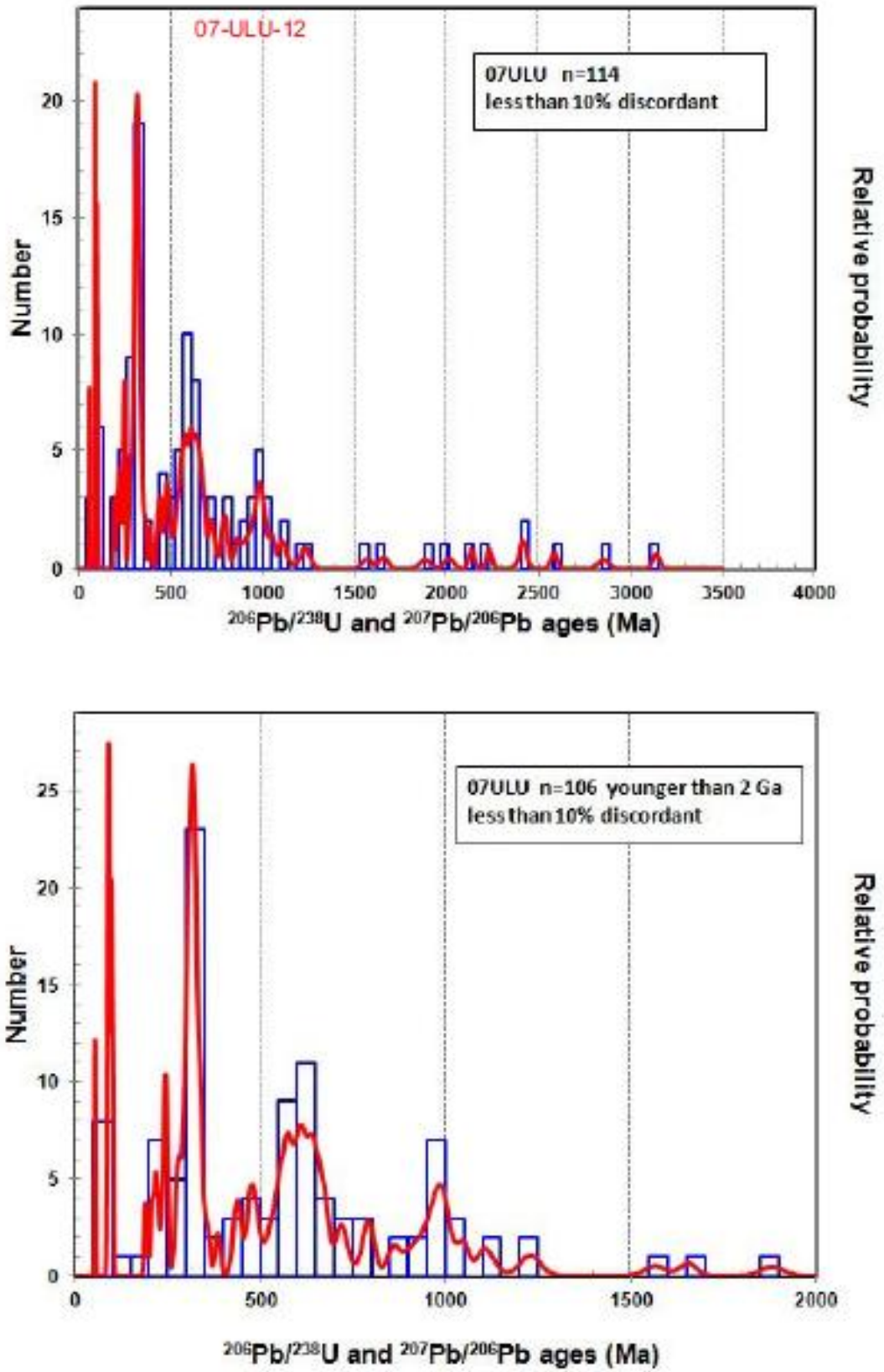
07-ULU-12
07ULU n=114
less than 10% discordant
Number
Relative probability
0
5
10
15
20
0
500
1000
1500
2000
2500
3000
3500
4000
206Pb/238U and 207Pb/206Pb ages (Ma)
07ULU n=106 younger than 2 Ga
less than 10% discordant
Number
Relative probability
0
5
10
15
20
25
0
500
1000
1500
2000
206Pb/238U and 207Pb/206Pb ages (Ma)

Figure 32

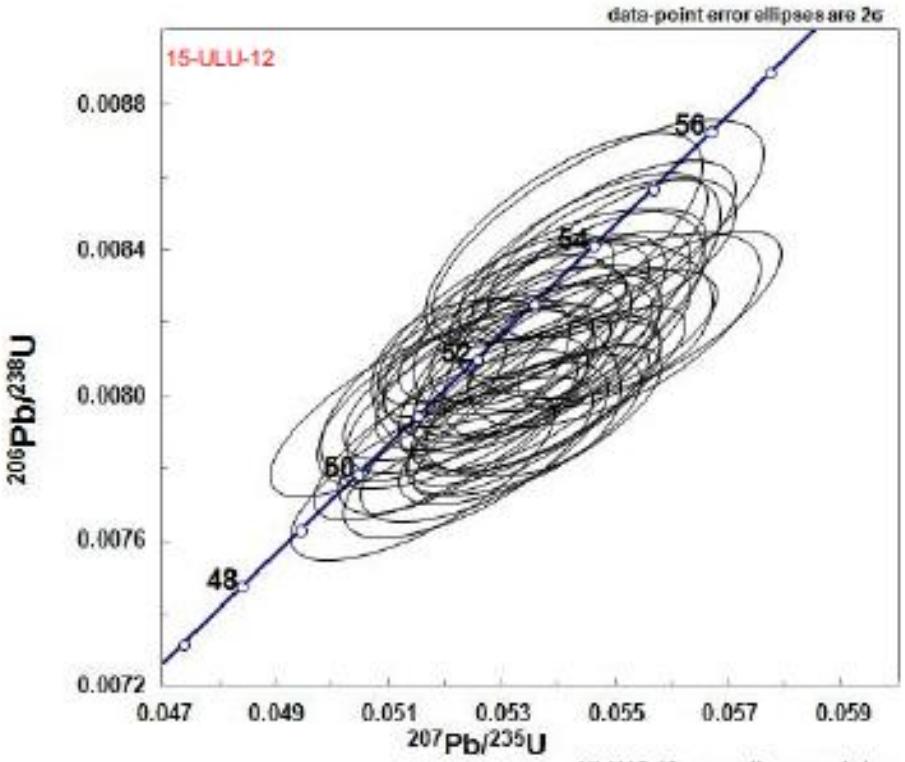

ULU15-12: overdispersed data, shown here in black used for best age estimate : 52+-0.5 Ma, robust median 206Pb/238U age.

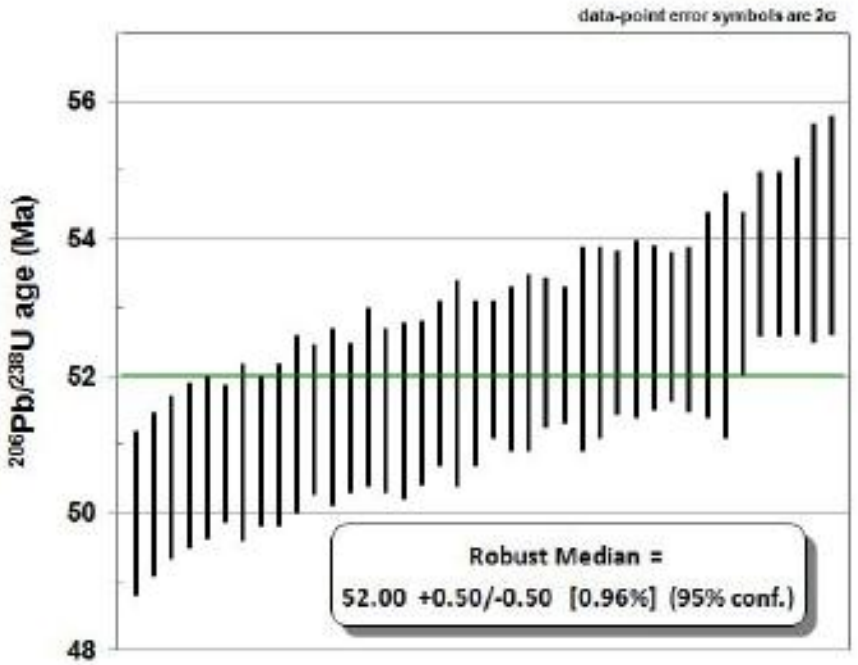

Figure 33A

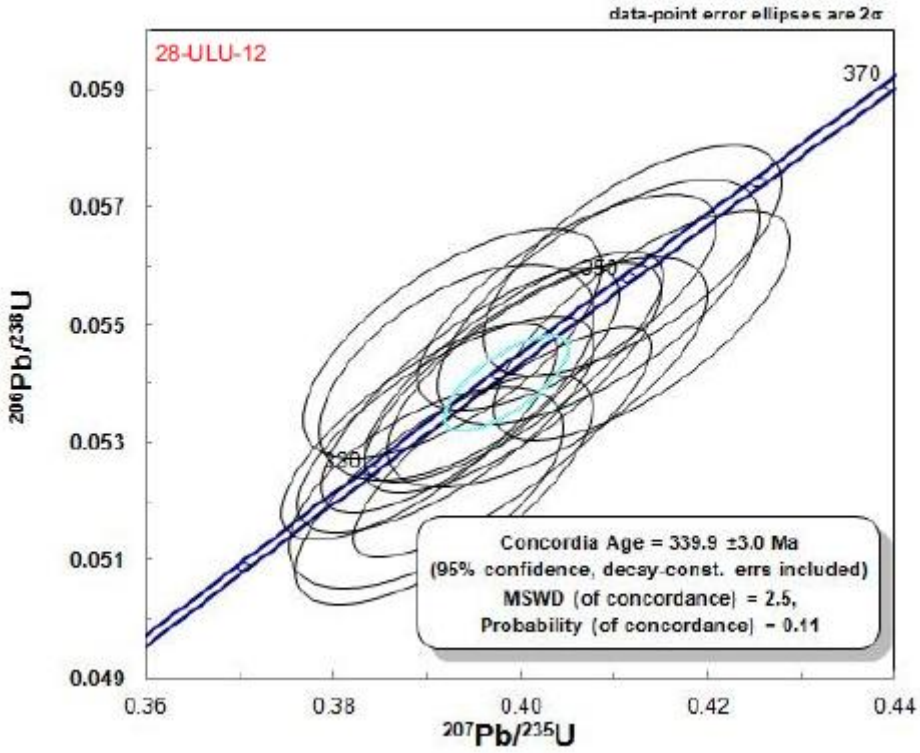
data-point error ellipses are 2σ
28-ULU-12
370
350
330
0.059
0.057
0.055
0.053
0.051
0.049
0.36
0.38
0.40
0.42
0.44
206Pb/238U
207Pb/235U
Concordia Age = 339.9 ±3.0 Ma
(95% confidence, decay-const. errs included)
MSWD (of concordance) = 2.5,
Probability (of concordance) = 0.11

Figure 33B

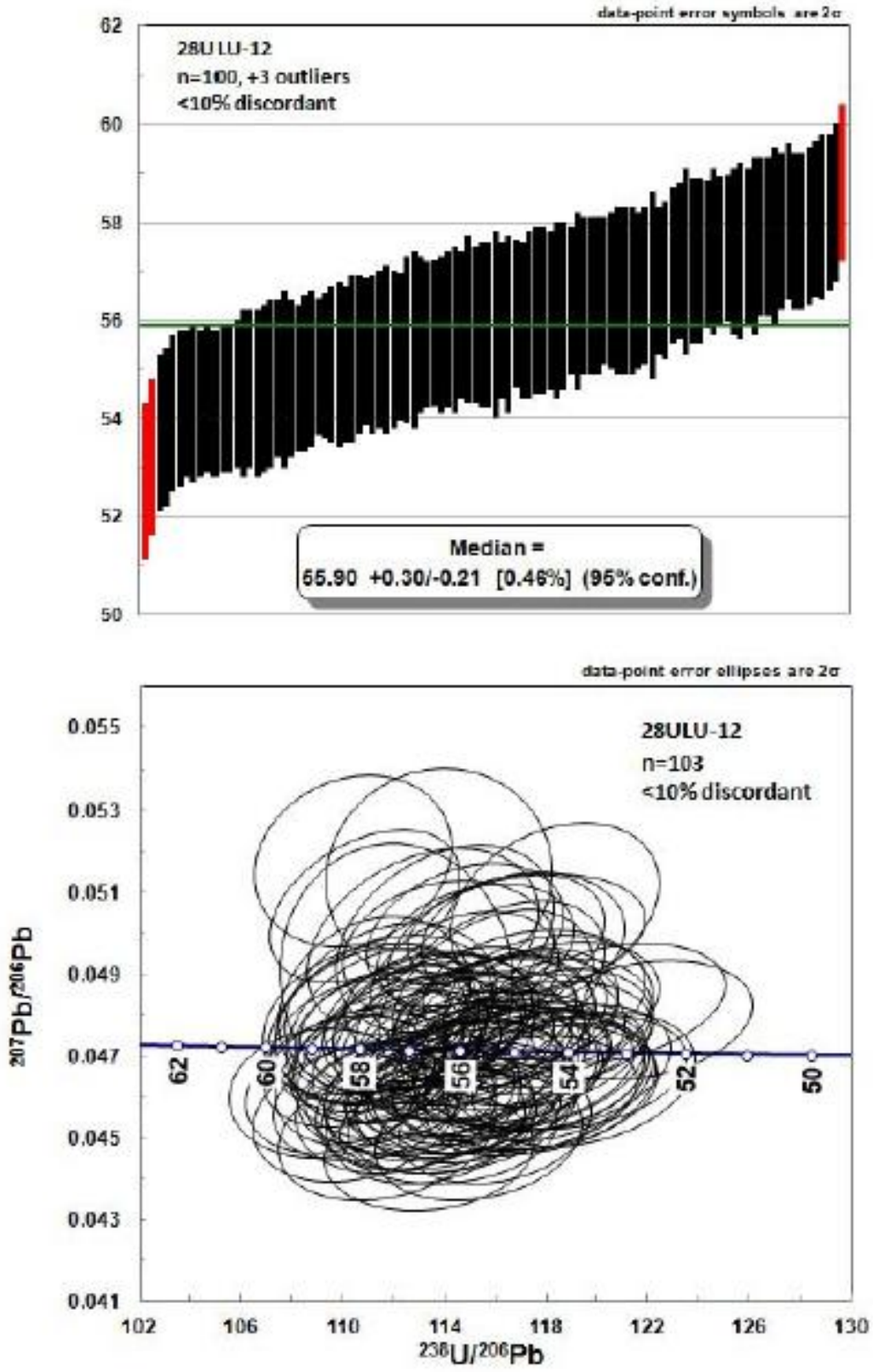
data-point error symbols are 2σ
28U LU-12
n=100, +3 outliers
<10% discordant
62
60
58
56
54
52
50
Median =
55.90 +0.30/-0.21 [0.46%] (95% conf.)
data-point error ellipses are 2σ
28ULU-12
n=103
<10% discordant
0.055
0.053
0.051
0.049
0.047
0.045
0.043
0.041
207Pb/206Pb
62
60
58
56
54
52
50
102
106
110
114
118
122
126
130
238U/206Pb

Figure 34A

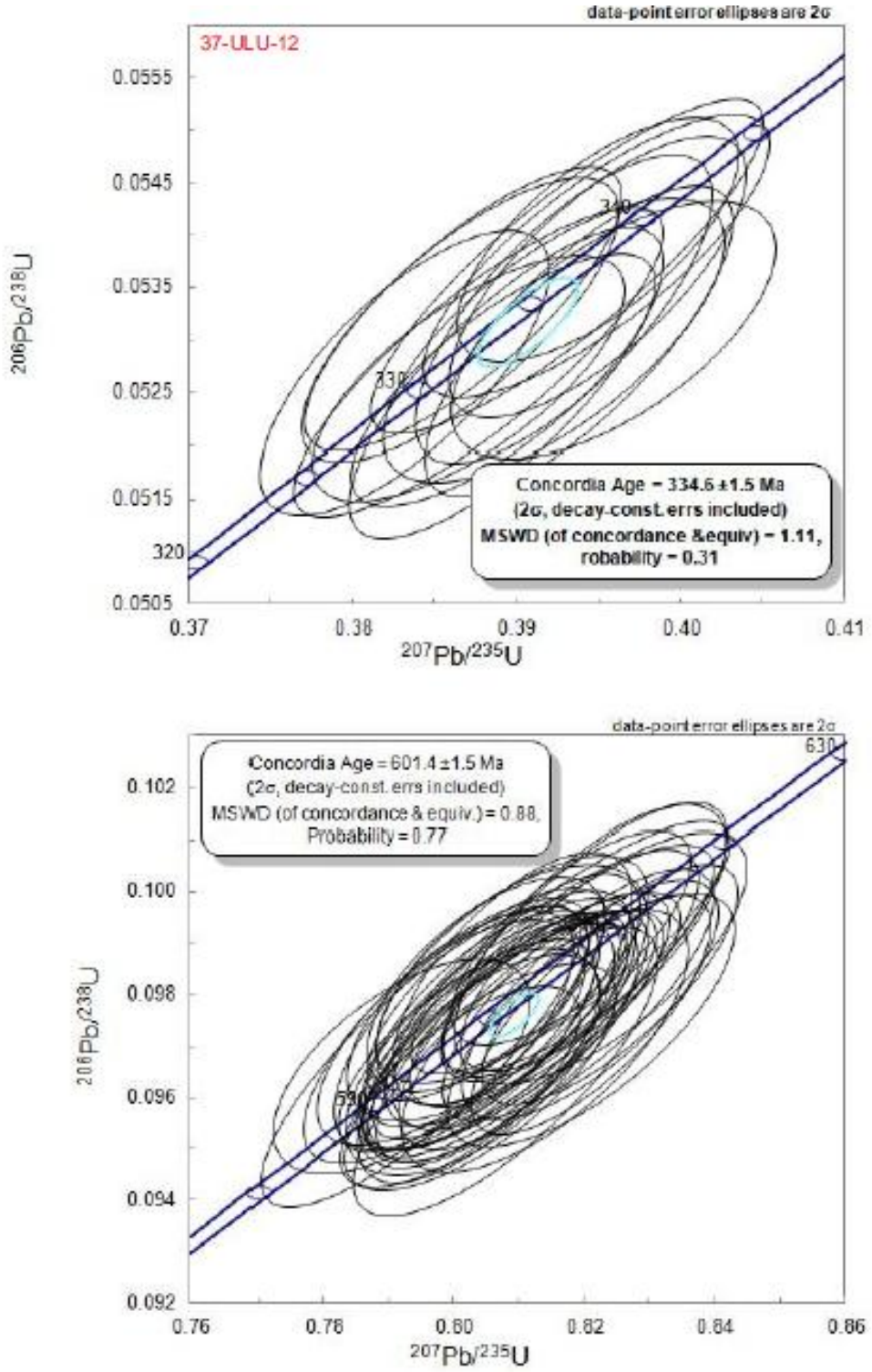
data-point error ellipses are 2σ
37-ULU-12
0.0555
0.0545
0.0535
0.0525
0.0515
0.0505
320
330
Concordia Age = 334.6 ±1.5 Ma
(2σ, decay-const.errs included)
MSWD (of concordance &equiv) = 1.11,
robability = 0.31
0.37
0.38
0.39
0.40
0.41
206Pb/238U
207Pb/235U
data-point error ellipses are 2σ
630
Concordia Age = 601.4 ±1.5 Ma
(2σ, decay-const. errs included)
MSWD (of concordance & equiv.) = 0.88,
Probability = 0.77
0.102
0.100
0.098
0.096
0.094
0.092
0.76
0.78
0.80
0.82
0.84
0.86
206Pb/238U
207Pb/235U

Figure 34B

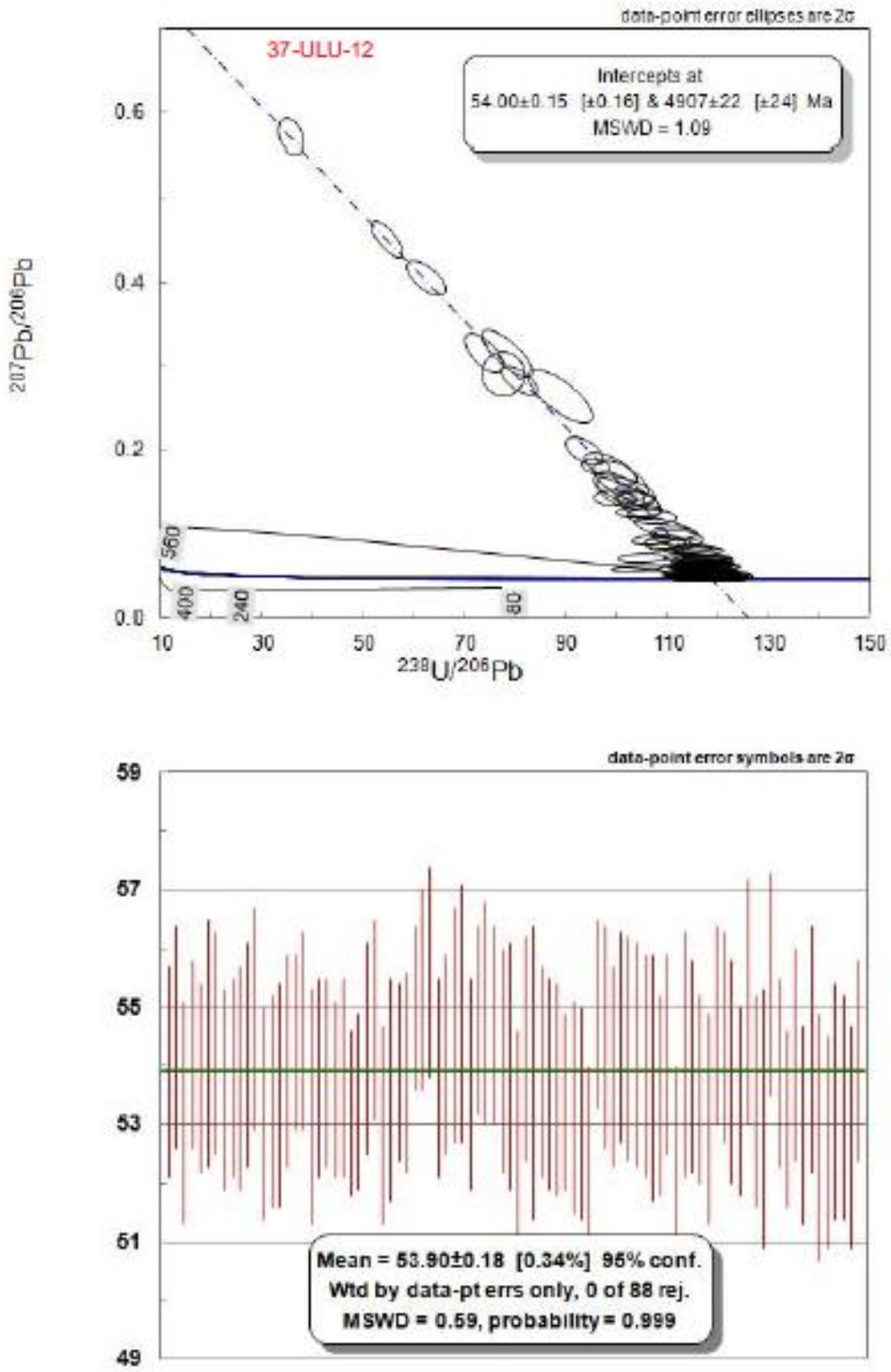
data-point error ellipses are 2σ
37-ULU-12
Intercepts at
54.00±0.15 [±0.16] & 4907±22 [±24] Ma
MSWD = 1.09
0.6
0.4
0.2
0.0
207Pb/206Pb
560
400
240
80
10
30
50
70
90
110
130
150
238U/206Pb
data-point error symbols are 2σ
59
57
55
53
51
49
Mean = 53.90±0.18 [0.34%] 95% conf.
Wtd by data-pt errs only, 0 of 88 rej.
MSWD = 0.59, probability = 0.999

Figure 35A

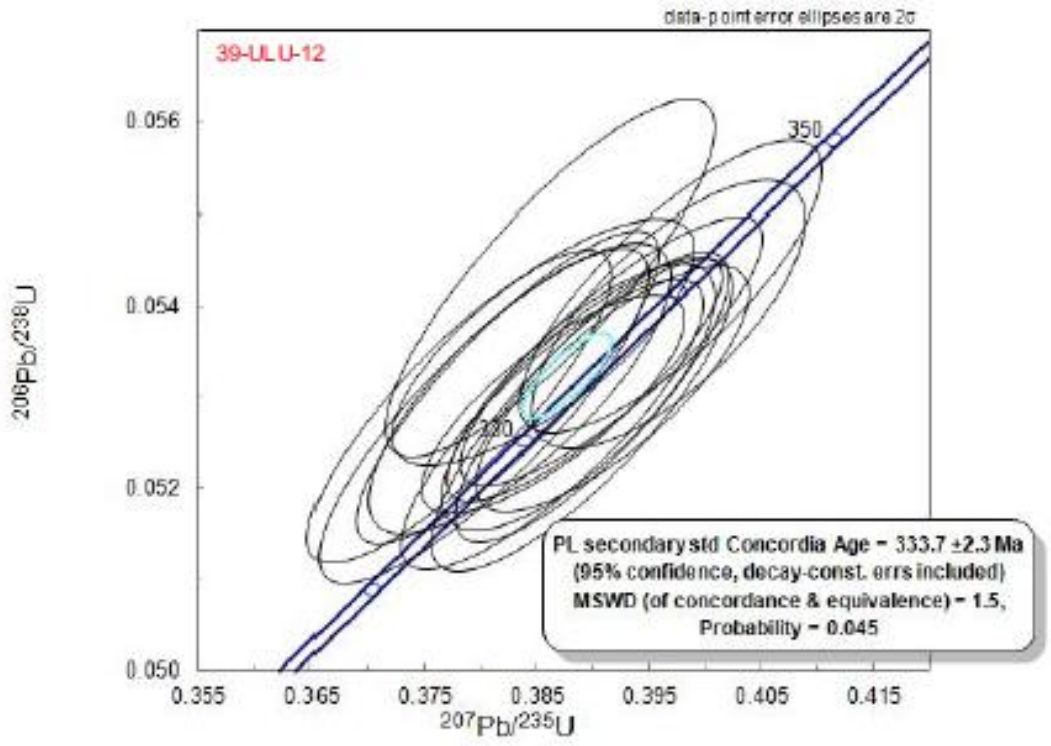
data-point error ellipses are 2σ
39-UL U-12
0.056
0.054
0.052
0.050
350
320
PL secondary std Concordia Age = 333.7 ±2.3 Ma
(95% confidence, decay-const. errs included)
MSWD (of concordance & equivalence) = 1.5,
Probability = 0.045
0.355
0.365
0.375
0.385
0.395
0.405
0.415
$^{206}Pb/^{238}U$
$^{207}Pb/^{235}U$

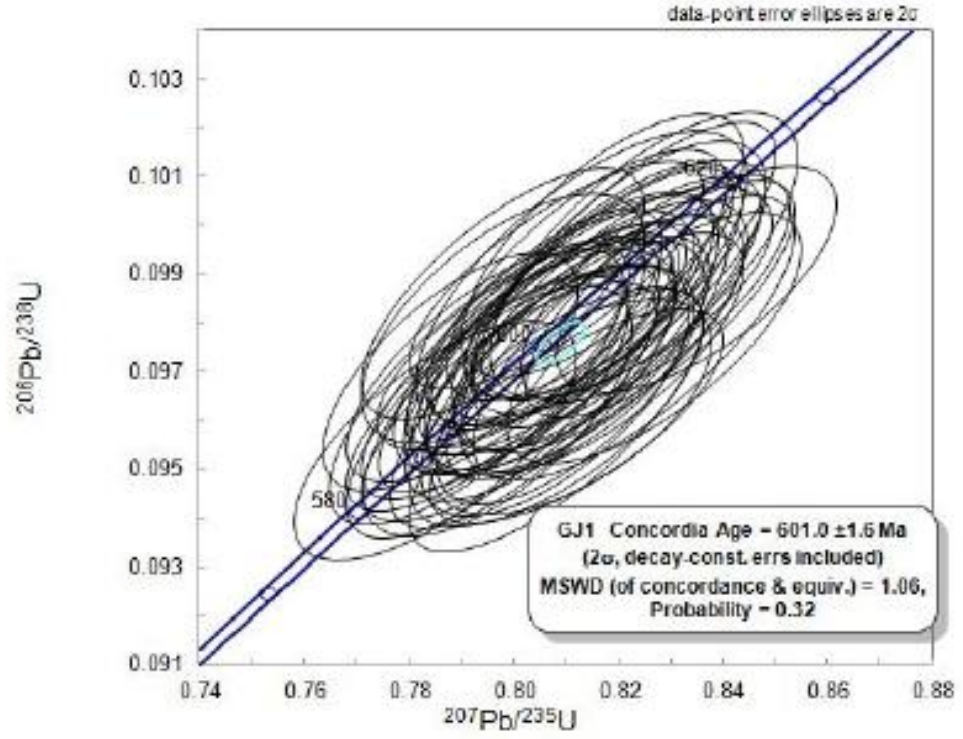
data-point error ellipses are 2σ
0.103
0.101
0.099
0.097
0.095
0.093
0.091
620
580
GJ1 Concordia Age = 601.0 ±1.6 Ma
(2σ, decay-const. errs included)
MSWD (of concordance & equiv.) = 1.06,
Probability = 0.32
0.74
0.76
0.78
0.80
0.82
0.84
0.86
0.88
$^{206}Pb/^{238}U$
$^{207}Pb/^{235}U$

Figure 35B

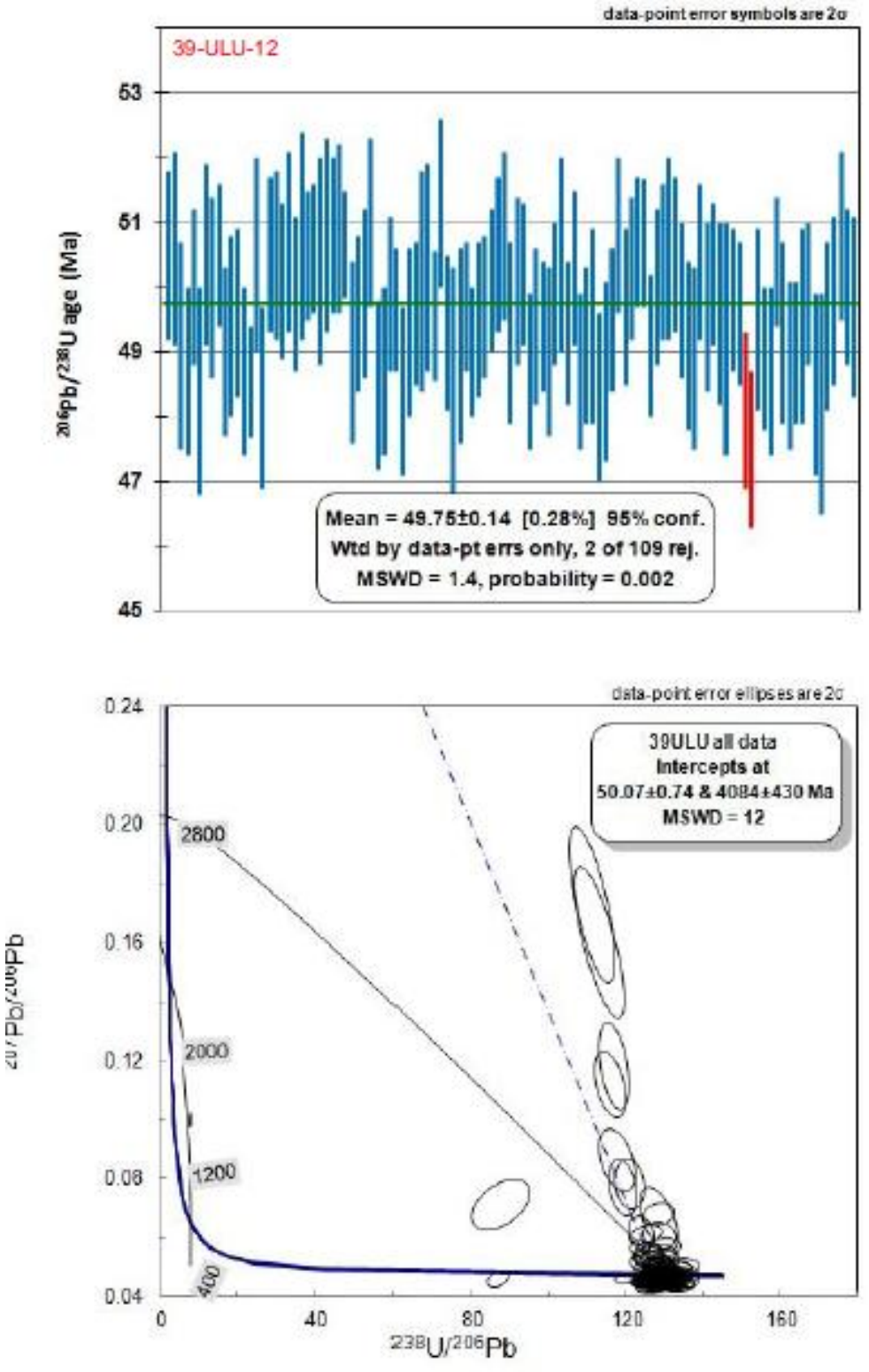
data-point error symbols are 2σ
39-ULU-12
53
51
49
47
45
$^{206}Pb/^{238}U$ age (Ma)
Mean = 49.75±0.14 [0.28%] 95% conf.
Wtd by data-pt errs only, 2 of 109 rej.
MSWD = 1.4, probability = 0.002
data-point error ellipses are 2σ
39ULU all data
Intercepts at
50.07±0.74 & 4084±430 Ma
MSWD = 12
0.24
0.20
0.16
0.12
0.08
0.04
$^{207}Pb/^{206}Pb$
2800
2000
1200
400
0
40
80
120
160
$^{238}U/^{206}Pb$

Figure 36A

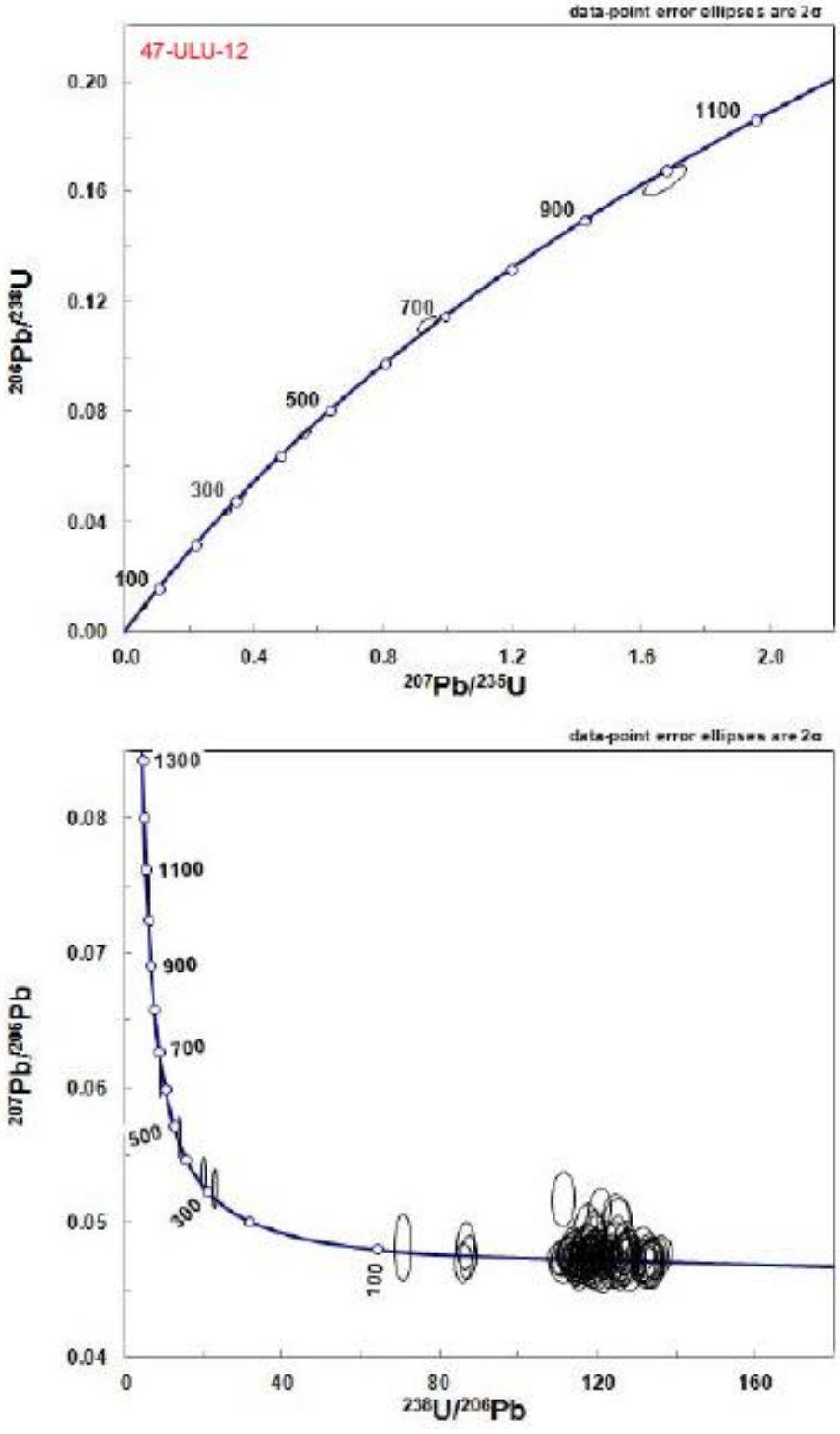
data-point error ellipses are 2σ
47-ULU-12
0.20
0.16
0.12
0.08
0.04
0.00
$^{206}Pb/^{238}U$
100
300
500
700
900
1100
0.0
0.4
0.8
1.2
1.6
2.0
$^{207}Pb/^{235}U$
data-point error ellipses are 2σ
0.08
0.07
0.06
0.05
0.04
$^{207}Pb/^{206}Pb$
1300
1100
900
700
500
300
100
0
40
80
120
160
$^{238}U/^{206}Pb$

Figure 36B

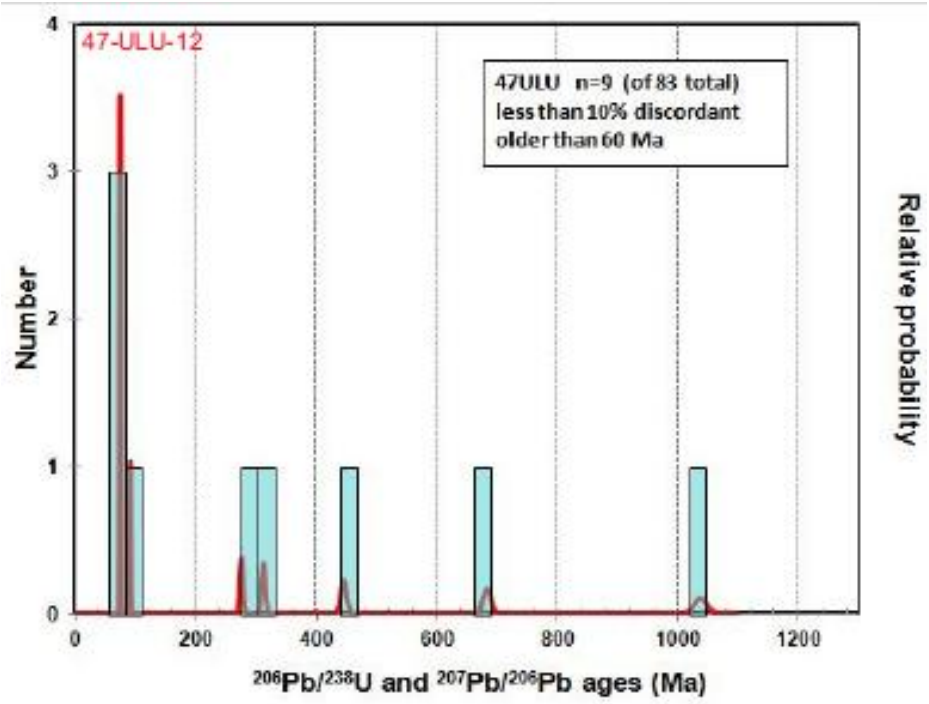
47-ULU-12
47ULU n=9 (of 83 total)
less than 10% discordant
older than 60 Ma
Number
Relative probability
0
1
2
3
4
0
200
400
600
800
1000
1200
206Pb/238U and 207Pb/206Pb ages (Ma)

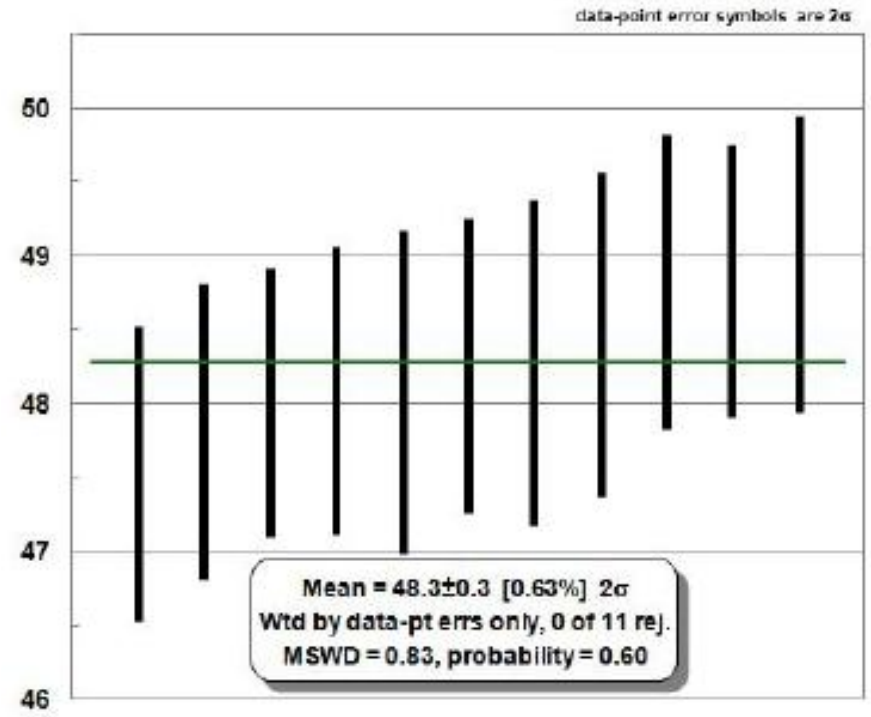
data-point error symbols are 2σ
50
49
48
47
46
Mean = 48.3±0.3 [0.63%] 2σ
Wtd by data-pt errs only, 0 of 11 rej.
MSWD = 0.83, probability = 0.60

Figure 36C

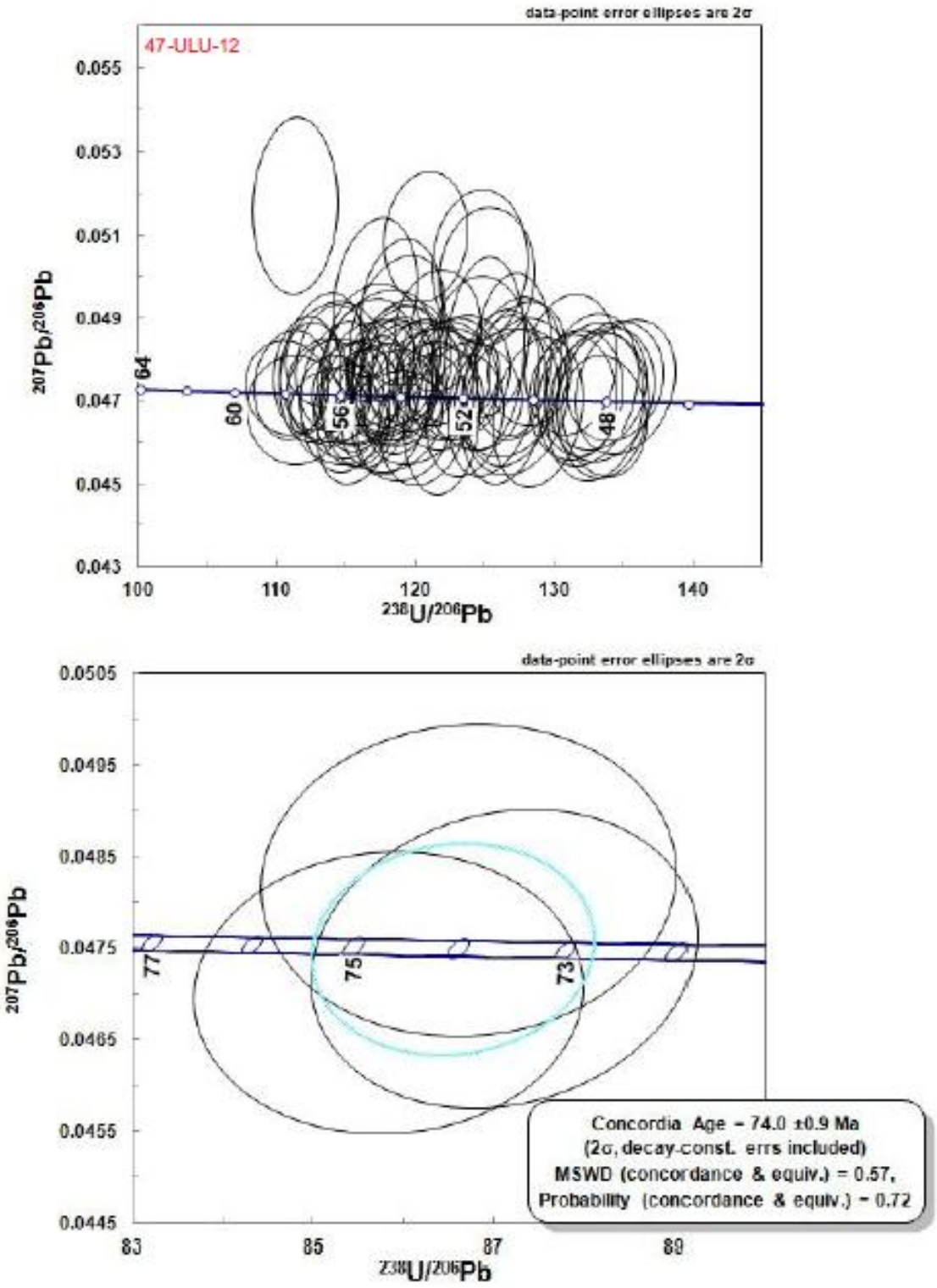
data-point error ellipses are 2σ
47-ULU-12
0.055
0.053
0.051
0.049
0.047
0.045
0.043
207Pb/206Pb
64
60
56
52
48
100
110
120
130
140
238U/206Pb
data-point error ellipses are 2σ
0.0505
0.0495
0.0485
0.0475
0.0465
0.0455
0.0445
207Pb/206Pb
77
75
73
83
85
87
89
238U/206Pb
Concordia Age = 74.0 ±0.9 Ma
(2σ, decay-const. errs included)
MSWD (concordance & equiv.) = 0.57,
Probability (concordance & equiv.) = 0.72

Figure 37A

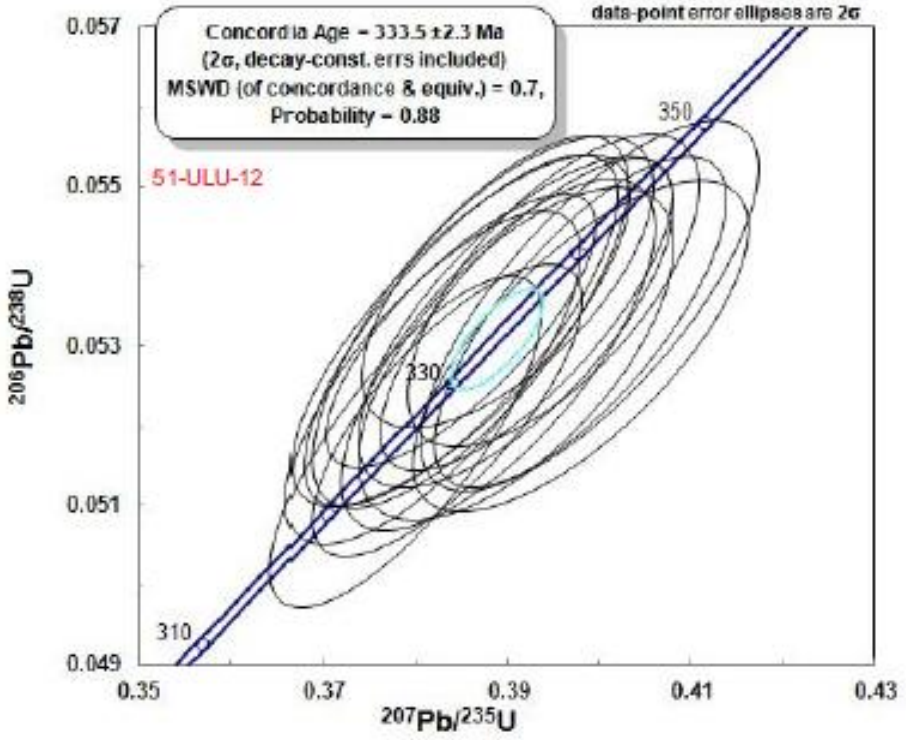
data-point error ellipses are 2σ
Concordia Age = 333.5 ±2.3 Ma
(2σ, decay-const. errs included)
MSWD (of concordance & equiv.) = 0.7,
Probability = 0.88
51-ULU-12
350
330
310
0.057
0.055
0.053
0.051
0.049
0.35
0.37
0.39
0.41
0.43
206Pb/238U
207Pb/235U

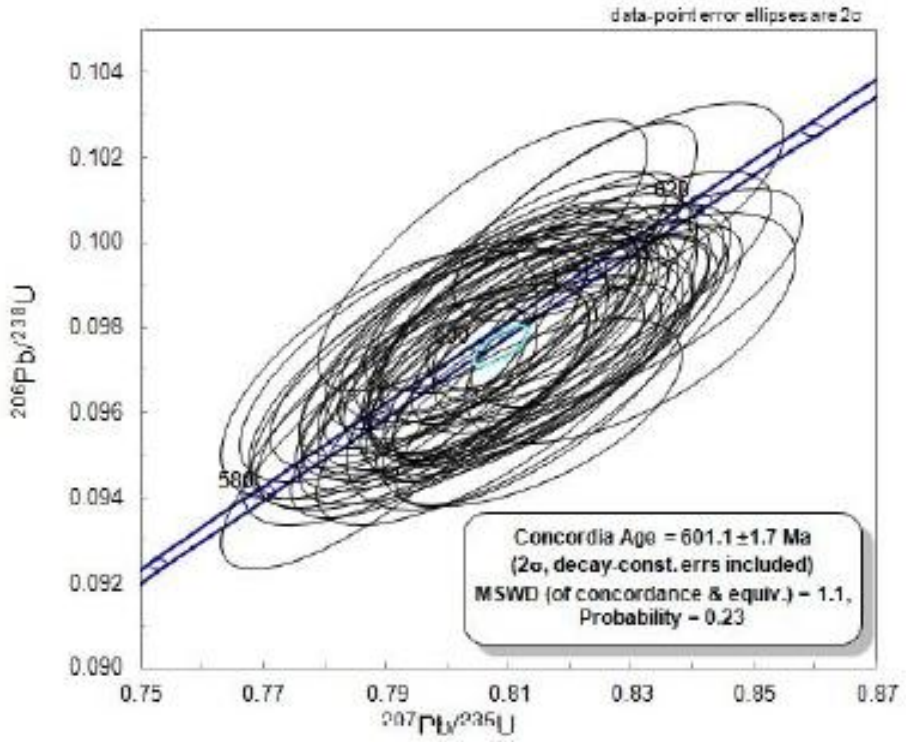
data-point error ellipses are 2σ
620
580
Concordia Age = 601.1 ±1.7 Ma
(2σ, decay-const. errs included)
MSWD (of concordance & equiv.) = 1.1,
Probability = 0.23
0.104
0.102
0.100
0.098
0.096
0.094
0.092
0.090
0.75
0.77
0.79
0.81
0.83
0.85
0.87
206Pb/238U
207Pb/235U

Figure 37B

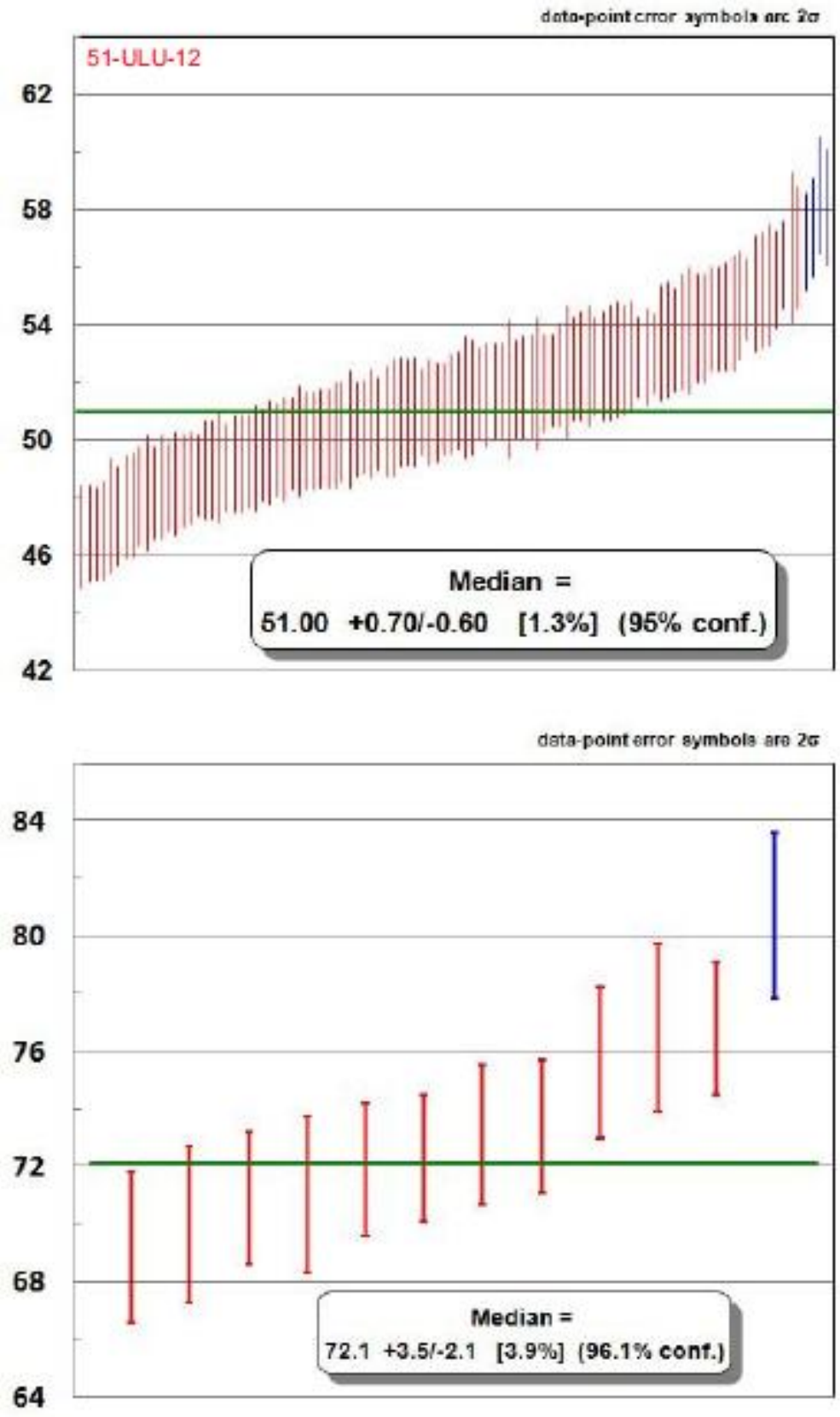
data-point error symbols are 2σ
51-ULU-12
62
58
54
50
46
42
Median =
51.00 +0.70/-0.60 [1.3%] (95% conf.)
data-point error symbols are 2σ
84
80
76
72
68
64
Median =
72.1 +3.5/-2.1 [3.9%] (96.1% conf.)

Figure 37C

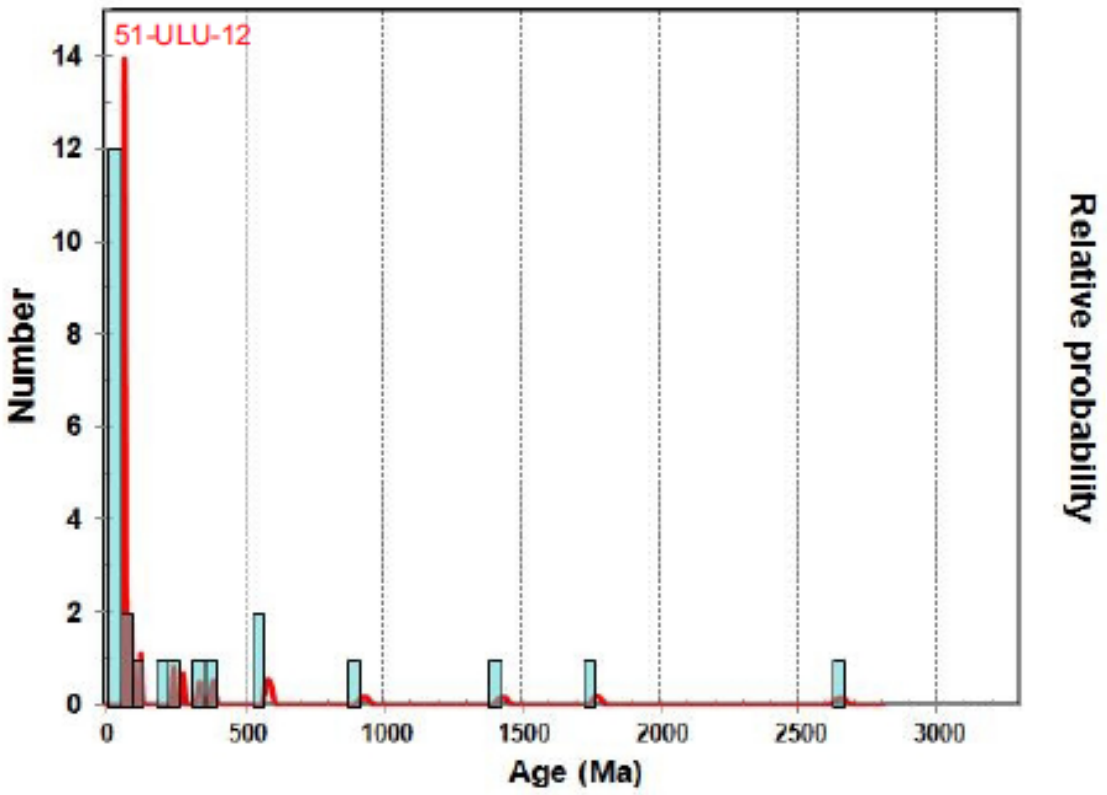
51-ULU-12
Number
Relative probability
Age (Ma)
0
2
4
6
8
10
12
14
0
500
1000
1500
2000
2500
3000

Figure 38

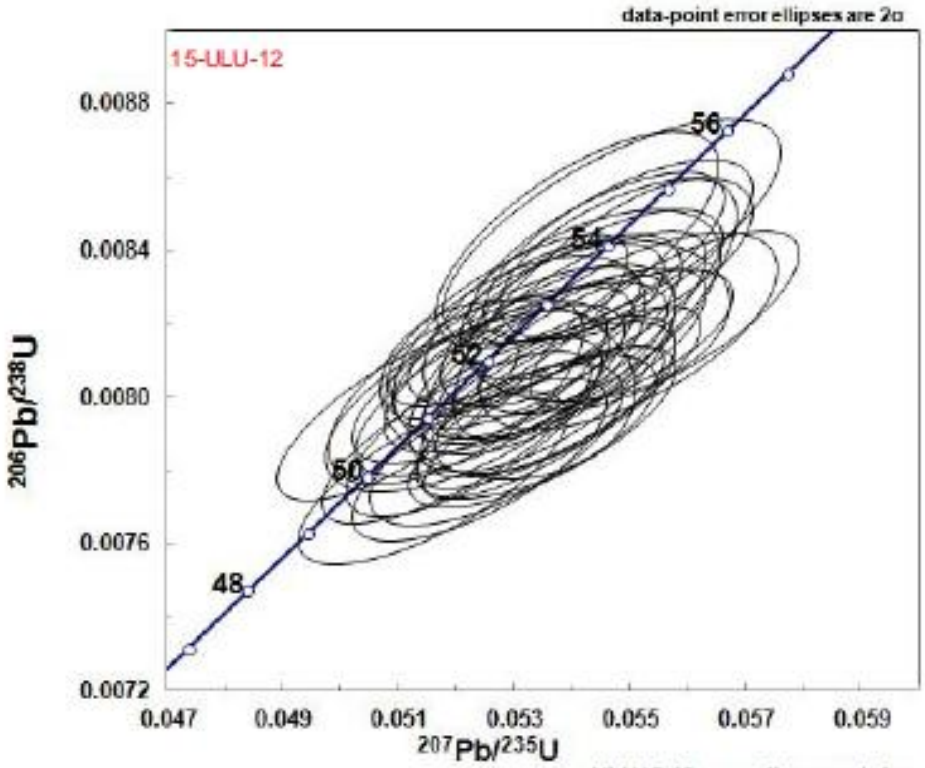

ULU15-12: overdispersed data, shown here in black used for best age estimate : 52+-0.5 Ma, robust median 206Pb/238U age.

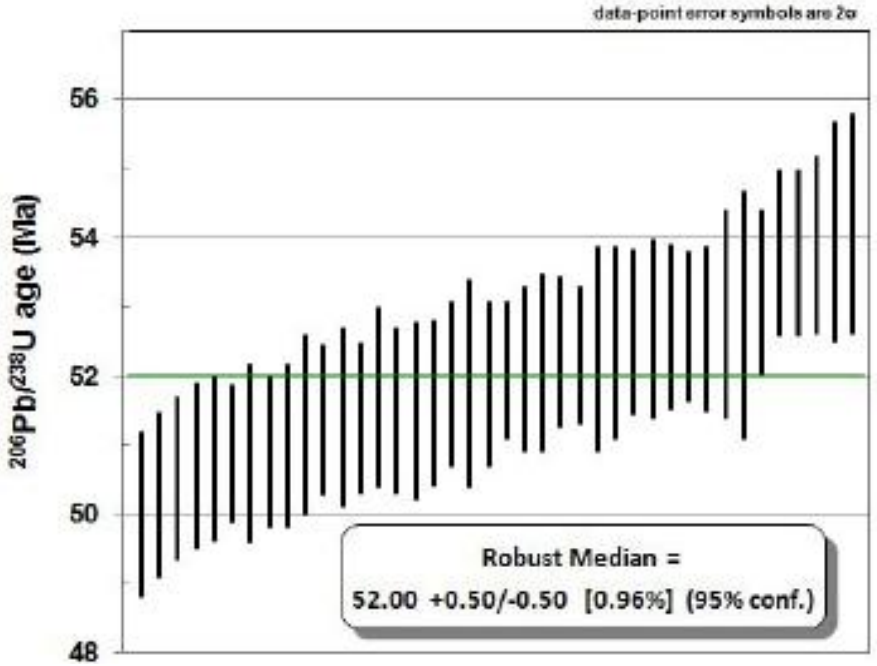

Figure 39

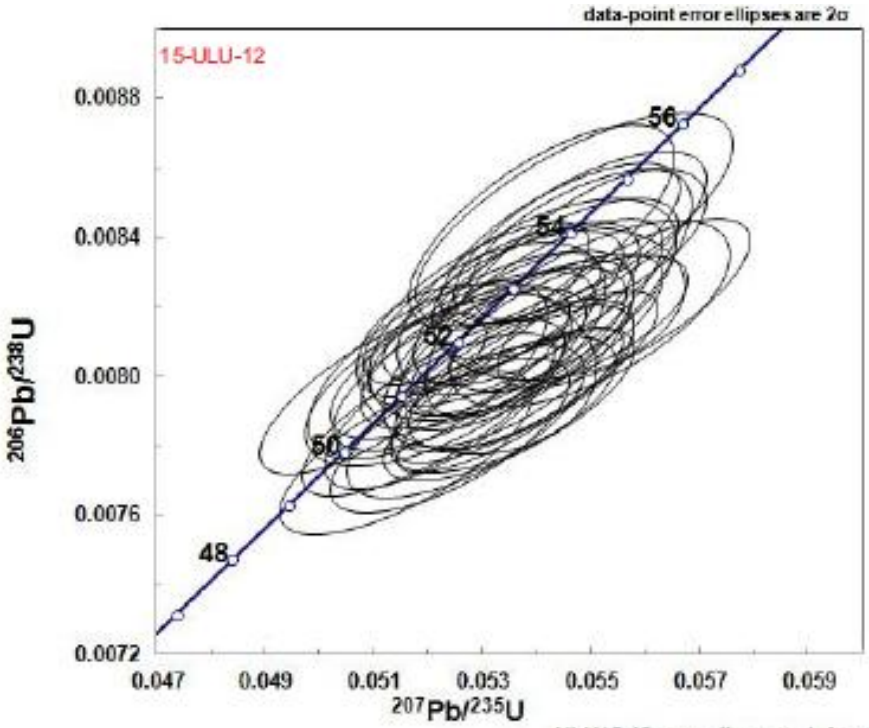

ULU15-12: overdispersed data, shown here in black used for best age estimate : 52+-0.5 Ma, robust median 206Pb/238U age.

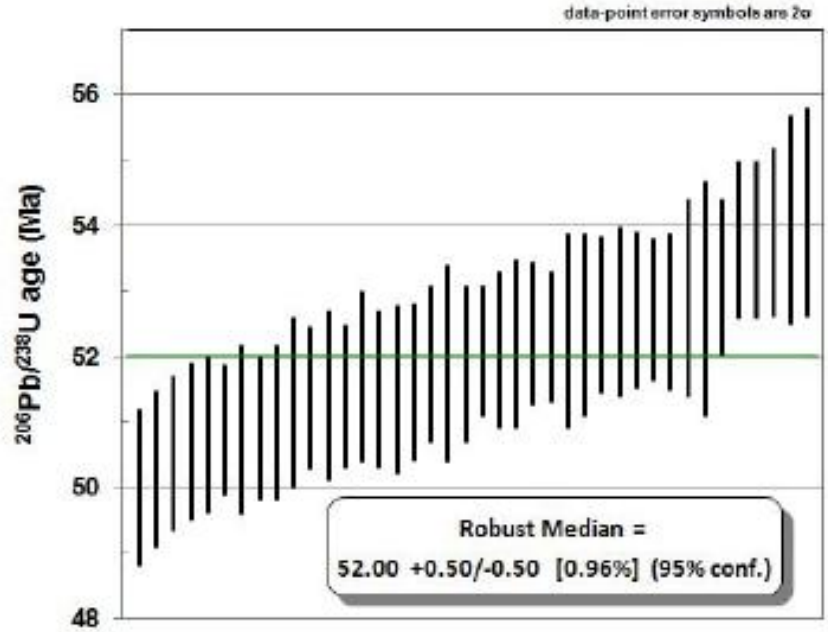

Figure 40

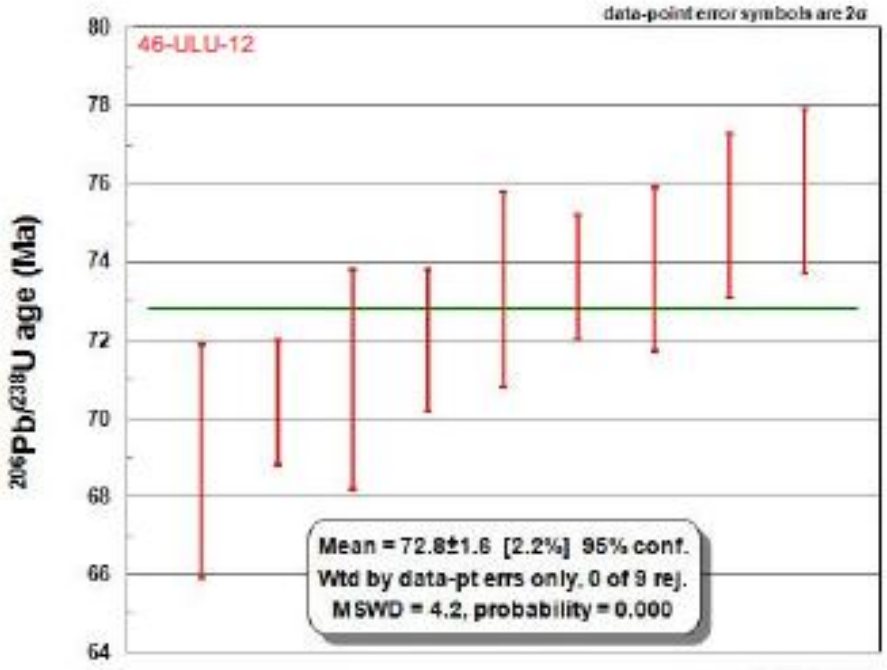

ULU46-12: don't use for age
dispersed data at ca. 73 Ma
1 analyses much younger at 62 Ma.
Will be repeated on polished mount.

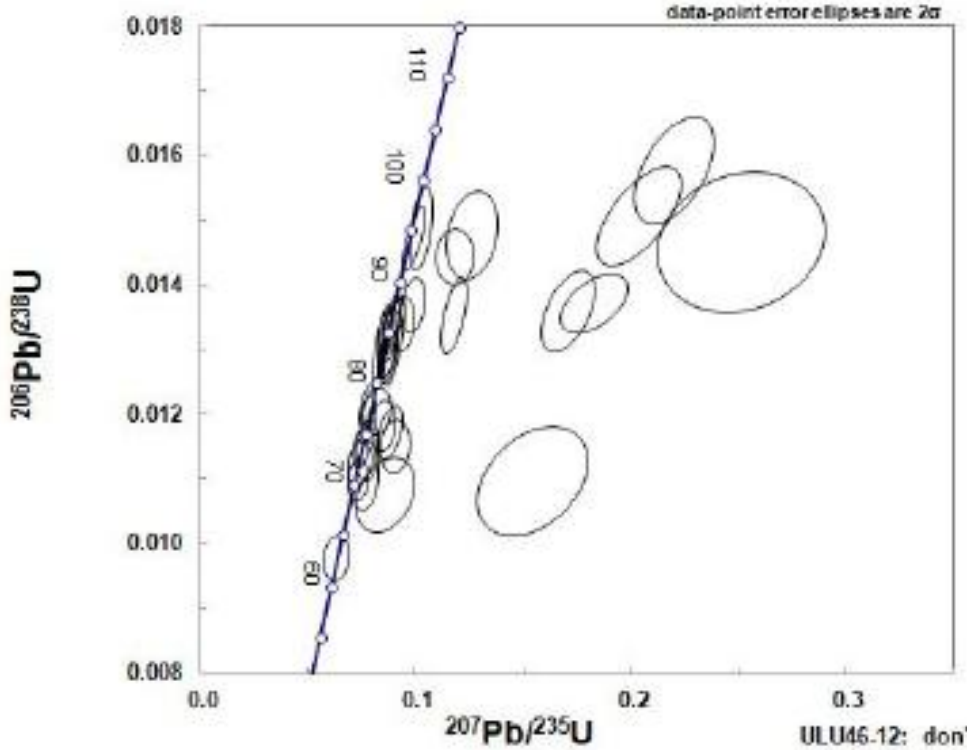

ULU46-12: don't use for age
very dispersed data, group at ca. 73 Ma
But 1 analyses much younger at 62 Ma.
Will be repeated on polished mount.

Figure 41

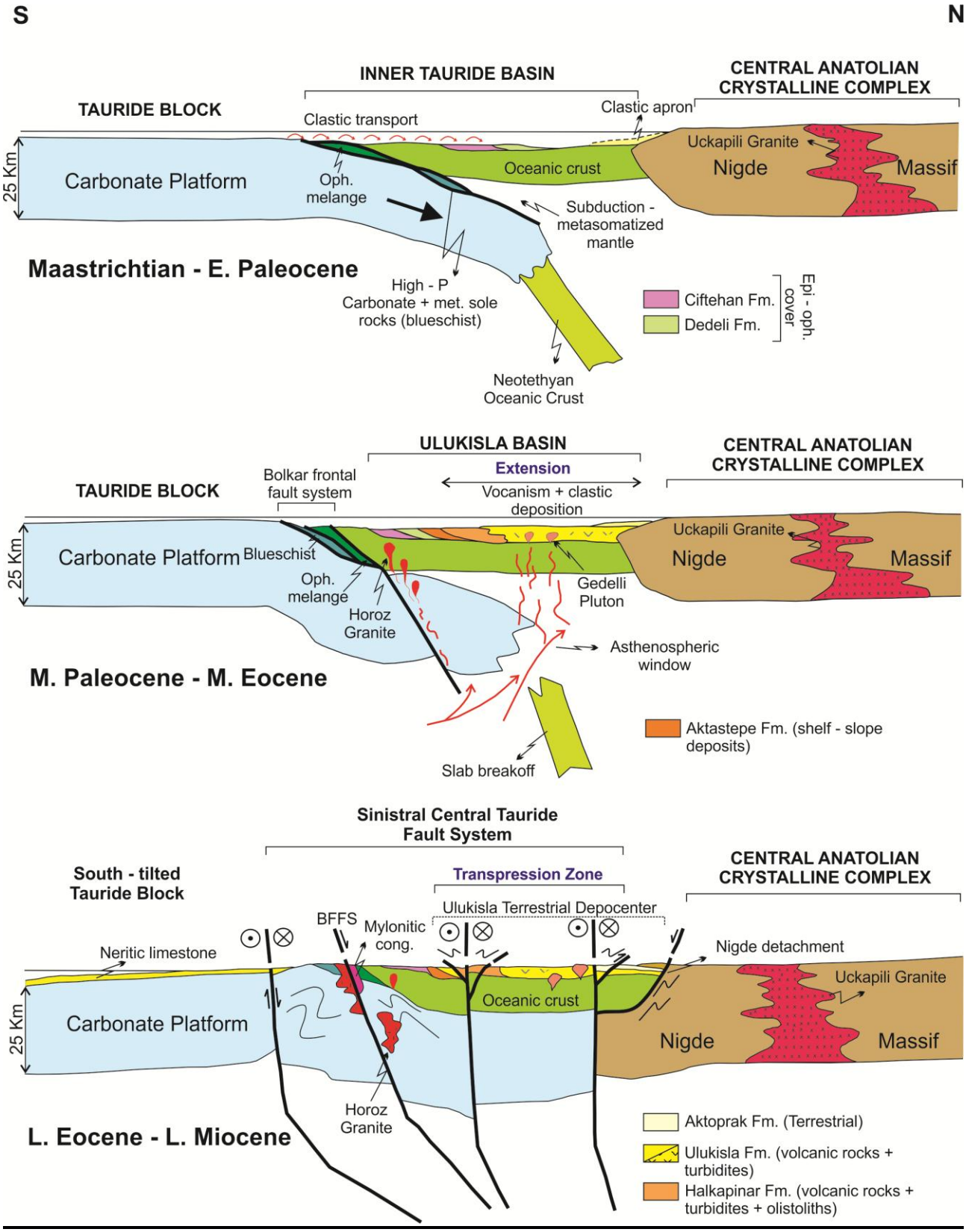
S
N
INNER TAURIDE BASIN
CENTRAL ANATOLIAN CRYSTALLINE COMPLEX
TAURIDE BLOCK
Clastic transport
Clastic apron
Uckapili Granite
Carbonate Platform
Oph. melange
Oceanic crust
Nigde
Massif
25 Km
Subduction - metasomatized mantle
Maastrichtian - E. Paleocene
High - P Carbonate + met. sole rocks (blueschist)
Ciftehan Fm.
Dedeli Fm.
Epi - oph. cover
Neotethyan Oceanic Crust
ULUKISLA BASIN
CENTRAL ANATOLIAN CRYSTALLINE COMPLEX
Extension
TAURIDE BLOCK
Bolkar frontal fault system
Vocanism + clastic deposition
Uckapili Granite
Carbonate Platform
Blueschist
Oph. melange
Horoz Granite
Gedelli Pluton
Nigde
Massif
25 Km
Asthenospheric window
M. Paleocene - M. Eocene
Aktastepe Fm. (shelf - slope deposits)
Slab breakoff
Sinistral Central Tauride Fault System
CENTRAL ANATOLIAN CRYSTALLINE COMPLEX
South - tilted Tauride Block
Transpression Zone
Ulukisla Terrestrial Depocenter
BFFS
Mylonitic cong.
Neritic limestone
Nigde detachment
Uckapili Granite
Oceanic crust
Carbonate Platform
Nigde
Massif
25 Km
Horoz Granite
L. Eocene - L. Miocene
Aktoprak Fm. (Terrestrial)
Ulukisla Fm. (volcanic rocks + turbidites)
Halkapinar Fm. (volcanic rocks + turbidites + olistoliths)

Table 1: Locations, formations and rock types of the collected samples from the Ulukisla Basin and its surroundings

Sample Number	Town/Village	Lon/Lat/Elevation (m)	Rock Type	Formation
01ULU12	Entrance to the Alihoca Village	N37°30'.381"/E034°44'.048"/1058	Sandstone	Ciftehan Formation
02ULU12	Alihoca Village	N37°29'.754"/E034°43'.059"/1079	Plagioglanite vein/dike	Alihoca Ophiolite
03ULU12	Alihoca Village	N37°29'.754"/E034°43'.059"/1079	Hornblende/poiklitic gabbro	Alihoca Ophiolite
04ULU12	Darbogazi Village Road	N37°28'.098"/E034°35'.171"/1686	Sandstone	Halkapinar Formation
05ULU12	Darbogazi Town Entrance	N37°28'.995"/E034°34'.185"/1385	Sandstone	Halkapinar Formation
06ULU12	Darbogazi Town Entrance	N37°28'.995"/E034°34'.185"/1385	Coarse-grained, highly-lithic Sandstone	Halkapinar Formation
07ULU12	After Exiting Darbogazi	N37°28'.382"/E034°34'.227"/1387	Lithic Sandstone	Halkapinar Formation
08ULU12	Darbogazi-Maden Road	N37°27'.693"/E034°35'.883"/1855	Basaltic Rock	Halkapinar Formation
09ULU12	Darbogazi-Maden Road	N37°27'.501"/E034°36'.748"/1996	A-Obsidian clast/lenses in the tuffaceous material/ B-Tuffaceous conglomerate with euhedral biotite	Halkapinar Formation
10ULU12	Darbogazi-Maden Karagol road intersection	N37°27'.398"/E034°36'.873"/2020	Sandstone (Fossileferous)	Halkapinar Formation
11ULU12	Karagol Road	N37°27'.172"/E034°36'.762"/2072	Sandstone	Halkapinar Formation
12ULU12	Karagol Road	N37°26'.651"/E034°35'.708"/2197	Blueschist Rock	Halkapinar Formation
13ULU12	Karagol Road	N37°26'.111"/E034°35'.002"/2247	Quartzite	Halkapinar Formation
14ULU12	Karagol Road	N37°25'.637"/E034°34'.487"/2318	Meta-Dolerite	Halkapinar Formation
15ULU12	Horoz Village Road	N37°29'.191"/E034°48'.474"/994	Granodiorite	Horoz Granite
16ULU12	Horoz Village Road	N37°28'.829"/E034°48'.072/1042	Dacite Dike	Horoz Granite
17ULU12	Horoz Vilage Road	N37°28'.639"/E034°47'.184"/1186	Aplitic/rhyolitic dikes intruding Horoz Gran.	Horoz Granite
18ULU12	Horoz Village Road	N37°28'.639"/E034°47'.184"/1136	Aplitic/rhyolitic dikes intruding Horoz Gran.	Horoz Granite
19ULU12	Ciftehan-Pozanti Road (E-S)	N37°30'.402"/E034°47'.158"/933	Sandstone	Ciftehan Formation

20ULU12	North of Alihoca Village	N37°30'.655"/E034°44'.563"/996	Rhyolite	Halkapinar Formation
21ULU12	North of Alihoca Village	N37°30'.655"/E034°44'.563"/996	Andesite	Halkapinar Formation
22ULU12	North of Alihoca Village	N37°30'.619"/E034°44'.621"/1015	Sandstone	Halkapinar Formation
23ULU12	North of Alihoca Village	N37°30'.619"/E034°44'.621"/1015	Tuffaceous Rock	Halkapinar Formation
24ULU12	North of Alihoca Village	N37°30'.619"/E034°44'.621"/1015	Rhyolite/Rhyodacite	Halkapinar Formation
25ULU12	North of Alihoca Village	N37°30'.619"/E034°44'.621"/1015	Rhyodacite-Dacite	Halkapinar Formation
26ULU12	Ciftehan-Gedelli Road	N37°31'.809"/E034°45'.663"/1388	Dirty Sandstone with abundant volc. Material	Hasangazi Formation
27ULU12	After Elmali Road Sign	N37°32'.327"/E034°46'.021"/1379	Trachybasalt	Ulukisla Formation
28ULU12	Elmali Rd	N37°32'.689'/E034°46'.323"/1243	Sandstone over Limestone	Ulukisla Formation
29ULU12	Elmali Rd	N37°32'.689'/E034°46'.323"/1243	Dirty Sandstone	Ulukisla Formation
30ULU12	Over the Tunnels Around Elmali Village	N37°33'.514"/N034°45'.840"/1116	Fine-grained andesite	Ulukisla Formation
31ULU12	Over the Tunnels Around Elmali Village	N37°33'.514"/N034°45'.840"/1116	Porphyritic andesite for zircon dating	Ulukisla Formation
32ULU12	After the tunnels, towards Gedelli Village	N37°34'.618"/E034°45'.194"/1107	Andesite Dike	Ulukisla Formation
33ULU12	After the tunnels, towards Gedelli Village	N37°34'.618"/E034°45'.194"/1107	Thick and dike	Ulukisla Formation
34ULU12	After the tunnels, towards Gedelli Village	N37°34'.618"/E034°45'.194"/1107	Monzonitic dike	Ulukisla Formation
35ULU12	Around previous location	N37°34'.768"/E034°45'.248"/1128	Biotite diorite	Ulukisla Formation
36ULU12	Around previous location	N37°34'.768"/E034°45'.248"/1128	Aplitic-rhyolitic dike	Ulukisla Formation
37ULU12		N37°35'.636"/E034°44'.557"/1147	Sandstone	Ulukisla Formation
38ULU12		N37°35'.636"/E034°44'.557"/1147	Pillow lava basalt	Ulukisla Formation
39ULU12	Between Hasangazi-Ciftehan E-5	N37°31'.376"/E034°42'.382"/1118	Sandstone	Hasangazi Formation
40ULU12	Ecemis Fault Zone	N37°29'.705"/E034°54'.863"/1203	Channel Sandstone	Camardi Formation
41ULU12	After Kamisli and before Aydinlar mahallesi	N37°38'.872"/E034°59'.382"/1219	Fine-grained sandstone	Camardi Formation

42ULU12	Camardi town exit	N37°50'.209"/E034°58'.996"/1523	Sandstone layer in the Camardi Fm.	Camardi Formation
43ULU12	Camardi town exit	N37°50'.209"/E034°58'.996"/1523	Mica-rich medium-grained sandstone	Camardi Formation
44ULU12	In the Nigde massif	N37°52'.301"/N034°56'.004"/1727	Muscovite-granite dike	Nigde massif
45ULU12	In the Nigde massif	N37°52'.301"/N034°56'.004"/1727	Biotite-muscovite schist	Nigde massif
46ULU12	Uckapili village	N37°54'.412"/N034°54'.391"/1876	Uckapili granite	Nigde massif
47ULU12	Nigde-Ulukisla Road	N37°42'.646"/N034°33'.291"/1184	Graywacke	Hasangazi Formation
48ULU12	Nigde-Ulukisla Road	N37°42'.646"/N034°33'.291"/1184	Volcanic airfall deposit	Hasangazi Formation
49ULU12	On the Yeniyildiz Road	N37°29'.472"/N034°19'.393"/1348	Dirty sandstone	Aktoprak Formation
50ULU12	Between Yeniyildiz and Aktoprak Villages	N37°28'.915"/E034°24'.778"/1604	Sandstone Calcareous Sandstone	Aktoprak Formation
51ULU12	Aktoprak (Kilan) Village	N37°28'.843"/N034°27'.190"/1649	Fossiliferous Sandstone	Aktoprak Formation
52ULU12	Caykavak GAP on the Nigde Ulukisla Road	N37°35".391"/N034°32'.329"/1606	Pillow basalt from the northern end	Ulukisla Formation
53ULU12	Caykavak GAP on the Nigde Ulukisla Road	N37°35".391"/N034°32'.329"/1606	Pillow basalt from a fault block in the center of the entire roadcut	Ulukisla Formation
54ULU12	Caykavak GAP on the Nigde Ulukisla Road	N37°35".391"/N034°32'.329"/1606	Plag-phyric,more felsic pillows	Ulukisla Formation
55ULU12	Caykavak GAP on the Nigde Ulukisla Road	N37°35".391"/N034°32'.329"/1606	Pillow lava from the southern end	Ulukisla Formation
56ULU12	Entrance of the Darbogaz town	N37°30'.844"/N034°34'.655"/1273	Kabaktepe Evaporites	Hasangazi Formation

Table 2: Strike and dip measurements of bedding planes in different formations in the Ulukisla Basin

Aktastepe Formation	Halkapinar Formation	Hasangazi Formation	Aktoprak Formation
71/60 SE	87/58 NW	60/65 NW	50/35 SE
78/65 SE	94/24 SW	230/85 SE	40/40 SE
73/60 SE	89/44 SE	210/52 SE	250/10 NW
75/60 SE	121/55 SW	60/75 SE	85/80 SE
80/87 NW	112/24 SW	60/80 SE	100/30 NE
82/62 NW	123/27 SW	110/85 NE	135/25 NE
133/36 SW	96/35 SW	110/40 NE	85/30 NW
130/42 SW	94/44 SW	261/49 NW	100/20 SW
151/50 SW	99/32 SW	85/65 SE	105/20 SE
152/42 SW	77/41 SE	90/85 S	86/70 NW
42/42 SE	41/34 SE	40/70 NW	85/70 NW
60/36 SE	62/43 SE	285/15 SW	95/70 NE
71/69 SE	39/38 SE	5/25 NW	89/70 NW
93/46 SW	71/33 SE	245/50 SE	86/60 NW
78/52 SE	141/42 NE	160/40 NW	88/60 SE
71/45 NW	82/61 NW	210/73 NW	81/21 NW
102/56 SW	102/27 NE	250/24 NW	98/20 NE
110/58 SW	126/46 NE	240/55 NW	78/40 SE
33/77 NW	163/19 NE	233/62 NW	70/60 SE
65/42 NW	132/44 SW	340/75 SW	75/40 SE
63/47 NW	97/38 SW	30/65 SE	81/35 SE
48/52 NW	112/12 NE	72/65 SE	50/35 NW
68/42 NW	68/25 NW	65/66 NW	110/20 SW
55/50 NW	165/23 SW	280/46 NE	89/25 SE
28/52 NW	135/28 SW	235/76 SE	131/26 SW

19/50 NW	161/30 SW	222/85 NW	35/32 NW
111/36 SW	163/32 NE	235/75 NW	45/32 NW
2/62 SE	124/45 SW	135/30 NE	50/50 NW
3/67 SE	70/35 SE	25/30 NW	60/46 NW
178/56 NE	93/38 SW	310/22 SW	68/50 NW
179/63 NE	90/42 S	78/25 NW	85/45 NW
177/64 NE	143/32 NE	79/41 NW	79/30 NW
5/70 SE	151/39 NE	78/43 NW	86/35 NW
8/64 SE	138/24 NE	82/42 NW	87/45 NW
12/48 SE	159/19 NE	86/41 NW	78/50 NW
163/43 NE	162/20 NE	81/47 NW	89/80 NW
171/34 NE	138/40 NE	80/39 NW	86/80 NW
165/32 NE	37/33 SE	78/48 NW	89/70 NW
172/25 NE	40/30 SE	87/46 NW	81/65 NW
42/32 SE	44/43 SE	60/39 NW	92/70 E
32/33 SE	68/28 SE	50/36 SE	82/67 NW
8/32 SE	65/30 SE	48/38 SE	83/65 NW
64/20 SE	39/18 SE	56/48 NW	91/60 NE
51/30 SE	133/10 NE	55/49 NW	96/55 NE
86/28 SE	29/18 SE	170/15 SW	88/53 NW
82/43 SE	61/31 SE	81/44 NW	94/70 NW
88/32 SE	13/23 SE	79/52 NW	85/60 NW
183/28 NW	94/12 NE	38/53 NW	88/65 NW
142/40 NE	98/15 NE	70/46 NW	88/70 NW
146/46 NE	170/25 NE	60/38 NW	90/50 N
138/42 NE		61/76 NW	88/70 SE
156/36 NE		76/50 NW	80/70 SE
139/41 NE		50/46 SE	87/50 NW

160/40 NE		53/46 SE	86/50 NW
175/44 NE		72/38 NW	86/58 SE
168/48 NE		68/36 NW	102/50 NE
159/22 NE		71/38 NW	78/60 SE
153/40 NE		73/29 NW	45/50 SE
170/28 NE		74/30 NW	44/60 SE
171/25 NE		62/40 NW	42/60 SE
149/25 NE		35/44 SE	40/60 SE
169/27 NE		36/38 SE	52/20 SE
161/24 NE		70/61 SE	78/20 SE
22/41 SE		72/45 SE	65/40 SE
22/61 SE		76/60 SE	125/22NE
18/24 SE		69/55 SE	128/20 NE
38/51 SE		65/49 SE	78/45 NW
46/44 SE		72/55 SE	79/43 NW
14/41 SE		49/60 SE	82/41 NW
14/55 SE		53/63SE	46/35 NW
51/35 NW		39/70 SE	42/54 NW
161/38 NE		88/30 SE	30/41 SE
171/35 NE		67/74 SE	135/20 NW
172/45 NE		71/78 SE	93/25 SW
152/42 NE		83/74 NW	110/20 SW
168/42 NE		84/59 NW	46/37 NW
179/45 NE		88/42 SE	50/42 NW
176/48 NE		131/32 SW	33/32 NW
148/21 NE		96/33 SW	48/32 NW
153/39 NE		122/135 W	50/47 NW
139/41 NE		152/25 SW	78/60 NW

3/25 SE		73/33 SE	79/60 NW
52/38 SE		74/28 NW	78/45 NW
39/34 SE		50/62 NW	80/50 NW
3/33SE		55/71 NW	78/46 NW
174 /42 NE		63/83 SE	94/50 NE
176/24 NE		113/35 SE	
175/33 NE		152/36 SW	
		82/43 SE	
		89/35 SE	
		88/58 NW	
		73/59 NW	
		81/59 NW	
		87/39 NW	
		79/34 SE	
		39/23 SE	
		89/37 SE	
		88/36 SE	
		84/38 SE	
		79/42 NW	
		77/41 NW	
		78/39 NW	
		68/40 NW	
		73/74 SE	
		75/71 SE	
		78/38 NW	
		82/52 NW	
		83/54 NW	
		88/54 NW	

		90/55 NW	
		90/59 NW	
		83/58 NW	
		86/55 NW	
		71/54 NW	
		79/56 SE	
		73/79 NW	
		67/74 NW	
		78/65 NW	
		81/63 SE	
		80/68 NW	
		82/65 SE	
		113/55 SW	
		93/60 NE	
		79/59 SE	
		90/64 S	
		78/78 SE	
		80/83 SE	
		86/55 SE	
		51/49 SE	
		123/33 SW	
		132/63 NE	
		51/45 SE	
		77/75 SE	
		91/56 SW	
		92/63 SW	
		79/83 SW	
		69/62 SE	

		92/74 NE	
		94/78 NE	

Table 3: Strike and dip measurements of the faults mapped and observed in the field

Early contractional deformation	Extensional deformation	Transpressional deformation
155/55 W	285/60 N	75/65 S
145/65 W	40/41 E	80/65 S
120/80 S	330/60 E	77/60S
160/70 W	325/75 E	67/70 S
105/70 S	290/85 N	88/65 S
100/70 S	250/35 N	85/59 S
110/67 S	160/85 W	95/60 S
115/85 S	135/75 S	115/70 S
340/75 E	135/45 S	120/65 S
310/65 N	260/50 N	82/64 S
335/82 E	340/30 E	120/60 S
305/70 N	225/30 W	115/65 S
320/80 E	300/85 N	100/65 S
325/77 E	210/25 W	98/65 S
350/75 E	155/63 W	86/67S
340/67 E	10/75 E	350 /20 E
110/80 S	250/32 N	175/88 W
335/82 E	335/69 E	165/45 W
105/75 S	105/65 S	130/70 S
320/60 E	130/82 S	130/55 S
104/50 S	155/52 W	90/53 S
355/85 E	225/60 W	100/51 S
90/65 S	315/85 N	115/40 S
165/35 W	130/74 S	95/58 S
90/70 S	275/65 N	75/59 S
0/72 E	130/80 S	260/30 N
0/75 E	335/45 E	71/65 S

	225/78 W	
	152/64 W	
	150/70 W	
	330/71 E	
	295/40 N	
	290/45 N	
	55/67 S	
	305/86 N	
	120/60 S	
	135/85 S	
	285/55 N	
	313/33 N	
	140/65 W	
	15/65 E	
	100/33 S	
	150/65 W	
	140/63 W	
	138/80 W	
	90/38 S	
	125/74 S	
	130/71 S	
	142/63 W	
	120/82 S	
	128/67 S	
	117/67 S	
	139/82 W	
	110/70 S	
	154/76 W	
	140 /55W	
	134/62 S	

	151/58 W	
	105/54 S	
	135/65 S	
	112/50 S	
	130/67 S	
	137/70 W	
	135/65 S	
	142/73 W	
	140/72 W	
	125/54 S	
	125/74 S	
	164/58 W	
	132/44 S	
	115/62 S	
	150/48 W	
	127/66 S	
	160/58 W	
	290/66 N	
	295/65 N	
	335/60 E	
	300/60 N	
	290/75 N	
	275/75 N	
	310/80 N	
	280/80 N	
	320/84 E	
	320/85 E	
	320/72 E	
	315/80 N	
	334/66 E	

	195/75 W	
	318/59 E	
	317/61 E	
	332/68 E	
	340/60 E	
	326/73 E	
	319/58 E	
	338/65 E	
	315 /58 N	
	322/63 E	
	315/67 N	
	322/62 E	
	318/58 E	
	320/66 E	